FORMATION FEATURES OF COMPOSITE MATERIALS CONTAINING COBALT NANOPARTICLES ACTIVE IN FISCHER-TROPSCH SYNTHESIS

M. V. Kulikova[a]*, M. I. Ivantsov[a,b], M. N. Efimov[a], L. M. Zemtsov[a], P. A. Chernavskii[b], G. P. Karpacheva[a] and S. N. Khadzhiev[a]

The influence of polymer matrix on the activity of composite material containing cobalt nanoparticles in Fischer-Tropsch synthesis was studied. It was found that the structure of the polymer matrix affects active centers formation. Magnetometry techniques *in situ* and XRD confirmed the presence of the metal cobalt and its oxide phases which are the active centers of different type effect.

*Corresponding Author
    Fax: +7(495)633-85-20
    E-Mail: m_krylova@ips.ac.ru
[a]   A.V. Topchiev Institute of Petrochemical Synthesis, Russian Academy of Sciences, 29 Leninsky prospect, Moscow 119991 Russia
[b]   Department of Chemistry Lomonosov Moscow State University, 1-3 Leninskie Gory, Moscow 119991 Russia

Introduction

Fischer-Tropsch synthesis (hydrocarbon synthesis from carbon monoxide and hydrogen) is a second stage of the most recycling processes of non-oil raw materials (coal, natural or associated gas, peat, etc.) to eco-friendly fuel components.[1]

Traditionally, the Fischer-Tropsch synthesis is catalyzed by VIII group metals (iron or cobalt) in bulk state or distributed on the surface of a highly porous support.[2] Their catalytic activity, selectivity and stability is defined by the shape and size of the applied active component particles.[3]

In 1925 F. Fischer and H. Tropsch published results for the catalytic hydrogenation of carbon monoxide to hydrocarbons at atmospheric pressure over an iron based catalyst.[4] Further study of this process has led to the development of cobalt catalysts which have proved to be more active than the iron ones.

In recent years, nanoscale metal-carbon materials as catalysts for the Fischer-Tropsch synthesis have increasingly garnered the interest of the researchers. The introduction of the catalytic active metal particles into carbon matrix is carried out at the stage of carbonization.[5] IR pyrolyzed polymer materials are used as carbon supports. Under the conditions of IR annealing the carbonization process leading to graphite structure formation occurs. Under the conditions of IR pyrolysis of precursors based on polymers and metal salts the ordered carbon structures are formed and simultaneously the metal reduction occurs with the participation of hydrogen released in the dehydrogenation of the backbone polymer chain.

IR pyrolysis process of the precursor allows to introduce catalytic active metals into the carbon matrix structure directly during its formation providing regular distribution of the active catalytic sites.[6,7]

Possibility to control nanocomposite structure and properties makes these systems very promising for the using them as catalysts for chemical and petrochemical processes such as Fischer-Tropsch synthesis. In this paper we distinguish the effect of the nature of initial polymer on the catalytic activity and selectivity of Co-containing nanocomposites.

Experimental

For the samples preparation the following polymers were used: polyacrylonitrile $((-CH_2-CH(CN)-)_n)$ (PAN) polydiphenylamine $((-C_6H_4-NH-C_6H_4-)_n)$ (PDPhA), polystyrene $((-CH\ (C_6H_5)-CH_2-)_n)$ (PS), polyvinyl alcohol $((-CH_2-CH(OH)-)_n)$ (PVA) and cellulose $((C_6H_{10}O_5)_n)$ (CE).

For the preparation of common solution of polymer and cobalt salt the following components were used: PAN – DMFA – $Co(NO_3)_2 \cdot 6H_2O$, PDPhA – DMFA - $Co(CH_3COO)_2$, PS – toluene - $C_{10}H_{14}CoO_4$, PVA - distilled water - $Co(NO_3)_2 \cdot 6H_2O$. The cellulose suspension in water was obtained after dissolving $Co(NO_3)_2 \cdot 6H_2O$. After common solution or suspension obtained the precursor was dried at 80 °C. IR pyrolysis was performed at temperatures of 250-700 °C in inert atmosphere. The cobalt content in the precursor was 20 wt. %.

Fischer-Tropsch synthesis was conducted in a fix bed reactor at a pressure of 2 MPa and a space velocity of 1000 h^{-1} (a molar ratio of CO: H_2 = 1: 2) in the temperature range 200-320 ºC. The temperature was increased by 20 °C step every 12 h. The gas and liquid samples were taken for analysis at the end of each isothermal mode.

Table 1. The influence of the polymer matrix nature on the basic indicators of the Fischer-Tropsch catalysts based on Co-CMNP (20 atm, 1CO+2H$_2$, liquid hourly space velocity 1000 h^{-1})

Sample	Temperature*, °C	Hydrocarbon yield, g m^{-3}		Liquid hydrocarbon productivity, g kg metal^{-1} ·h^{-1}	Liquid hydrocarbon selectivity, %
		Gaseous hydrocarbons	Liquid hydrocarbons		
Co-PVA	280	100.4	25.4	2084	20.2
Co-PDPhA	300	46.8	33.3	1744	41.6
Co-CE	300	76.6	38.7	279	33.6
Co-PS	300	36.2	18.9	137	34.3
Co-PAN	300	54.0	72.0	2600	57.0

- The temperature at which the maximum yield of liquid hydrocarbons is shown

The catalytic tests were carried out without pre-reduction stage. The initial synthesis gas and gaseous products of the synthesis were analyzed by a chromatograph "Kristallux-4000M" with two chromatographic columns. Helium was applied as a carrier gas and TCD as a detector. A column packed with CaA molecular sieve (3 mm × 3 m) was applied for CO and N$_2$ separation. Temperature mode – isothermal, 80 °C. A column packed Haye Sep R (3 m × 3 mm) was applied for CO$_2$ and C$_1$-C$_4$ hydrocarbon separation. Temperature mode - programmed, 80-200 °C, 8 °C min^{-1}.

The catalyst activity review was based on the following parameters: specific activity (CO moles reacted on 1 g of Co per 1 s), CO conversion (percentage ratio of reacted CO weight to the weight of CO logged into the reaction zone), the product yield (number of grams of product obtained by passing of synthesis gas through 1 m^3 of catalyst reduced to normal conditions), the selectivity (percentage ratio of carbon, taking participation in the formation of the reaction products, to the total amount of carbon introduced into the reaction zone), productivity (the amount of products produced by 1 kg of catalyst per 1 h).

The magnetic characteristics of the composites were measured with a vibration magnetometer.[8] Oxidation of the nanocomposites was carried out in an air stream in vibrating magnetometer cell at a programmed temperature rise of 0.42 °C s^{-1} speed.

X-ray diffraction analysis was performed at room temperature on a DIFREY-401 diffractometer (Russia) (Cr Kα radiation, Bragg–Brentano focusing).

Results and discussion

The most active catalysts for Fischer-Tropsch synthesis are cobalt systems characterized by high selectivity in hydrocarbon formation. In the presence of these systems the synthesis proceeds with a minimum amount of carbonaceous by-products such as CO$_2$ and monohydric alcohols.[9] The composite materials containing Co nanoparticles (Co-CMNP) were synthesized via IR pyrolysis of the precursor based on PAN and cobalt salt. The Co-CMNP catalytic activity dependence on the cobalt salt nature, preparation temperature and Fischer-Tropsch synthesis conditions was shown in the previous study.[10]

This paper describes the effect of the polymer nature used for Co-CMNP preparation on the catalyst activity in the Fischer-Tropsch process.

Every prepared sample showed activity in the synthesis of hydrocarbons from CO and H$_2$ (Fig. 1).
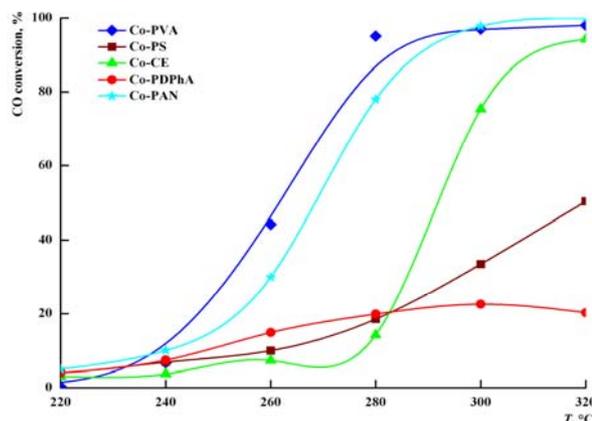
Figure 1. Temperature dependence of CO conversion of Co-CMNP.

The maximum activity was shown by the samples based on PVA and PAN. These samples CO conversion reached 100% at 300 °C. Also Co-CMNP based on CE showed high catalytic activity. CO conversion tended to 100% at 320 °C. However, this sample CO conversion was started to rise much later than the samples based on PVS or PAN. The drastic increase of the sample was observed only after 280 °C. This indicates that Co-CMNP based on CE has carbon matrix of structure differs from the structure of the carbon matrix formed during the pyrolysis of Co-PAN or Co-PVA. Therefore, adsorption of reagents (first catalytic action) on the surface of the active metal sites may occurs at higher temperatures than in the case of the samples based on Co-PVA or Co-PAN.

The influence of the polymer matrix nature on the basic indicators of the Fischer-Tropsch catalysts based on Co-CMNP is presented in Table 1.

Table 1 show that the synthesized samples with different support have not very high yield of liquid hydrocarbons in comparison with commercial catalysts (~ 100 g m^{-3}).

However, the productivity of Co-PAN, CoPDPhA and Co-PVA is extremely high and is ten times much as industrial catalyst productivity.

The Co-PVA sample showed a low yield (25.4 g m^{-3}) whereas its productivity was very high - 2084 g kg metal^{-1}·h^{-1}.

The similar indicators were achieved in the presence of Co-PDPhA. The yield of liquid hydrocarbons was 33.3 g m^{-3}, while the productivity reached 1744 g kg metal^{-1}·h^{-1}. It should be noted that the yield of gaseous hydrocarbons in the presence of the Co-PDPhA sample was two times lower than in the presence of the Co-PVA sample (46.8 g m^{-3} and 100.4 g m^{-3}, respectively). The highest yield of liquid hydrocarbons (72 g m^{-3}) and liquid hydrocarbon productivity (2600 g kg metal^{-1}·h^{-1}) were reached in the presence of Co-PAN.

The samples of Co-CE and Co-PS showed low yield of liquid hydrocarbons (38.73 g m^{-3} and 18.91 g m^{-3}, respectively) as well as the productivity of the catalysts (< 279 g kg metal^{-1}·h^{-1}).

It's important to note that the yield of the main by-product formed in the presence of cobalt catalysts - methane - depends on the nature of the polymer used (Fig. 2).
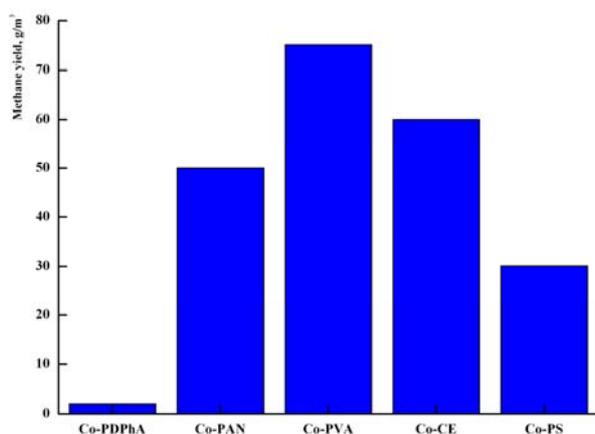

Figure 2. Methane yield in Fischer-Tropsh synthesis in the presence of Co-CMNP.

Co-PVA and Co-CE were characterized by the highest methane yield (~ 70 g m^{-3} and 60 g m^{-3}, respectively). The smallest selectivity of liquid hydrocarbons (Table 1) was observed in the presence of the same samples.

Methane yield was 50 g m^{-3} in the presence of Co-PAN catalyst and in the case of Co-PDPhA the methanation was almost completely suppressed. The same samples are characterized by the highest liquid hydrocarbon selectivity (57 % and 41.6 %, respectively) (Table 1). It indicates that the use of PDPhA or PAN as the polymer matrix allows to form different active sites for Co-CMNP.

Thus, in the case of Co-CMNP based on PAN some of the active sites responsible for hydrocarbon formation, are crystallites of metallic Co (so-called type A sites). These sites take part in dissociative adsorption of CO with generation of active surface carbon followed by its

hydrogenation led to the formation of methane.[9] As concerns Co-CMNP based on PDPhA bicomponent active sites consisted of metallic and oxide cobalt are mainly formed (so-called type B sites). These sites cause the growth of the hydrocarbon chain in the Fischer-Tropsch synthesis conditions.[11, 12] Probably, formation of different active sites caused by the formation of polyconjugated systems with different structure due to polymer nature. Thus, in the case of PAN polyconjugated polycyclic system is formed, as opposed to polyconjugated linear cyclic structures in PDPhA.

Magnetometric technique *in situ* was applied in order to explain the features of the synthesis gas conversion in the presence of Co-PDPhA, Co-PAN and Co-PVA which showed the highest liquid hydrocarbon productivity.
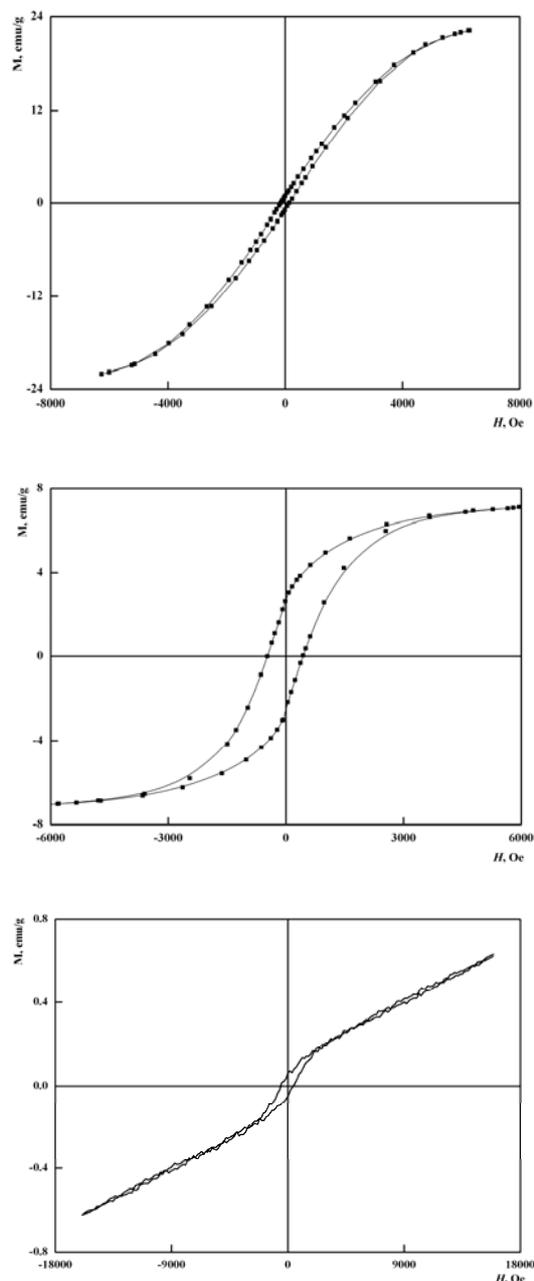

Figure 3. Field dependence of magnetization reversal of Co-PDPhA (*a*), Co-PAN (*b*) and Co-PVA (*c*) samples.

Field dependence of magnetization reversal of Co-PDPhA and Co-PAN samples showed hysteresis loop (Fig. 3a, b). This shape of the dependence is caused by the presence of ferromagnetic particles in the samples, i.e. cobalt crystallites with an oxidation degree equal to zero. Co-PAN sample hysteresis loop is characterized by a relatively high coercive force (Fig. 3b). This fact can be explained by the presence of particles with size of 15-20 nm in the sample. The hysteresis loop shape of Co-PVA sample (Fig. 3c) differs from the curves of Co-PDPhA and Co-PAN samples (Fig. 3a, b). The distorted hysteresis loop of Co-PVA sample indicates the dominance of the oxide paramagnetic phase of cobalt in the sample.

The synthesized composite samples were studied by the magnetometry method in situ. Fig. 3 shows that Co-PDPhA and Co-PAN samples contain metallic cobalt which forms the active sites of cobalt catalysts of Fischer-Tropsch synthesis. In Co-PVA sample cobalt has the oxide form and metallic cobalt is lack.

The degree of the metal reduction was determined via comparison of the magnetization value of bulk Co (1 mg) and the magnetization value of the studied. The metal reduction degree was approximately 90%, 64% and 1% for systems with Co-PDPhA, Co-PAN and Co-PVA, respectively. However, the fact that all three samples showed activity in the synthesis of hydrocarbons from CO and H_2 (Table 1), indicates that the sample Co-PVA was activated directly in the synthesis.

These conclusions were confirmed by XRD analysis.[10,13,14]. It was shown that metallic cobalt of α- (hexagonal) and β- (face-centered cubic) modifications and amorphous carbon phase were formed in the composite material based on PDPhA.[13,14] Reflection peaks relating to metallic cobalt of α- (hexagonal) and β- (face-centered cubic) modifications and carbon phase as a PAN pyrolysis product were presented in all diffraction patterns of Co-PAN.[10] Cobalt oxide phase reflection peaks were detected for Co-PAN samples.[10] The XRD pattern of Co-PVA sample is shown in Fig. 4.
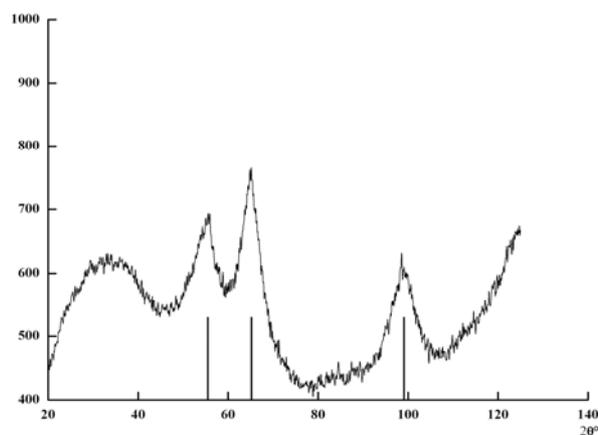
The XRD pattern of Co-PVA sample (Fig. 4) indicates that cobalt oxide phase (where Co^{2+}) prevails in the diffractogram. The width of the reflection peaks shows poor crystallinity which can be explained by small size of cobalt oxide particles caused by rapid particle formation under non-equilibrium conditions. Reflection peaks corresponding to metallic cobalt or its other oxides (e.g., Co_3O_4 or Co_2O_3) were not detected. Wide halo around 30° is associated with the amorphous carbon matrix.

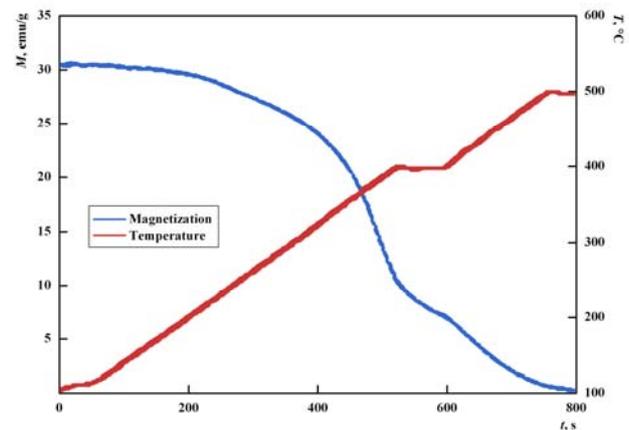**Figure 4.** The XRD pattern of Co-PVA sample. The straight lines show CoO phase.
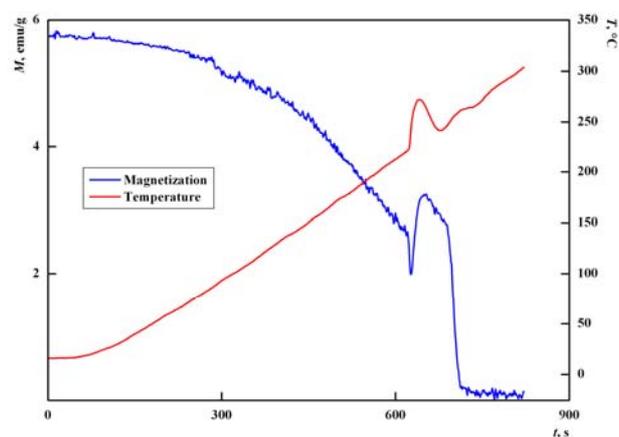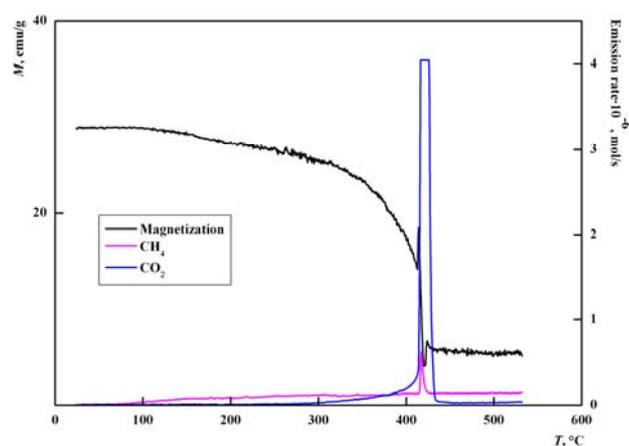
Figure 5. The TPO curves of Co-PDPhA, Co-PAN and Co-PVA samples.

Temperature programmed oxidation (TPO) curves of Co-PDPhA, Co-PAN Co-PVA samples are shown in Fig. 5. The data of Fig. 5a and 5b show that the oxidation of Co-PDPhA and Co-PAN samples occurs via similar scheme - after a "plateau" there is rapid drop of the magnetization indicating burnout of the polymer shell and oxidation of the metal particles. The magnetization rapid drop in Fig. 5 occurs simultaneously with a rapid CO_2 emission that additionally confirms the hypothesis of burnout carbon shell. Also, there is methane emission which may be associated with simultaneous oxidation and pyrolysis processes of the polymer leading to hydrogen and other gaseous products release at the temperature. Methane is formed on the metallic particles due to hydrogenation of oxidation and decomposition products. In Fig. 5a and 5b there is a jump in the magnetization, indicating cobalt reduction partly by oxidation products. At the same time calorification is observed, indicating exothermic process (oxidation of the matrix and cobalt). In the case of Co-PAN the magnetization decrease is observed at 150 °C, and for Co-PDPhA – at 320 °C. Such temperature difference indicates that the applying PDPhA as polymer matrix leads to "covering" active metal particles as described in.[13] It seems that such a dense shell prevents adsorption of synthesis gas on the active site surface. That is explains the low CO conversion for this catalyst.

There is no rapid drop of the magnetization in the whole investigated temperature range and no rapid calorification in the oxidation curve of Co-PVA sample (Fig. 5c). Burning of the polymer matrix occurs gradually in the case of the PVA.

Conclusions

Thus, the effect of the polymer matrix nature on Co-CMNP activity in the Fischer-Tropsch process was shown. The system based on polyconjugated cyclic structure formed during pyrolysis reaction of polymer exhibited the highest activity. Obviously, different matrix-nanoparticle systems are formed as various types of polymers are applied. In the case of PDPhA the composite formation and cobalt reduction is caused by hydrogen released during the condensation reaction of DPhA oligomer fragments. As a result of thermolysis the system with tightly encapsulated particles is formed. In the case of Co-PAN system the metal reduction occurs with the participation of hydrogen released in the dehydrogenation of the main polymer chain. The system with weakly encapsulated particles is formed. In the Co-PVS the metal reduction does not occur and forming cobalt oxide particles are encapsulated by thermalized polymer matrix.

In the case of PVS conjugation system formation occurs due to the side groups decoupling opposite to PAN where there is formation of conjugated cyclic structures during backbone substituents cyclization followed by carbonization.

Co and CoO phases presence in Co-PDPhA and Co-PAN samples were proved by XRD and *in situ* magnetometry. The phases are responsible for the active sites of different nature activity. In Co-PVA sample metallic cobalt was not found. However, the high catalytic activity of this sample indicates that its activation occurs in synthesis gas medium under reaction condition.

References

[1]Kozukov E. A., Krylova A. Yu., *Synthetic flammable gases and liquid fuels*, MosCow: MAI, **2008**.

[2]Slivinskij, E. V., Kliger, G. A., Kuz'min, A. E., Abramova, A. V., Kulikova, E. A., *Russ. Khim. Zhurn. (Zhurn. Russ. Khim. Ob-va im. D. I. Mendeleeva)*. **2003**, *47*, 6.

[3]Bezemer, G. L., Bitter, J. H., Kuipers, H., Oosterbeek, H., Holewijn, J. E., Xu X. D., Kapteijn F., van Dillen A. J., de Jong K. P., *J. Am. Chem. Soc.*, **2006**, *128*, 3956.

[4]Puntes V. F., Krishnan K. M., Alivisatos A. P., *Science*, **2001**, *291*, 2115

[5]Efimov, M. N., Dzidziguri, E. L., Sidorova, E. N., Chuprunov, K. O., Zemtsov, L. M., Karpacheva, G. P., *Russ. J. Phys. Chem. A.*, **2008**, *82*, 1175.

[6]Yongmin, L., Huamin, Zh., Baolian, Y., Zhiheng, Zh., Zhiheng, T., *Carbon*, **2005**, *43*, 3144.

[7]Ermilova, M. M., Karpacheva, G. P., Zemtsov, L. M., Orekhova, N. V., Efimov, M. N., Maksimov, A. M., Tereshchenko, G. F., Int. Sci. J. Altern. Energy Ecol., **2006**, *35(3)*, 53.

[8]Chernavskij, P. A., Pankina, G. V., Chebotarev, B. P., Kiselev, V. V., Lunin, V. V.*, RU 2 444 743 C2*

[9]Lapidus, A. L., Krylova, A. Yu., *Russ. Khim. Zhurn. (Zhurn. Russ. Khim. ob-va im. D. I. Mendeleeva)*. **2000,** *44*, 43

[10]Kulikova, M. V., Zemtsov, L. M., Sagitov, S. A., Efimov, M. N., Krylova, A. Yu., Karpacheva, G. P., Khadzhiev, S. N., *Solid Fuel Chem.*, **2014**. *48(2)*, 105.

[11]Minachev, Kh. M., Lapidus, A. L., Krylova, A. Yu., *Solid Fuel Chem.*, **1993**, *6*, 7.

[12]Lapidus A. L., *Bull. Acad. Sci. USSR, Div. Chem. Sci.*, **1991**, *40(12)*, 2335.

[13]Ozkan, S. Zh., Dzidziguri, E. L., Chernavskii, P. A., Karpacheva, G. P., Efimov, M. N., Bondarenko, G. N., *Nanotechnol. Russia*, **2013**, *8(7-8)*, 452.

[14]Dzidziguri, E. L., Sidorova, E. N., Bagdasarova, K. A., Zemtsov, L. M., Karpacheva, G. P., *Crystall. Reports.* **2008**, *53(2)*, 316.

DISTRIBUTION OF Co(II) IONS FROM AQUEOUS MEDIA INTO CHCl₃ SOLUTION OF N,N'-ETHYLENEBIS(4-PROPIONYL-2,4-DIHYDRO-5-METHYL-2-PHENYL-3H-PYRAZOL-3-ONE IMINE) (H₂PrEtP)

F. C. Nwadire[a], V. I. E. Ajiwe[a] and P. A. C. Okoye[a]

Liquid-liquid extraction of cobalt (II) ions have been carried out using 0.05 M solution of N,N'-ethylenebis (4-propionyl-2,4-dihydro-5-methyl-2-phenyl-3H-pyrazol-3-oneimine) (H₂PrEtP) Schiff base in chloroform. Various parameters for the extraction such as effect of pH, concentrations of the extractant, cobalt(II) ion , phase ratio and synergistic effect of 4-propionyl-2,4-dihydro-5-methyl-2-phenyl-3H-pyrazol-3-one (HPrP) have been investigated and optimized. Extraction with single ligand was observed to have a $pH_{1/2}$ of 7.05 with percentage extraction of 53.24 % corresponding to log$D$ value of 0.0563, and optimum pH of 9.25 with percentage extraction of 98.43 %, log$D$ value of 1.7971. The synergistic effect of HPrP on the extraction significantly lowered the $pH_{1/2}$ from pH 7.05 (near neutral) to pH 6.25 (slightly acidic) with percentage extraction of 52.60 % corresponding to log$D$ value of 0.0451. Optimum extraction of 99.30 was observed at pH 8.26 when the mixed ligands, H₂PrEtP and HPrP were used. The extraction of cobalt (II) ions increased rapidly as the concentrations of the ligands H₂PrEtP increased from 2.5×10^{-3} M to 4.0×10^{-2} M and that of HPrP from 2.5×10^{-3} M to to 2.5×10^{-2}. Variation of the metal concentration did not have much effect on the extractions, hence the percentage extraction was relatively high over all the metal concentrations studied.

*Corresponding Authors
    E-Mail: nwadirefc2014@yahoo.com; Vaj.04@yahoo.com; pacnau05@yahoo.com
    Tel.: +2348035509598
[a]   Department of Pure and Industrial Chemistry, Nnamdi Azikiwe University, P.M.B., 5025 Awka, Nigeria.

Introduction

The extraction of metal ions from aqueous media into chloroform solution of 1-phenyl-3-methyl-4-acylpyrazolone and its derivatives have been extensively reported.[1,2,3,4] Pyrazolones are prominent analytical reagents and potent drugs or pharmaceutical agents.[5,6,7] Presently the bis derivatives of these 4-acylpyrazolones, known as Schiff bases, are being used for the complexation of metal ions from aqueous media. Earlier studies on isolation and characterization of metal complexes of Schiff bases have shown that they form stable metal complexes with Cu(II) and Ni(II) and unstable complexes with Mo(VI), Co(II), Cd(II) and many other transition metals.[1,8] The new Schiff bases such as N,N'-ethylenebis(1-phenyl-3-methyl-4-acylpyrazoloneimine) and its derivatives, N,N'-ethylenebis(4-butanoyl-2,4-dihydro-5-methyl-3H-py-razol-3-oneimine) (H₂BuEtP), N,N'-ethylenebis(1-phenyl-3-methyl-4-acylpyrazoloneimine)-1,2-propane(H₂ADPP) and N,N'-ethylenebis(1-phenyl-3-methyl-4-propionylpyrazolo-neimine) (H₂PrEtP) have been successfully synthesized and characterized using ultraviolet, infrared, ¹H and ¹³C NMR spectroscopy.[9,11,12,13] The synthesis provides an opportunity for a N=C-C-OH bonding moiety and extends the scope of coordination to involve quadridentate ligands from initial bidentate 4-acylpyrazolone.[8,10,11,12,13]

In continuation of our work on the synthesis and characterization of 1-phenyl-3-methyl-4-acylpyrazolone-5 derivatives and their application in the extraction of transition metal ion such as Ni(II),[8] we report the use of the Schiff base N,N'-ethylenbis(4-propionyl-2,4-dihydro-5-methyl-2-phenyl-3H-pyrazol-3-oneimine) as a potential extractant for cobalt(II) ions.

In studying the solvent extraction of cobalt(II) ions from aqueous media using N,N'-ethylenbis(4-propionyl-2,4-dihydro-5-methyl-2-phenyl-3H-pyrazol-3-one imine) (H₂PrEtP) as an organic extractant the synergistic effect of 4-propionyl-2,4-dihydro-5-methyl-2-phenyl-3H-pyrazol-3-one (HPrP), effect of pH of buffered media, variation in phase ratio and concentrations of both ligands and cobalt(II) ions were studied and optimized.

Materials and Methods

All reagents were of analytical grade. H₂PrEtP (Schiff base) was synthesized by the method reported elsewhere.[9,11] The ligand's purity after recrystallization from aqueous ethanol was established by elemental analysis for C, H and N; analysis of IR and NMR spectral data at Institute for Inorganic Chemistry Technology, University of Dresden Germany.[9,11]

All other reagents were used as purchased from Aldrich and BDH.

Doubly distilled deionised water was used in all dilutions. Stock solution of 0.05 M H_2PrEtP was prepared by dissolving the required amount of the ligand in chloroform. 0.05 M solution of HPrP was similarly prepared in chloroform. Stock solution of 1.697×10^{-2} M of Co(II) was also prepared similarly by dissolving cobalt(II) chloride hexahydrate in 0.1 ml of 10 M HNO_3 and making up to mark in a 50 ml volumetric flask with deionized water. Buffer solutions of pH range 1 to 10 were prepared with; 0.1 M HCl/0.1 M NaCl (pH 1.0 to 2.9), 0.1 M CH_3COOH/0.1 M NaCl (pH 3.0 to 3.5), 0.1 M CH_3COOH/0.1 M CH_3COONa (pH 3.6 to 5.6), 0.1 M KH_2PO_4/0.1 M NaOH (pH 5.7 to 10.0). The pH of the buffered solutions were measured using a digital labtech pH meter.

Extraction procedure

A buffered solution (2 ml) containing 8.48×10^{-4} M of Co(II) ions at the required pH was prepared in a 10 ml extraction bottle. Equal volume (2 ml) of 0.05 M solution of H_2PrEtP in chloroform was added. For the mixed ligand extractions a mixture of 0.05 M H_2PrEtP and 0.05 M HPrP solution in chloroform was mixed in the ratio of 9:1 by volume. The mixture was mechanically agitated for 30 minutes at room temperature, 30 °C, to enable the attainment of equilibrium. The phase (aqueous and organic) were allowed to settle and separated with the aid of a micropipette. Concentration of Co(II) ions in the aqueous phase was determined with a Buck Scientific Atomic Absorption Spectrophotometer (AAS) at 240.7 nm. The concentration of Co(II) ion extracted into the organic phase was determined by the difference between the concentration of Co(II) ion in the aqueous phase before and after the extraction. The distribution ratio D can be expressed as c_{org}/c_{aq} where c_{org} and c_{aq} are the concentrations of cobalt(II) in the chloroform and the aqueous phase, respectively.

Results and Discussion

Effect of buffer solutions.

Distribution of Co(II) from aqueous phase into chloroform phase having the Schiff base H_2PrEtP can be represented by the Eqn. (1)

$$Co^{2+}{}_{(aq)} + H_2PrEtP_{(org)} \leftrightarrow Co(PrEtP)_{(org)} + 2H^+{}_{(org)} \quad (1)$$

The Eqn. (1) is based on the assumption that the Co(II) from aqueous phase is extracted into chloroform by the Schiff base by forming a complex with the Co(II) ion in the 1:1 mole ratio. Thus the extraction constant K_{ext} can be expressed by the Eqn. (2).

$$K_{ext} = \frac{\left[Co(PrEtP)_{(org)}\right]\left[H^+\right]^2}{\left[Co^{2+}{}_{(aq)}\right]\left[H_2PrEtP_{(org)}\right]} \quad (2)$$
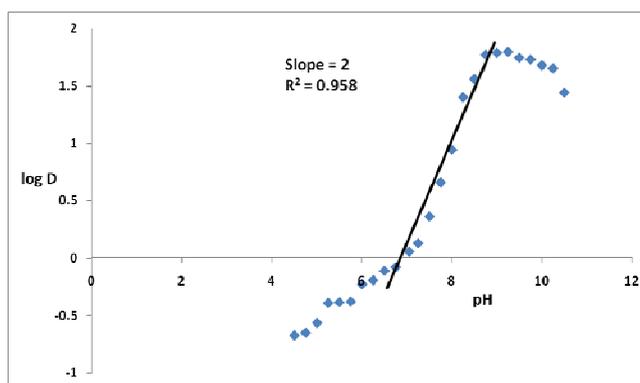

Figure 1. Graph of log D against pH for the extraction of 8.48×10^{-4} M Co(II) ions from buffered aqueous solution into chloroform solution of 0.05 M H_2PrEtP.

The plot in Fig. 1 shows the effect of pH of aqueous solution on the distribution of Co(II) into chloroform solution of H_2PrEtP and a slope of two was obtained from the graph indicated that 2 mole of hydrogen ions were displaced. This confirms that there were ligand–metal interaction through the oxygen atoms of the hydroxyl functional groups of ligand according to the Eqn. 1.

The distribution ratio of the metal ions between the two liquid phases becomes

$$D = \frac{\left[Co(PrEtP)_{(org)}\right]}{\left[Co^{2+}{}_{(aq)}\right]} \quad (3)$$

and substituting D into equation 2 after arrangement gives

$$\log D = \log K_{ext} + \log\left[H2PrEtP\right] + 2pH \quad (4)$$

The above mentioned result shows that the extraction of cobalt(II) ions into chloroform solution of H_2PrEtP increased with increase in pH of aqueous solution and reached a peak at pH 9.25 where an extraction of 98.43% was achieved. Thereafter, further increase in pH resulted into a decrease in percentage extraction of the metal. The partition coefficient, $\log D$ was determined statistically from the plot and found to be 1.78±0.02. The pH$_{1/2}$ was found to be 7.05. Statistical analysis of the data for all the extraction processes are recorded in Table 1, where pH*opt* and %E_{opt} means optimum pH and percentage extraction at optimum pH, respectively.

Effect of addition of HPrP (synergist) on the distribution of Co(II).
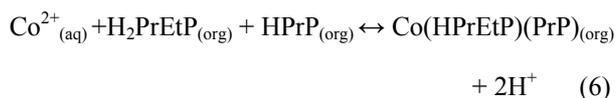
On addition of HPrP, quantitative extraction of 99.30 % was obtained at pH 8.26. The pH$_{1/2}$ was significantly lowered from pH 7.05 (near neutral) to a slightly acidic pH of 6.25.

Table 1. Analysis of extraction data for the effect of pH of aqueous phase on the distribution of 8.48×10^{-4} M of Co(II) into 0.05M chloroform solution of H_2PrEtP.

Organic phase	pH$_{1/2}$	% E at pH$_{1/2}$	pH$_{opt}$	% E at optimal pH	Log D	LogK$_{ex}$	Species extracted
0.05 M H$_2$PrEtP	7.05	53.24 %	9.25	98.43 %	1.78±0.02	-14.12±0.4	Co(PrEtP)
9:1, 0.05 M H$_2$PrEtP and 0.05 M HPrP	6.25	52.60	8.26	99.30	2.06±0.10	-11.8±0.33	Co(HPrEtP)(PrP)
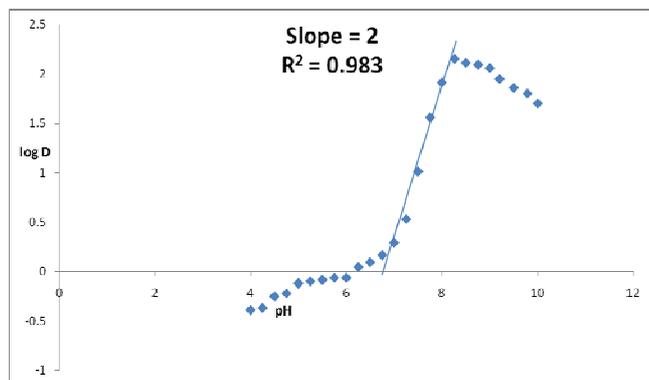
Figure 2. Graph of LogD against pH for the extraction of 8.48×10^{-4} M Co(II) ions from buffered aqueous solution into chloroform solution of 0.05 M 9:1 H$_2$PrEtP and HPrP

Figure 3. Plot of LogD against Log [Co(II)] for the extraction of Co(II) from buffer solution into chloroform solution of 0.05 M H$_2$PrEtP.

The partition coefficient was found to be 2.06 ± 0.10 and was determined statistically from the plot shown in Fig. 2. Plot of Log*D* against pH in the mixed ligands system in Fig. 2 gave a slope of 2 indicating that 2 moles of hydrogen ions were displaced during the extraction process thus the possible reaction equation for the extraction may be written as:
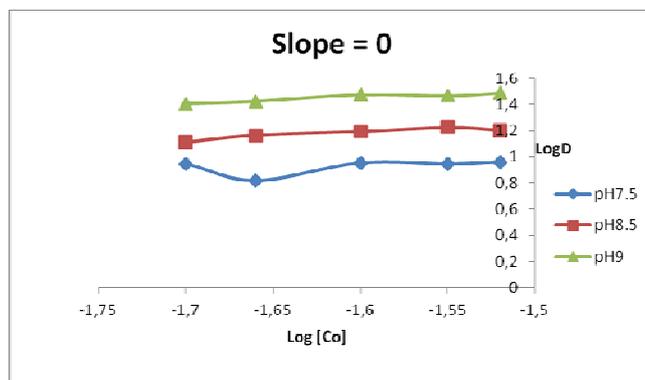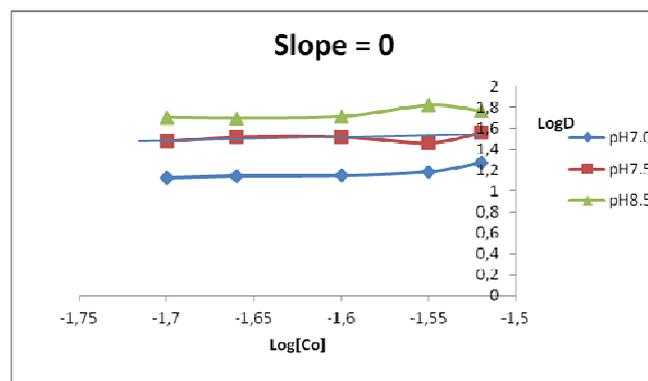
$$Co^{2+}_{(aq)} + H_2PrEtP_{(org)} + HPrP_{(org)} \leftrightarrow Co(HPrEtP)(PrP)_{(org)}$$
$$+ 2H^+ \quad (6)$$

Hence,

$$K\text{ext} = \frac{\left[Co(HPrEtP)(PrP)_{(org)} \right]\left[H^+ \right]^2}{\left[Co^{2+}_{(aq)} \right]\left[H_2PrEtP_{(org)} \right]\left[HPrP_{(org)} \right]} \quad (7)$$

Statistical analysis of the data for all the extraction processes is recorded in Table 1.

Effects of metal ions (Co^{2+}) concentrations.

Variation of the metal ion concentration did not have much effect on the distribution pattern of the cobalt into chloroform solution of H$_2$PrEtP. Very high percentage extractions were achieved at all concentrations of the metal ions, studied both in the presence and absence of (synergist) HPrP, as shown in Fig. 3 and Fig. 4.

Figure 4. Plot of LogD against Log [Co(II)] for the extraction of Co(II) from buffer solution into chloroform solution of 0.05 M H$_2$PrEtP and 0.05 M HPrP in 9:1 ratio.

Extraction plots for the variation of metal concentrations gave a zero slope indicating that the extraction is independent of the concentrations of the metal ions. Data obtained from the extraction processes shows that Co^{2+} distributes better into chloroform solution of H$_2$PrEtP in the presence of HPrP as synergist at pH 7.0, 7.5 and 8.5. In absence of the synergist, the maximum extraction of Co^{2+} ions occurred at 3.0×10^{-2} M Co(II) concentration at pH 9.0 where an extraction of 96.85 % was obtained. The least percentage extraction was observed at metal concentration of 2.2×10^{-2} M, pH 7.5 which gave a % E of 86.85 %. In the presence of HPrP as synergist the maximum extraction was achieved at 2.8×10^{-2} M metal ion concentration and pH 8.5 corresponding to 98.52 % extraction.

Effect of ligand (H₂PrEtP) and synergist (HPrP) concentrations.

All extraction processes studied showed that the extraction of Co^{2+} into chloroform solution of H₂PrEtP and HPrP increases as the ligands concentrations increased. The extractions follow similar trends on variation of the concentrations of the ligand either in the presence or absence of synergist as shown in Figs. 5, 6 and 7.
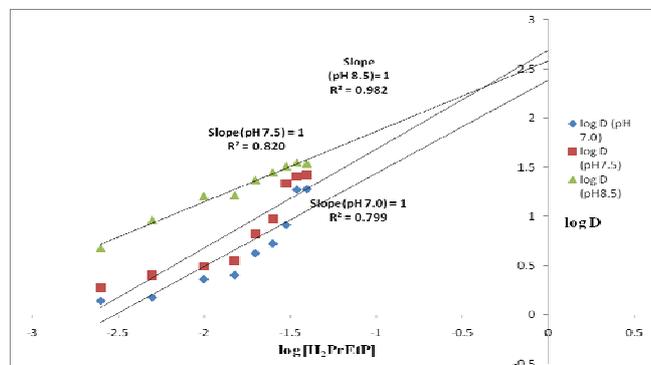

Figure 5. Plot of logD against log[H₂PrEtP] for the extraction of 8.48×10^{-4} M of Co(II) from aqueous solutions into chloroform solution of H₂PrEtP with HPrP kept constant.

Figure 6. Plot of logD against log[HPrP] for the extraction of 8.48×10^{-4} M of Co(II) from aqueous solutions into chloroform solution of H₂PrEtP with H₂PrEtP kept constant.
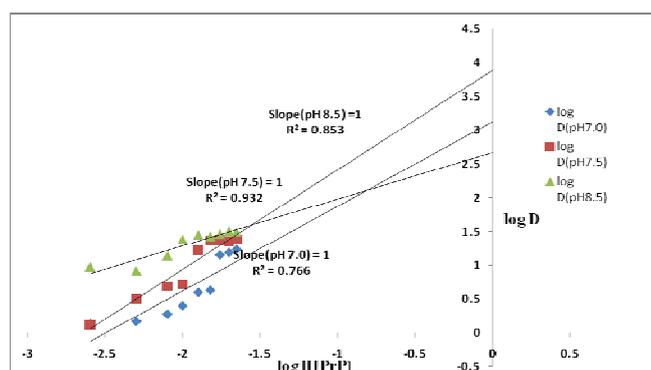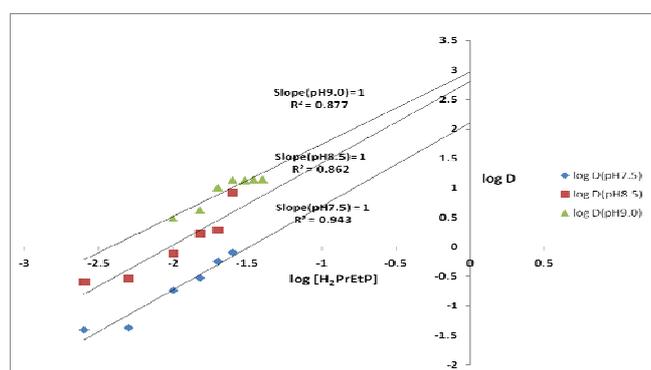

Figure 7. Plot of logD against log [H₂PrEtP] for the extraction of 8.48×10^{-4} M of Co(II) from aqueous solutions into chloroform solution of H₂PrEtP in the absence of synergist at constant pH of 7.5, 8.5 and 9.0.

Based on the results presented in Figures 5, 6 and 7, the conclusion is that the extraction of Co(II) ions is dependent on both pH of the aqueous medium and the concentration of the ligand. The studied ligand gives a better extraction of cobalt in a moderately alkaline pH.

Conclusion

On studying the distribution of Co(II) in buffered aqueous medium with a chloroform solution of H₂PrEtP alone a $pH_{1/2}$ of 7.05 was observed. The synergistic effect HPrP shifted the $pH_{1/2}$ from 7.05 (near neutral) to 6.25 (slightly acidic). The partition coefficients were; H₂PrEtP alone D_1 1.78±0.02 and H₂PrEtP/HPrP mixture D_2 2.06±0.10, indicating that there is a slight difference in the distribution of Co(II) ions into chloroform solution of H₂PrEtP as Co(PrEtP)$_{(org)}$ and into mixture of H₂PrEtP/HPrP as Co(HPrEtP)(PrP)$_{(org)}$. The extraction constant $K_{ext}Co_1$ for H₂PrEtP is -14.12±0.40 and is less than $K_{ext}Co_2$ -11.8±0.33 for H₂PrEtP/HPrP. Hence Co^{2+} distributes better into the mixed ligand system from the buffered media. From all the observation, we concluded that the extraction of Co(II) ions in buffered media with H₂PrEtP or its mixture with HPrP is more efficient in slightly alkaline medium.

Acknowledgement

References

[1]Chukwu U. J. and Godwin J., *Am. Chem. Sci. J.*, **2013**, *3*(4), 479-488.

[2]Okafor, E. C. and Uzoukwu, B. A., *Radiochim. Acta*, **1990,** *51*, 167-172.

[3]Kalagbor, A. L., Uzoukwu, B. A. and Chukwu, U. J., *Nat. Sci.*, **2011**, *9*(3), 37-42.

[4]Uzoukwu, B. A. and Mbonu J. I., *Solvent. Extr. Ion Exch.,* **2005**, *23*, 750.

[5]Onyedika G., Arinze J. and Ogwuegbu M., *J. Min. Mater. Charact. Eng.*, **2013**, *1,* 90-94.

[6]Flett, D.S. and West, D.S. *M.J Jones, Ed., Complex metallurgy 78, London,* **1975**, 49-57.

[7]Devi, N.B., Nathsaram, K.C. and Chakravortly, V. *Hydrometallurgy*, **1988**, *49*(2), 49-61.

[8]Godwin, J., Nwadire, F.C. and Uzoukwu, B. A., *Eur. Chem. Bull.,* **2012**, *1*(7), 269-273.

[9]Uzoukwu, B.A., Gloe, K. and Duddeck, H., *Synth. React. Inorg. Met. Chem.*, **1998**, *28*(5), 819-831.

[10]Amarasekara, A. S, Owereh, O. S., Lyssenko, K. A. and Timofeeva, T.V., *J. Struct. Chem.*, **2009**, *50*(6), 1159.

[11]Uzoukwu, B. A, Gloe, K. and Duddeck, H., *Indian J. Chem.*, **1998**, *37B*, 1180-1183.

[12]Godwin , J. and Uzoukwu, B. A., *Int. J. Chem.,* **2012**, *4*(4), 105.

[13]Godwin, J and Uzoukwu, B. A., Int. Org. Sci. Res.-J. Appl. Chem., **2012**, *1*(3), 14.

SAMARIUM(III) REMOVAL BY LIQUID–LIQUID AND SOLID-PHASE EXTRACTION. KINETICS AND THERMODYNAMICS ASPECTS

Afaf Amara-Rekkab,[a] Mohamed Amine Didi,[a]* and Didier Villemin[b]

The liquid–liquid and liquid-solid extractions of samarium(III) from aqueous nitrate solution using D2EHPA (di-2-ethylhexyl phosphoric acid) and chelating resin "Chelex 100" as extractants is investigated to recover samarium(III) from aqueous solution. The effect of operating parameters, such as time, nitrate ion, aqueous phase acidity, concentration of the extractant, resin mass, ion strength, temperature on the samarium extraction and various acid solutions on the metal stripping from the loaded organic phase and resin are investigated. The synergistic effect showed that addition of D2EHPA to TOP (Tri-iso-octyl-phosphate) extraction was obtained for the volume ratio 4.5/0.5. The thermodynamic functions like free energy (ΔG), enthalpy (ΔH) and entropy (ΔS) of extraction mechanism are discussed. Solid phase extraction is found to be more suitable than the liquid–liquid extraction for samarium(III) recovery. By liquid-liquid extraction the removed quantity was 93.26 mg g^{-1}; for the liquid-solid extraction by Chelex 100 resin the removed quantity was 19 mg g^{-1}. The stripping efficiency was found to be quantitative in HNO$_3$ and HCl 1 M. The robustness of the procedure is demonstrated by the average recoveries obtained (>99.6 %) for samarium(III).

* Corresponding Authors
Fax: +21343213198
E-Mail: madidi13@yahoo.fr; ma_didi@mail-univ.tlemcen.dz

[a] Laboratory of Separation and Purification Technologies, Department of Chemistry- Faculty of Sciences, Box119., University of Tlemcen -13000, Algeria.

[b] Laboratoire de Chimie Moléculaire et Thioorganique, ENSICAEN, UMR CNRS 6507, INC3M, FR 3038, Labex EMC3, 14050 Caen, France.

Introduction

The recovery of heavy metals by removal from dilute aqueous system has required the development of new technique for their concentration and separation.[1] In recent years, rare earth elements (REE) have been regarded as vitally important components from an industrial point of view. The major reason for this is the high application of the REE in many fields as these elements and their compounds find various commercial applications. Samarium is primarily used in the production of samarium-cobalt permanent magnets, which are used in lightweight electronic equipments where the size or space is a limiting factor, and where function at high temperature is of a great concern. Stable samarium titanate compounds with useful dielectric properties are suitable for coatings and in capacitors of microwave frequencies. The specific applications of samarium in different fields of technology have turned samarium into an industrial material of outstanding significance.[2]

Intricately similar in their chemical properties, lanthanides pose an exigent problem in their separation. Therefore, separation of trivalent lanthanides is still a very important and serious problem. Among the different methods used for this purpose, solvent extraction and solid phase extraction are the most popular and versatile techniques.[3]

This paper describes the extraction of samarium(III) by liquid-liquid and liquid–solid using D2EHPA (di(2-ethylhexyl)phosphoric acid) diluted with dichloromethane and resin Chelex 100 as extracting agent.

Solvent extraction is widely applied to processes of metal ions recovery, ranging from aqueous solutions in hydrometallurgical treatment to environmental applications. It is also considered a useful technique to increase the initial concentration of the solute, commonly used in the separation processes of analytical applications.[4] Di-2-ethylhexyl-phosphoric acid (D2EHPA) is extensively used as an extractant for the extraction of Sm(III) from aqueous solutions.[2] Other applications of this popular extractant include the removal of Zn(II)[5], Mn(II)[6], Fe(III).[7]

Chelex-100, used in this work, is a polystyrene divinylbenzene copolymer incorporating iminodiacetate chelating groups. The iminodiacetate groups coordinate metals by means of oxygen and nitrogen bonds and the resins have a particularly strong affinity for trace metals. Its use was first proposed for the preconcentration of total trace metals from seawater. Chelex-100 retains free metal ions and loosely bound trace metals.[8] It has been used in numerous studies for the binding of several metals including Cr (III), Ni (II), Cu (II), Zn(II), Tl (III) and La (III).[9-14]

The objective of this study is to investigate the best conditions for samarium(III) extraction by D2EHPA and Chelex 100 by varying diverse parameters as shaking time, the initial samarium(III) ion concentration, initial pH of aqueous solution, ion strength and the temperature. The extraction mechanism is also investigated and the processes of liquid-liquid extraction or liquid-solid Extraction are compared.

Materials and methods

Chemicals and reagents

Samarium(III) nitrate hexahydrate is procured from Sigma (ALDRICH), Hydrochloric acid, used for adjusting pH of samarium(III) solutions, is from Stinnes chemicals, sodium thiosulfate (Sigma Aldrich). Tri-iso-octyl-phosphate (Alfa Aesar), tri-butyl-phosphate (Sigma Aldrich) and di (2-ethylhexyl) phosphate (Sigma Aldrich) were dissolved in dichloromethane (Sigma Aldrich) to achieve the required concentration. All other reagents such as buffer at pH = 4.0 (VWR Prolabo) and Arsenazo III (Alfa Caesar) were used for the analysis of the results by UV-Visible spectrometer (SPECORD 210 plus).

Chelex-100 (Bio-Rad Laboratories, CA, USA) is a chelating resin which uses ion exchange to bind transition metal ions. The resin is composed of polystyrene divinylbenzene copolymers containing paired imino-diacetate ions, which act as chelators for polyvalent metal ions (see Table 1).[10] This group can interact via its nitrogen and oxygen atoms with the samarium according a tridentate interaction.

Table 1. General description and some properties of resin

Type	Chelex 100
Ionic form	Na$^+$
Functional group	Iminodiacetic acid
Matrix	Polystyrene-divinylbenzene
Structure	Macroporous
pH range	0–14
Bead size	0.3-1.0 mm
Capacity	0.4 mmol mL^{-1}
Appearance	White, translucent

Liquid-liquid and liquid-solid extractions and determination procedure for samarium(III)

General extraction and stripping experiments were carried out by contacting equal volumes (5 mL) of the aqueous (samarium(III) at 1 mmol L^{-1}) and organic phases (D2EHPA at 2 mmol L^{-1}) ($V_{Aq.}/ V_{Org.} = 1$) in reagent bottles. After equilibrium between two phases is established, the phases were separated by decantation.

The recovery of Sm(III) onto Chelex 100 resin was studied. An exactly weighted amount (0.1 g) of Chelex 100 in Na$^+$ form was mixed with 5 mL of (Sm(NO$_3$)$_3$.6H$_2$O) solution at 1 mmol L^{-1} initial concentration.

The removal of Sm(III) onto Chelex 100 resin in three different extractants D2EHPA, TBP and TOP was investigated as a function of contact time between 2 and 15 minutes at initial concentration of samarium(III) = 1 mmol L^{-1}. The effect of solution pH on the equilibrium uptake of samarium(III) from aqueous solution by D2EHPA and Chelex 100 resin was investigated between initial pH 1.3 and 5.05. Dilute nitric acid was used to adjust the pH of samarium solutions using a pH meter (model WTW, pH 3310 SET 2).

Kinetic experiments were carried out by agitating 5 mL of samarium(III) solution of concentration ranging from 0.2 to 5.0 mmol L^{-1} with 0.1 g of Chelex 100 resin and 5 mL of D2EHPA respectively in an Erlenmeyer flasks of 10 mL at 20 ± 1 °C, pH = 5.05 and at a constant agitation speed of 1000 rpm.

The effect of the ionic strength was studied with 5 mL of samarium(III) solution (1 mmol L^{-1})and varying concentration of sodium thiosulfate from 0.1 to 0.4 mol L^{-1}. Under constant pH and constant concentrations of Chelex 100 resin and D2EHPA, samarium(III) extraction was enhanced by varying temperature in the range of 298–328 K. The concentration of Sm(III) in the aqueous phase was analyzed with a SPECORD 210 plus spectrophotometer using the method described in the literature.[15]

All procedures of the extraction liquid-liquid and liquid-solid were carried out at room temperature 298 K and stirring rate at 1000 rpm. In these experiments percentage extraction (%E) was determined as follows:

$$\%E = 100 \, \frac{C_0 - C}{C_0} \qquad (1)$$

where C_0 and C are the concentrations (mol L^{-1}) of samarium ions before and after extraction, respectively.

Results and discussion

Effect of contact time

The kinetic of extraction that describes the solute uptake rate governing the residence time of the sorption reaction is one of the important characteristics that define the efficiency of sorption.

In order to establish equilibrium time for maximum uptake and to know the kinetics of extraction process; the sorption of Sm(III) for initial concentrations 1 mmol L^{-1} by Chelex 100 resin in three different extractants D2EHPA, TBP and TOP is shown in Figure 1.
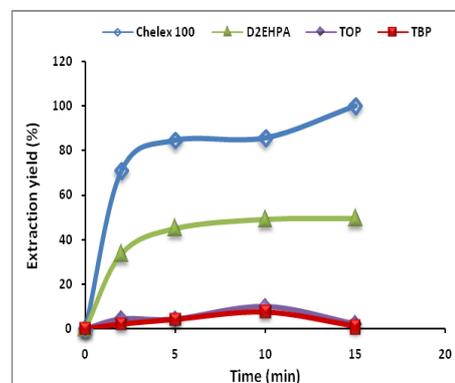

Figure 1. Effect of contact time on the ion exchange of Sm(III) using Chelex 100 resin, D2EHPA, TBP and TOP. Initial concentration of Sm(III) 1 mmol L^{-1}, T = 20 ± 1 °C, stirring speed 1000 rpm and initial pH 5.05.

The results in Figure 1 suggest that the maximum extraction is achieved in Chelex 100. The curve suggests that the % extraction increases after 10 minutes reaching the highest value in 15 min. The next better extractant is D2EHPA. It is to be noted that in this case the maximum extraction is obtained in the first 10 minutes which rises slowly to reach the maximum in 15 min. The extraction in TOP and TBP is almost parallel reaching maximum at 10 min beyond which the extraction touches minimum at 15 min.

The amount of Sm(III) adsorbed onto Chelex 100 increased with increase in contact time, the maximum percentage of Sm(III) extraction was 85.67 % at 10 min for initial concentration of Sm(III) 1 mmol L^{-1} which is used as a suitable contact time for samarium(III) adsorption. Thereafter, attained equilibrium at 15 min. This is apparent from the fact that the Chelex 100 has a large number of vacant surface sites available for adsorption during the stage of extraction of samarium(III).

Also, Fig. 1 shows the effect of time on the extraction of samarium(III) by D2EHPA, TBP and TOP. It is observed that 15 min is the maximum of sorption of samarium corresponding to 49.53 % was obtained by D2EHPA. However, the maximum percent Sm(III) extraction were 9.86 and 7.7 % obtained at 10 min by TOP and TBP respectively, Thereafter, becomes slower.

Effect of samarium concentration

Several experiments were made to study the effect of the initial samarium concentration on its percent removal. The initial Sm(III) concentrations tested were 0.2, 0.6, 0.8, 1, 2 and 5 mmol L^{-1} at an amount of adsorbent of 0.1 g of Chelex 100 and at an initial D2EHPA concentration 2 mmol L^{-1}.
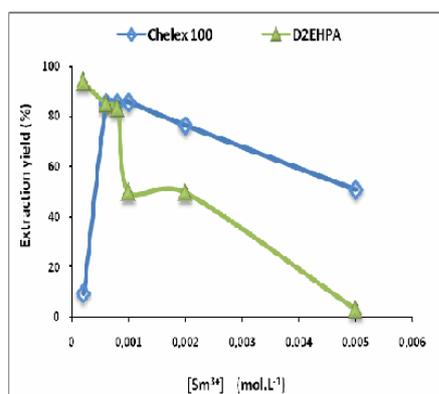

Figure 2. Effect of initial concentration of Sm(III) sorption using Chelex 100 resin and D2EHPA. $T = 20 \pm 1$°C, stirring speed 1000 rpm and initial pH 5.05, contact time 10 min for Chelex 100 and 15 min for D2EHPA.

The results shown in Fig. 2 indicate that the removal of the samarium(III) is optimum at the low concentration beyond which the % removal diminishes continuously and it becomes almost zero in case of D2EHPA at 0.005 M samarium (III). removal is initial samarium concentration dependent and the necessary initial samarium concentration

to reach quantitative sorption is in the range of 0.6 to 1 mmol L^{-1} and at 0.2 mmol L^{-1} for removal of samarium by Chelex 100 resin and D2EHPA, respectively.

Effect of initial pH

In the adsorption the solution pH plays an important role for controlling the high sorption capacity and selectivity of the target lanthanide ions.[16-18] This is partly because hydrogen ions themselves compete strongly with adsorbents.[19]

To determine the optimum pH for the adsorption of Sm(III) ions onto Chelex 100 resin and D2EHPA, the percentage removal of Sm(III) ion as a function of hydrogen ion concentration was examined at an initial concentration of samarium = 1 mmol L^{-1}.
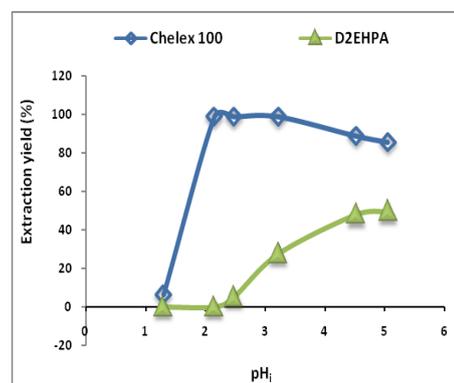

Figure 3. Effect of initial pH for efficient extraction of samarium ion by Chelex 100 resin and D2EHPA. $T = 20 \pm 1$°C, stirring speed 1000 rpm, contact time 10 min for Chelex 100 and 15 min for D2EHPA.

The results shown in Figure 3 suggests that the sorption is strongly pH-dependent. For Chelex 100 the equilibrium sorption capacity is minimum at pH 1.3 (6.35 %) and increases with the pH reaching the maximum value between pH 2.15-3.22 (99 %). It then decrease thereafter. The corresponding sorption in D2EHPA, however, continuously increased with increasing pH acquiring a maximum value around pH 5.

The nature of the functional groups of the resin at different pH are shown in Figure 4. The functional groups shown under (a) predominate at pH$_i$ between pH 2.15- 3.22.

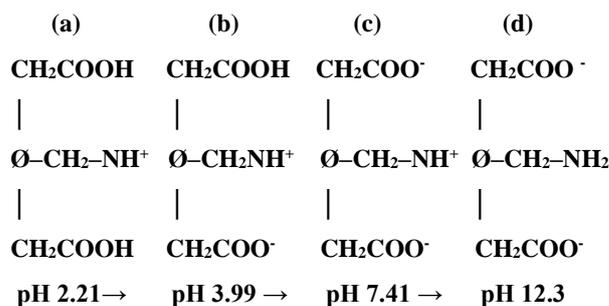| (a)	(b)	(c)	(d)
CH$_2$COOH	CH$_2$COOH	CH$_2$COO$^-$	CH$_2$COO$^-$
|	|	|	|
Ø–CH$_2$–NH$^+$	Ø–CH$_2$NH$^+$	Ø–CH$_2$–NH$^+$	Ø–CH$_2$–NH$_2$
|	|	|	|
CH$_2$COOH	CH$_2$COO$^-$	CH$_2$COO$^-$	CH$_2$COO$^-$
pH 2.21→	pH 3.99 →	pH 7.41 →	pH 12.3

Figure 4. Different forms of the resin Chelex 100 depending on the pH.

The sorption capacity of D2EHPA to remove Sm(III) is lowest at lower pH conditions because hydrogen ions occupy most of sites on the surface of D2EHPA. However, with increasing pH of the solution, the competition by hydrogen ions is weakened because of the low hydrogen ion concentration and therefore Sm(III) ions occupy the sites more easily that results in the higher rate of removal of Sm(III) ions. The optimum pH for the maximum percentage (49.5 %) removal of Sm(III) in presence of D2EHPA is found to be pH 5.05.

Effect of ionic strength

The effect of ionic strength on samarium(III) sorption was studied by stirring Chelex 100 resin and D2EHPA with increasing $Na_2S_2O_3$ concentration in the aqueous solutions from 0.1 to 0.5 mol L^{-1}.

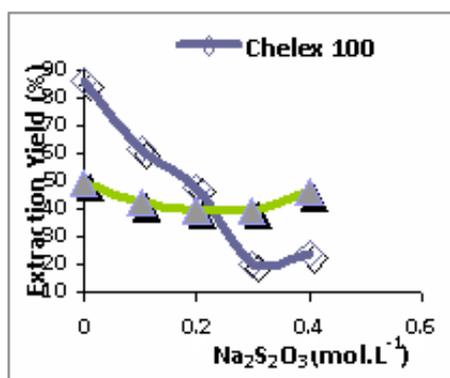**Figure 5.** Effect of $Na_2S_2O_3$ concentration on the extraction yield. Initial concentration of samarium(III) 1 mmol L^{-1}, T = 20 ± 1°C, stirring speed 1000 rpm, initial pH = 5.05, contact time 10 min and 15 min for Chelex 100 and D2EHPA respectively.

Results, summarized in Fig. 5, show that the sorption of samarium by Chelex 100 is greatly influenced by the ionic strength whereas the ionic strength does not appreciably influences the sorption in the presence of of D2EHPA. It is evident in Fig. 5, that there is a negative and null impact on increasing of extraction yield of Sm(III) by Chelex 100 and D2EHPA at concentration of $Na_2S_2O_3$ from 0.1 to 0.5 mol L^{-1}, respectively.

Elution

Desorption of adsorbed samarium ions from Chelex 100 was evaluated by distilled water, HNO₃ and HCl acid treatment. 5 mL of HNO₃ and HCl solution at (0.5 – 1 – 2 M) concentrations were added at 0.1g of saturated resin on Samarium(III) respectively; the mixture was stirred for 1 h. After this time, the two phases were separated, then the samarium(III) present in the aqueous phase was determined by UV-Visible.

The extraction yield of elution was determined by the equation:

$$Yield(\%) = 100 \frac{absorption\ of\ the\ aq.\ phase\ after\ elution}{absorption\ of\ the\ initial\ treated\ solution} \quad (2)$$

Good regeneration properties of the adsorbent and reversibility of the adsorption process was obtained (Fig. 6). From these results it can be concluded that the Chelex 100 can be used repeatedly for the removal of samarium ions from aqueous solution.
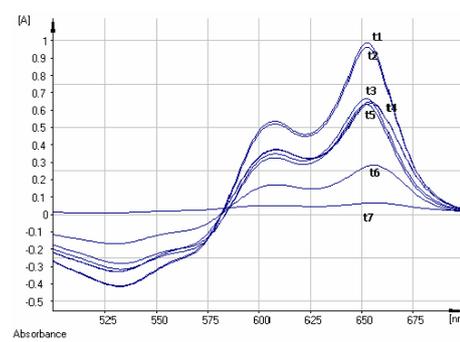

Figure 6. Evolution of the absorbance on the desorption of Sm(III) at different time (t_1=5 min, t_2= 10 min, t₃=15 min, t_4=20 min, t_5=30 min, t_6=45 min and t_7=60 min).
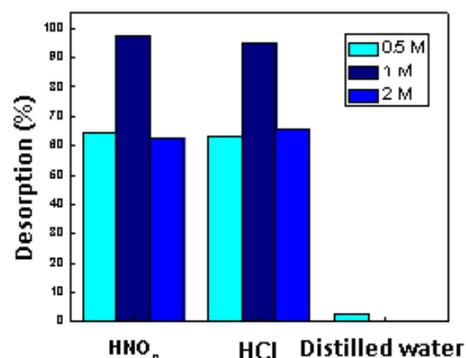

Figure 7. Effect of the eluent concentration on the desorption; V=5 mL ; t = 60 min ; m= 0.1 g.

The Fig. 7 shows that a solution of HCl or HNO₃ (1.0 M) is sufficient for the elution of more than 95 % of Sm(III) retained on the Chelex 100 resin. The ratio between the aqueous volume (acid solution) and the mass of the saturated resin is taken equal to 50 g mL^{-1}; and that the desorption of the Sm^{3+} ions was insignificant (2.5 %) during the use of the distilled water without acid.

Thermodynamic studies

Thermodynamic parameters, such as the Gibbs energy ($\Delta G°$), enthalpy ($\Delta H°$), and entropy ($\Delta S°$) changes are determined by using the following equations:

$$K_d = \frac{q_e}{C_e} \quad (3)$$

where

q_e (mg g^{-1}) was the adsorption capacity at equilibrium time and

C_e was the concentration capacity at equilibrium time.

Table 2. Gibbs free energy, enthalpy and entropy changes for Sm(III) sorption on Chelex 100 and D2EHPA.

Resin	$\Delta H°$ kJ mol^{-1}	$\Delta S°$ J K^{-1}·mol^{-1}	$\Delta G°$ (kJ mol^{-1})			
			313 K	318 K	323 K	328 K
Chelex 100	-40.6	-106.17	-7.37	-6.84	-6.31	-5.78
D2EHPA	-15.0	-52.2	+1.07	+1.33	+1.6	+2.12

$$\Delta G^0 = -RT \ln K_d \qquad (4)$$

$$\ln K_d = \frac{\Delta S^0}{R} - \frac{\Delta H^0}{RT} \qquad (5)$$

where

R (8.3145 Jmol^{-1} K^{-1}) is the ideal gas constant,

T (K) is the absolute temperature and

K_d is the thermodynamic equilibrium constant.

The values of changes of enthalpy (ΔH^0) and entropy (ΔS^0) are calculated from the slopes and intercepts of the plot of ln K_d vs. $1/T$ by using Eq. (5).[2]
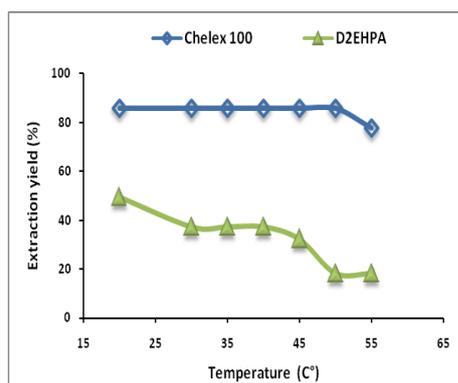

Figure 8. Effect of temperature on extraction of samarium(III). Initial concentration of samarium(III) 1 mmol L^{-1}, T= 20±1°C, stirring time 1000 rpm, initial pH=5.05, contact time 10 min for Chelex 100 and 15 min for D2EHPA.

The relative parameters and correlation coefficient calculated from Eqs. 2–4 are listed in Table 2. The negative ΔG^0 values show that, the sorption of ions of samarium by Chelex 100 occurs spontaneously in 298–328 K, while it is not spontaneous in case of D2EHPA system as indicated by the positive sign of ΔG^0.

The enthalpy of the sorption, ΔH^0, is a measure of the energy barrier that must be overcome by reacting molecules.[16] The value of $\Delta H°$ for sorption of Sm^{3+} by Chelex 100 and D2EHPA is negative, indicating that the extraction procedure of samarium is exothermic in nature. The negative value of entropy for two extractants indicates the formation of a stable complex which makes the extraction system more ordered resulting in the decrease of entropy value.

Conclusions

Sorption of samarium(III) by the Chelex 100 resin and D2EHPA were performed. The methods were optimized using various parameters such as contact time, the initial samarium(III) ion concentration, initial pH of aqueous solution, ion strength and the temperature.

The maximum sorption of samarium(III) by Chelex 100 took place in the initial pH 2.15 to 3.22 and the initial concentration of metal 1 mmol L^{-1} with a equilibrium time equal to 10 min.

D2EHPA is shown to be a good and stable extractant. It is more selective for recovery of Sm^{3+} from aqueous media. It should be noted that at pH 5.05, maximum extraction efficiency is obtained with 2 mmol L^{-1} D2EHPA in kerosene at initial concentration of Sm^{3+} 1 mmol L^{-1}. D2EHPA extracts Sm^{3+} very rapidly. Equilibrium was reached within 15 min.

Thermodynamic functions of extraction reaction were calculated and discussed. The reaction of extracting samarium(III) was found to be spontaneous by Chelex 100 resin and not spontaneous by D2EHPA extractant.

Acknowledgements

References

[1]Oliveira, R. C., Jouannin, C., Guiba, E., Garcia, Jr. O., *Proc. Biochem.,* **2011,** *46,* 736.

[2]Wang, X., Du, M., Liu, H., *Sep. Purif. Technol.,***2012,** *93,* 48.

[3]Mandhare, A. M., Han, S. H., Anuse M. A., Kolekar. S. S. *Arabian J. Chem.,* **2011,** http://dx.doi.org/10.1016/j. arabjc. 2011.01.026.

[4]Teng, T. T., Yusup, Y., Low, L. W., *Heavy Metal Ion Extraction Using Organic Solvents: An Application of the Equilibrium Slope Method. Stoichiometry and Research – The Importance of Quantity in Biomedicine,*Dr Alessio Innocenti (Ed.), ISBN: 978-953-51-0198-7, InTech, doi:10.5772/33199, **2012.**

[5]Pereira, D. D., Ferreira Rocha, S. D., Mansur, M. B., *Sep. Purif. Technol.,* **2007,** *53,* 89.

[6]Pérez-Garibay, R., Martínez-Jiménez, J., Uribe-Salas, A., Martínez – Luévanos, A., *Engineering* **2012,** *4,* 526.

[7]Jin, Y., Ma, Y., Weng, Y., Jia, X., Li, J., *J. Ind. Eng. Chem.,* **2014,** *20(5),* 3446.

[8]Wen, L. S., Jiann, K. T., Santschi, P. H., *Marine Chem.,* 101 (**2006**) 104.

[9]Gode, F., Pehlivan, E., *J. Hazard. Mater.,* **2006,** *136B,* 330.

[10]Leinonen, H., Lehto, J., *React. Funct. Polym.,* **2000,** *43***,** 1.

[11]Lin, L. C., Juang, R. S., *Chem. Eng. J.,* **2007**, *132*, 205.

[12]Tser-Sheng, L., Nriagu, J. O., *Anal. Chim. Acta,* **1999,** *395,* 301.

[13]Wu, R. S. S., Lam, K. H., Lee, J. M. N., Lau, T. C. *Chemosphere,* **2007,** *69,* 289.

[14]Etou, A., Bai, S., Saito, T., Noma, H., Okaue, Y., Yokoyama, T., *J. Colloid Interface Sci.,* **2009,** *337,* 606.

[15]Lu, Y-W., Keita, B., Nadjo, L., *Polyhedron,* **2004,** *23,* 1579.

[16]Zhao, X., Zhang, G., Jia, Q., Zhao, C., Zhou, W., Li, W., *Chem. Eng. J.,* **2011,** *171,* 152.

[17]Awual, Md. R., Kobayashi, T., Miyazaki, Y., Motokawa, R., Shiwaku, H., Suzuki, S., Okamoto, Y., Yaita, T., *J. Hazard. Mater.,* **2013,** *252-253*, 313.

[18]Igberase, E., Osifo, P., Ofomaja, A., *J. Environ. Chem. Eng.,* **2014,** http://dx.doi.org/10.1016/ j.jece.2014.01.008.

[19]Li, D., Chang, X., Hu, Z., Wang, Q., Li, R., Chai, X., *Talanta,* **2011,** *83,* 1742.

MOLECULAR STRUCTURE OF BRIDGED *peri*-AROYL-NAPHTHALENE COMPOUND HAVING CYCLOHEXANE-*cis*-1,2-DIOXY-HINGE MOIETY IN SOLUTION

Sayaka Yoshiwaka[a], Kazuki Ogata[a], Noriyuki Yonezawa[a], and Akiko Okamoto[a]*

Keywords: molecular structure in solution, bridged *peri*-aroylnaphthalene compound, cyclohexane-*cis*-1,2-dioxy-hinge, stable conformational isomer.

The bridged *peri*-aroylnaphthalene compound having cyclohexane-*cis*-1,2-dioxy-hinge moiety connecting two benzoyl groups was successfully synthesized through the nucleophilic aromatic substitution of 1,8-bis(4-fluorobenzoyl)-2,7-dimethoxynaphthalene and cyclohexane-*cis*-1,2-diol. The compound consists of two ingredients in solution. The ingredients were successfully separated by repeated preparative thin layer chromatographical treatments to give stable solids. By the aid of ^{1}H NMR spectroscopic time course tracing, the ingredients have proved to undergo mutual transformations between them to yield an equilibrium mixture of constant fraction values by standing the individual solution within several weeks, revealing that the ingredients are conformational isomers to each other. Spatial organizations of the isomers of the bridged compound in solution have been elucidated by difference NOE measurement showing rough geometry of the isomers as two "extended" forms.

* Corresponding Authors
Fax: +81–42–388–7601
E-Mail: aokamoto@cc.tuat.ac.jp

[a]   Department of Organic and Polymer Materials Chemistry, Tokyo University of Agriculture and Technology, 2–24–16 Naka-machi, Koganei, Tokyo 184–8588, Japan

Introduction

Non-coplanarly accumulated aromatic ring compounds have received much attention from organic chemists and material scientists. Some of these compounds show characteristic physical and chemical properties including semiconductivity, photochromic nature, and molecular recognition ability probably originated from their unique spatial structures.[1–5] Therefore, accurate structural understanding of the fine spatial organization and the conformational alteration behaviour of this type of molecules in solution are of great important to design the novel functional molecules of this category as well as crystal structure analysis. [6–9]

The authors have studied on structure and reaction behaviours of naphthalene derivatives having two aroyl substituents at 1- and 8-positions (*peri*-positions)[10–13] especially focusing on X-ray crystal structure analysis.[14–22] In the single crystal molecular structures of *peri*-aroylnaphthalene compounds aromatic rings accumulate non-coplanarly. Two aroyl groups are situated almost perpendicularly against the naphthalene ring and generally oriented in an opposite direction. Only a few of the *peri*-aroylnapthalene compounds show *syn*-oriented conformation where the two aroyl groups situate in a same direction.[19,20,21,22] The X-ray crystal structure of the molecular packing of homologous and analogous compounds as well as the single molecular spatial organization has been determined and analysed comparatively to elucidate hitherto unknown or slighted stabilizing interactions functioning in the crystal of such non-coplanarly accumulating aromatic ring compounds. In addition, the structures of these compounds in solution have been investigated with the aid of ^{1}H NMR spectroscopy to reveal the rather dynamic feature of the molecular structure accompanying with the motion capability of the parts in molecule, flexibility, and interconversion behaviour giving the structural parameters such as the rotational barrier of linkages of ketonic bondings.[12, 13]

Recently, the authors have designed and synthesized intramolecularly bridged homologous molecules, which share terminal benzene ring connected to the benzoyl groups at 1- and 8-positions of the naphthalene ring.[23] And crystal structure of one of the bridged homologues has been clarified [Figure 1, compound **1b**].
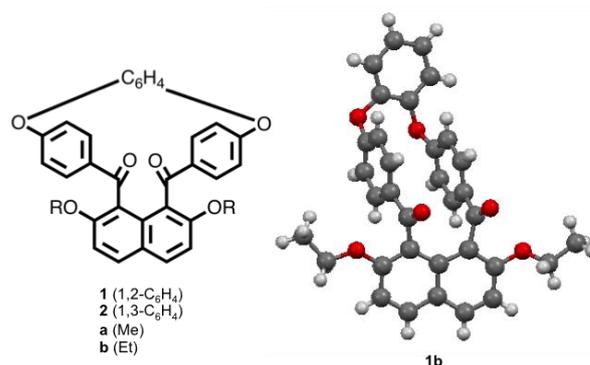

Figure 1. Bridged *peri*-aroylnaphthalene compounds having benzenedioxy-hinge moiety **1** and **2** with the example of crystal structure of compound **1b**

The molecular structure of these molecules in solution has been studied with the aid of ^{1}H NMR spectroscopy, disclosing the unsymmetrical circumstance of the phenylene ring of the benzoyl groups of the bridged compounds (**1b** and **2b**) against the apparently symmetric shape in chemical formulae (Figure 2).
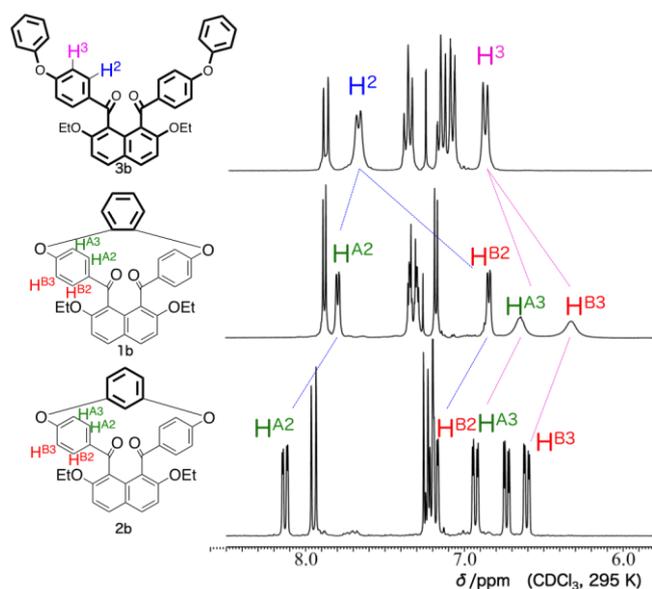
Figure 2. ^{1}H NMR spectra of compounds **3b**, **1b**, and **2b**.

These results indicate that the spatial mobility of the aromatic rings in the benzoyl groups is strongly restricted. In a natural consequence of design and synthesis of bridged *peri*-aroylnaphthalene compounds, those having cyclohexanedioxy-hinge moiety in place of benzenedioxy unit (**4**) as the objected homologous bridged molecules [Figure 3] were triggered. In this paper, the authors report the synthesis of novel-bridged *peri*-aroylnaphthalene compound having cyclohexane-*cis*-1,2-dioxy-hinge unit (compound **4**) and discuss the structural characteristic especially focusing on the existence of two stable conformational isomers, isolation of the ingredients, the spatial organization of them, and interconversion behaviours with the aid of ^{1}H NMR spectroscopy.
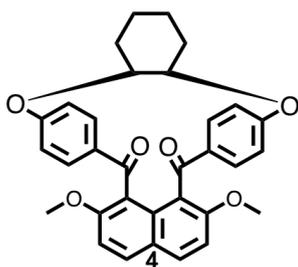

Figure 3. Bridged *peri*-aroylnaphthalene compound **4**.

Experimental

All reagents were of commercial quality and were used as received. Solvents were dried and purified using standard techniques.[24] 2,7-Dimethoxynaphthalene, the bridged *peri*-aroylnaphthalene compounds connected with 1,2-benzenedioxy moiety (**1**) and 1,3-benzenedioxy one (**2**), and 2,7-diethoxy-1,8-bis(4-phenoxybenzoyl)naphthalene (**3**) were prepared according to literatures.[22,23,25,26]

Measurement

^{1}H NMR spectra were recorded on a JEOL JNM-AL300 spectrometer (300 MHz) and a JEOL ECX400 spectrometer (400 MHz). Chemical shifts are expressed in ppm relative to internal standard of Me_4Si (δ 0.00). ^{13}C NMR spectra were recorded on a JEOL JNM-AL300 spectrometer (100 MHz). Chemical shifts are expressed in ppm relative to internal standard of $CDCl_3$ (δ 77.0). IR spectra were recorded on a JASCO FT/IR-4100 spectrometer. High-resolution FAB mass spectra were recorded on a JEOL MStation (MS700) ion trap mass spectrometer in positive ion mode.

Synthesis of bridged *peri*-aroylnaphthalene 4

To a solution of 1,8-bis(4-fluorobenzoyl)-2,7-dimethoxynaphthalene (0.3 mmol, 130.7 mg) in *N,N*-dimethylacetamide (7.5 mL), NaH (1.5 mmol, 60 mg) and *cis*-1,2-cyclohexanediol (0.3 mmol, 35 mg) were added and the resulting solution was stirred at 423 K for 24 h. The reaction mixture was poured into aqueous 2 M HCl (75 mL) at rt resulting in formation of pale yellow precipitates. The precipitates were collected by filtration and dried in vacuo. giving crude product (156 mg; conv. 32%). The crude material was purified by column chromatography repeatedly [silica gel, toluene : AcOEt = 3 : 1 (two times) and $CHCl_3$: AcOEt = 20 : 1 (ten times)] to give two ingredients of conformers of the target compound (**4**) (isolated yields **I**: 10%; **II**: 18%). Isolated conformer **I**: ^{1}H NMR δ (300 MHz, $CDCl_3$): 7.93 (2H, d, J = 9.0 Hz), 7.83 (2H, dd, J = 8.7 Hz and 2.7 Hz), 7.23 (2H, d, J = 9.0 Hz), 6.81 (2H, dd, J = 8.7 Hz and 2.7 Hz), 6.62 (2H, dd, J = 8.7 Hz and 2.7 Hz), 6.27 (2H, dd, J = 8.7 Hz and 2.7 Hz), 4.64–4.73 (2H, m), 3.78 (6H, s), 1.42–2.19 (8H, m) ppm; ^{13}C NMR δ (100 MHz, $CDCl_3$): 22.15, 29.78, 56.89, 111.30, 113.95, 122.09, 122.17, 125.09, 125.59, 129.14, 130.80, 131.47, 131.99, 134.00, 156.23, 162.14, 193.67 ppm; IR ν (KBr): 2937, 2859 (C–H, cyclohexane), 1670 (C=O), 1598, 1511, 1460 (Ar, naphthalene), 1260, 1240 (C–O–C) cm^{-1}; HRMS (m/z): [M+H]$^+$ calcd for $C_{32}H_{29}O_6$, 509.2000 found 509.1964. Isolated conformer **II**: ^{1}H NMR δ (300 MHz, $CDCl_3$): 7.95 (2H, d, J = 9.0 Hz), 7.81 (2H, dd, J = 8.4 Hz and 2.4 Hz), 7.23 (2H, d, J = 9.0 Hz), 6.87 (2H, dd, J = 8.4 Hz and 2.4 Hz), 6.60 (2H, dd, J = 8.4 Hz and 2.4 Hz), 6.37 (2H, dd, J = 8.4 Hz and 2.4 Hz), 4.70–4.78 (2H, m), 3.78 (6H, s), 1.46–2.22 (8H, m) ppm; ^{13}C NMR δ (100 MHz, $CDCl_3$): 22.14, 29.86, 56.87, 111.30, 115.48, 120.65, 122.00, 125.49, 130.10, 131.66, 132.06, 134.41, 156.35, 162.38, 193.88 ppm; IR ν (KBr): 2935, 2859 (C–H, cyclohexane), 1671 (C=O), 1596, 1510, 1460 (Ar, naphthalene), 1261, 1238 (C–O–C) cm^{-1}; HRMS (m/z): [M+H]$^+$ calcd for $C_{32}H_{29}O_6$, 509.2000 found 509.1964.

Results and Discussion

The authors attempted the synthesis of the newly designed bridged *peri*-aroylnaphthalene compound having a cyclohexane-*cis*-1,2-dioxy-hinge connecting at the edge of the aroyl groups by two synthetic protocols: one is the dual S$_N$2 reaction of 1,8-bis(4-hydroxybenzoyl)-2,7-dimethoxynaphthalene compound with dibromocyclohexane and the other is dual S$_N$Ar reaction of 1,8-bis(4-fluorobenzoyl)naphthalene analogue with dihydroxy-

cyclohexane in the presence of base. Though the former approach gave a complex mixture comprised of significant amount of undesirable products of cyclohexenyl ether compounds, the latter choice of the starting materials constructed the targeted bridged *peri*-aroylnaphthalene structure in a rather good conversion. Under the optimized conditions that are almost same with the synthetic reaction conditions for catechol- or resorcinol-hinge *peri*-aroylnaphthalene analogues briefly reported in the preceding paper, the reaction of 1,8-bis(4-fluorobenzoyl)naphthalene and *cis*-1,2-cyclohexanediol was allowed to proceed in a satisfied conversion, still accompanying with several types of by-products such as 2 : 1 adduct of *peri*-aroylnaphthalene substrate and *cis*-1,2-cyclohexanediol molecule, and 2,7-dimethoxynaphthalene, and so on. Furthermore, the ^{1}H NMR spectrum of the crude product shows the existence of two major ingredients of the structures possibly fit as cyclohexane-*cis*-1,2-dioxy-hinge bridged *peri*-aroylnaphthalene (compound **4**) molecules. In solution, two isolated ingredients were observed apparently as stable species at rt by ^{1}H NMR spectrometrically.

The two major ingredients of the structures were successfully isolated by repeated preparative thin layer chromatography (PTLC) on silica-gel as almost pure forms (Figure 4, top; isolated ingredient **I**, Figure 5, top; isolated ingredient **II**). For each of the ingredients, four kinds of protons for the benzene ring of the benzoyl moiety are distinguished as respective chemical shifts (see Figure 2). The authors have recently reported ^{1}H NMR spectroscopic structural analysis of phenylene-hinge-bridged *peri*-aroylnaphthalene compounds **1** and **2**. The spectra of phenylene-hinge-bridged *peri*-aryloxybenzoylnaphthalene compounds show unique non-equivalency in chemical shift that the protons of the phenylene rings in the oxybenzoyl groups at 1- and 8-positions appear at δ 7.80, 6.84, 6.54–6.74 (broad), 6.20–6.40 (broad) ppm for compound **1b** (catechol-hinge derivative) and δ 8.14, 7.18, 6.94, and 6.62 ppm for compound **2b** (resorcinol-hinge derivative) [Figure 2], whereas for non-bridged compound **3b** a couple of equivalent signals at 7.66 ppm and 6.86 ppm are observed. The ^{1}H NMR spectra of the isolated ingredients show non-equivalency in chemical shift that the protons of the phenylene-hinge appear at δ 7.83, 6.81, 6.62, and 6.27 ppm for isolated ingredient **I** and at δ 7.81, 6.87, 6.60, and 6.37 ppm for isolated ingredient **II**. The resemble signals feature manifests that the two ingredients have essentially the same situation of the phenylene ring of oxybenzoyl groups to each other and also with the phenylene bridged *peri*-aryloxybenzoylnaphthalene compounds. Consequently, both of the ingredients have quite large similarity in structure, having more intimate relationship than structural isomers. Accordingly, bridged *peri*-aroylnaphthalene compound **4** is proved composed of two independent structurally isomeric molecules.

The findings prompted the authors to follow the structure transformation behaviour of the two independent molecules in solution. First, the authors attempted to observe rather long ranged time-course of the product distribution by ^{1}H NMR spectroscopy (Figures 4 and 5). After standing of CDCl₃ solutions containing each of the ingredients at rt for 2 weeks, the counter ingredient formed. Then, the ratio of the ingredients in solution varied gradually. Standing for additional 6 weeks, the molecular ratio became equally constant value (ingredient **I** : ingredient **II** = 67 : 33) in both

solutions initially contain one of almost pure ingredient solely. The time-course of the interconversion behaviour also showed that the structural transformation of one ingredient (ingredient **II**) to the other one (**I**) proceeds much slowly. Based on the facts described above, the ingredients are considered as conformational isomers having high energy barrier against interconversion.
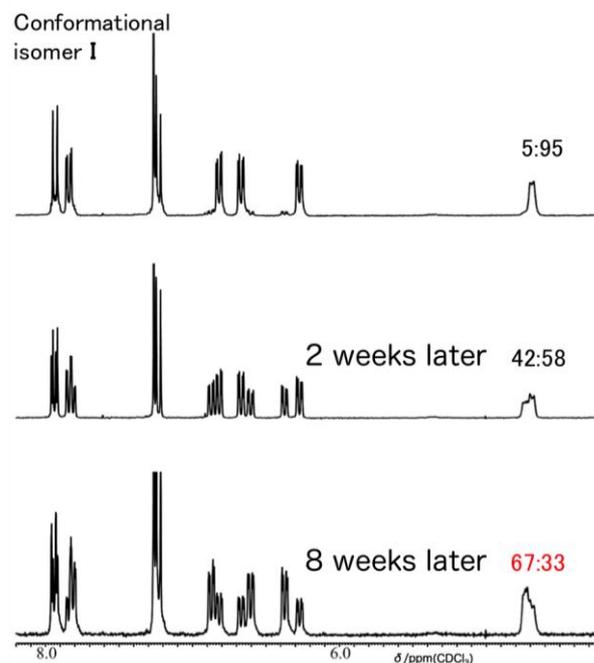

Figure 4. Time-course of ^{1}H NMR spectra of compound **4** (conformational isomer **I**).
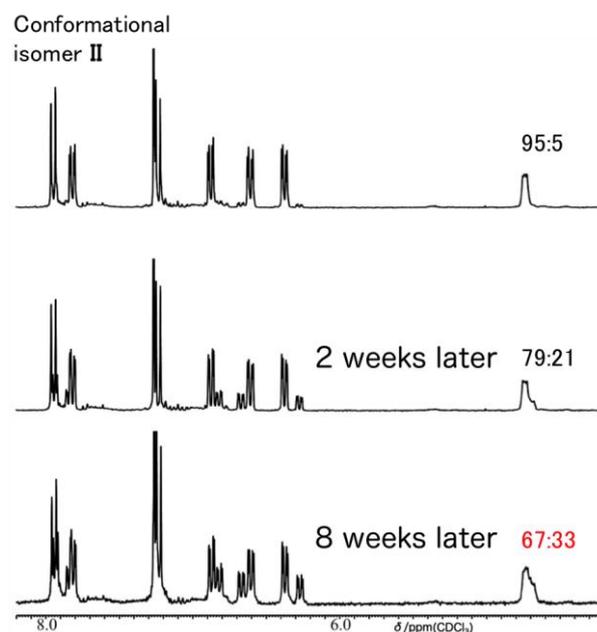

Figure 5. Time-course of ^{1}H NMR spectra of compound **4** (conformational isomer **II**).

From the standpoint of linkage flexibility of the molecular formulae, this means that there are possible two modes of structural conversion for this equilibrium: one is the inversion of linkages at cyclohexanedioxy-hinge moiety and

the other is reversion of ketonic carbonyl-groups. Accordingly, there are possible four independent isomeric molecules in solution (Figure 6). Two of the extended-type derivatives bear the cyclohexanedioxy-hinge situated outward from the aroyl groups. On the other hand, in other two independent molecules, the cyclohexanedioxy-hinge overspreads the aroyl groups to make the molecular figure as categorized "Bent-type". The other category of classification of the conformational isomers is *exo/endo*: the former designates that the cyclohexane and naphthalene rings situate on the same side against the plane of *o*-benzoyl and C(=O)– phenylene bonds of the two benzoyl groups.
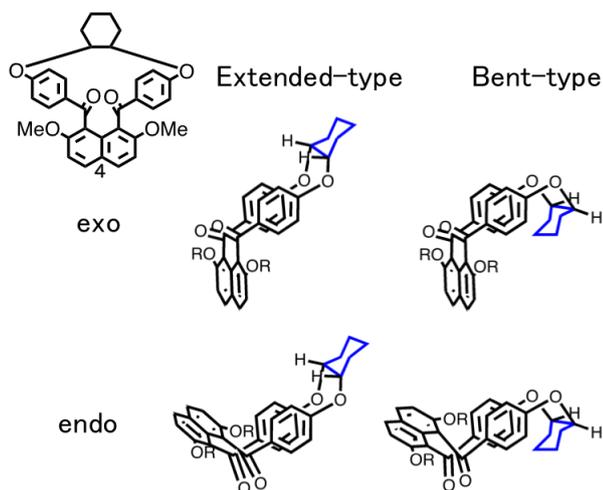

Figure 6. Plausible structure of conformation for bridged compound **4** in solution.

In other words, the interconversion between "Extended-type" structure and "Bent-type" one depends on the mobility of the linkage of cyclohexane ring and ethereal oxygen and the exchange between "*exo*" structure and "*endo*" one on the flexibility of the ketonic carbonyl bonds as displayed in Figure 6. Therefore, specification of two conformers from four candidates targeted required.

Finally, the spatial organization of cyclohexanedioxy-hinge bridged *peri*-aroylnaphthalene compound has been elucidated by the aid of difference Nucleus Overhauser Effect (NOE) measurement (Figures 7 and 8). In all cases, the signals of the protons at the *m*-positions of the benzoyl groups are correlated with the corresponding neighbouring signal of the *o*-positions of the benzoyl groups (Figure 7: δ 6.27 and 6.81 ppm, 6.66 and 7.81 ppm; Figure 8: δ 6.37 and 6.87 ppm, 6.61 and 7.81 ppm). Moreover, the signal of the methine protons of the 1- and 2-positions of the cyclohexanedioxy-hinge correlates with one of the protons at the *m*-position of the benzoyl groups. In the case of isolated conformer **I**, the signals of the *m*-positions of the benzoyl groups at the higher magnetic field correlate with the signal of the protons of the 1- and 2-positions of the cyclohexanedioxy-hinge moiety (Figure 7: δ 6.27 and 4.69 ppm). In the case of isolated conformer **II**, however, the signals of the *m*-position of the benzoyl groups at the low magnetic field correlate with the signal of protons at the 1- and 2-positions of the cyclohexanedioxy-hinge moiety (Figure 8: δ 6.60 and 4.73 ppm). On the other hand, there are no correlated signals of protons of the methylene moiety

of cyclohexanedioxy-hinge moiety with the signals of the *m*-position of the benzoyl groups at higher magnetic field (Figure 8: 6.37 ppm).
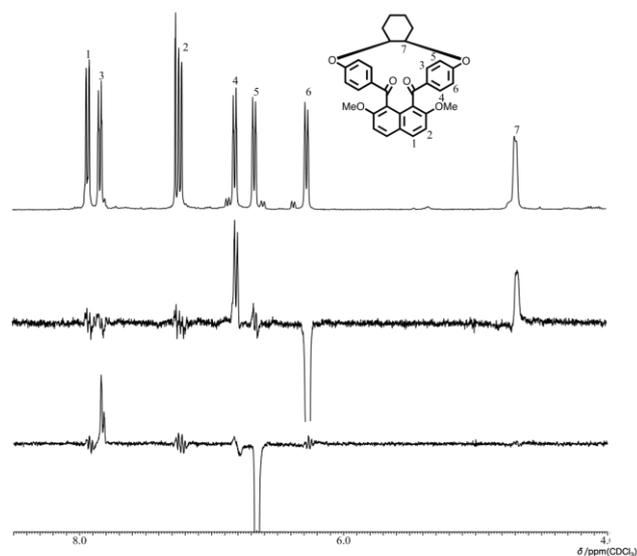

Figure 7. Difference NOE spectra of compound **4** (conformer **I**).
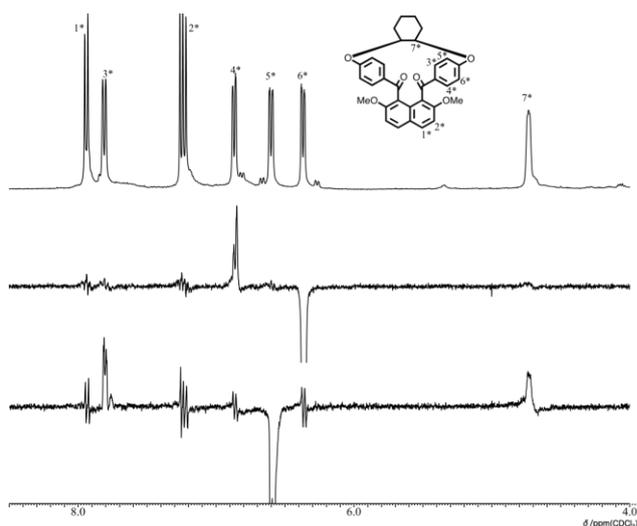

Figure 8. Difference NOE spectra of compound **4** (conformer **II**).

Accordingly, the presence/absence of correlation between the 1- and 2-positioned protons of the cyclohexanedioxy-hinge and *m*-positioned protons of the benzoyl moiety disclosed the conformation of the isomers, "Extended-type" or "Bent-type." Based on the difference NOE spectra, both of the isolated conformer have correlation between 1- or 2-proton of cyclobutane ring and *m*-proton of benzoyl moiety, the authors conclude that there are no conformers for "Bent-type" in compound **4**. No correlation of the protons at the 1- and 2-position of cyclohexanedioxy-hinge with the signals of the protons of the benzoyl groups should be observed if the shapes of conformer were "Bent-type."

Here, the authors have referred the spatial organization elucidation of bridged *peri*-aroylnaphthalene compound bearing butylene-hinge by the aid of NOESY measurement (see Note). The results show that one of the *m*-positioned

protons of the benzoyl group appeared at split chemical shifts and the higher field one corresponds to the *m*-positioned proton more closely to the naphthalene ring. According to the above observation, isolated conformer **I** is probably categorized as "*endo*-type" in the extended-classification. In the case of isolated conformer **I**, the signal of protons at the 1- and 2-positions of cyclohexane-hinge has correlation with the higher field signal of a proton at *m*-position of the benzoyl group. So, the protons of cyclohexanedioxy-hinge of isolated conformer **I** have orientation toward the naphthalene ring (Figure 9, *endo*-type). On the other hand, in the case of isolated conformer **II**, the protons at the 1- and 2-positions of cyclohexanedioxy-hinge correlate with the lower field signal of the protons at the *m*-position of the benzoyl groups (Figure 9, *exo*-type).
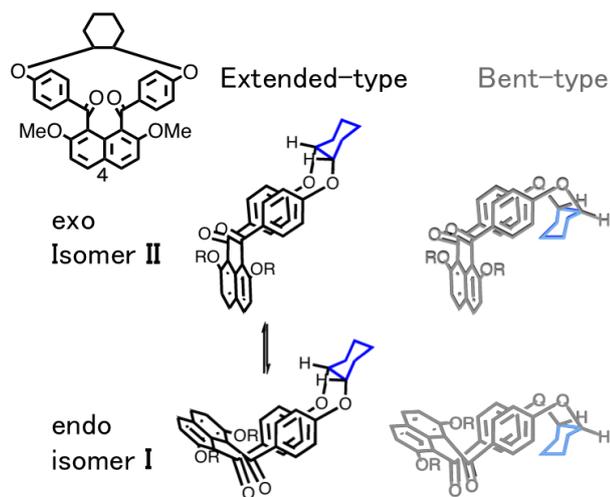

Figure 9. Plausible structure of compound **4** in solution.

The authors consider that the conformers in solution are going back and forth between *exo*-type and *endo*-type in extended-conformation (Figure 9). Based on pretty slow transformation of the cyclohexanedioxy-hinge compound **4**, two of four conformational isomers are isolated and characterized. In the case of bridged *peri*-aroylnaphthalene compound bearing catechol-hinge, although no transformation is observed like bridged compound bearing cyclohexanedioxy-hinge in solution, the shapes of the signals of the protons at the *m*-position of the benzoyl groups are broad. The shapes are interpreted as displaying a vertical motion of the catechol-hinge (Figure 10).
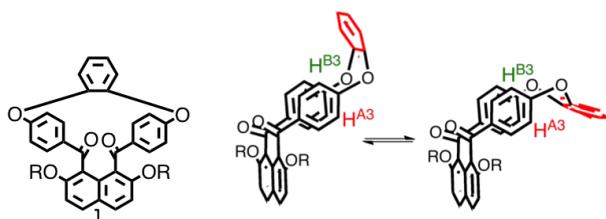

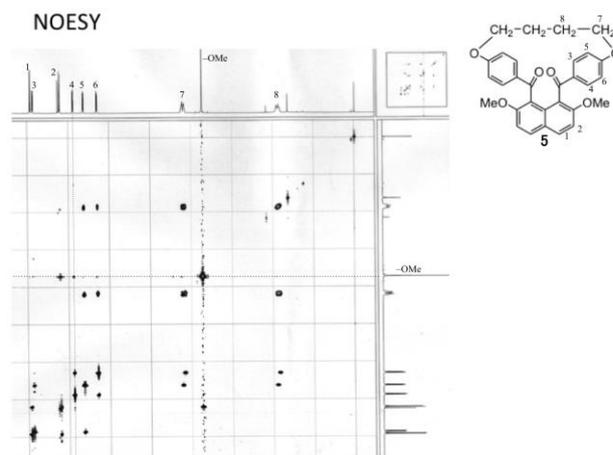**Figure 10.** Plausible structure of compound **1** in solution.

Figure 11. Nucleus overhauser effect correlated spectra of bridged *peri*-aroylnaphthalene compound bearing butylene-hinge moiety (**5**).

Conclusion

The authors synthesized novel bridged *peri*-aroylnaphthalene compound bearing cyclohexane-*cis*-1,2-dioxy-hinge moiety at the terminal carbons of the benzoyl groups. The compound has two stable conformational isomers in solution that can be successfully separated. Though two isomers are sufficiently stable in solid. Furthermore, the structures of the isomers have been revealed as two extended-type conformers. Tracing of the time-course of these conformers by ^{1}H NMR spectroscopy has revealed interconversion of the isomers to each other proceeds slowly in solution finally giving a mixture of constant ratio.

Note

A signal of methoxy groups at the 2- and 7-positions of naphthalene ring correlate not only with the signal of the protons of the *β*-position of the naphthalene rings but also with the signal of the protons at the *o*-position of the benzoyl groups, which shows that the protons situate toward the naphthalene ring rather than outward. The latter signal of one of the *o*-position of the benzoyl groups correlates with one of the signals of the protons at the *m*-position of the benzoyl group that is deviated to the higher field in the aromatic region. The observation that one of the signals of the *m*-positioned protons of the benzoyl groups has correlation with the protons of CH_3O-moiety suggests that a proton attributing to the signal at the higher field situates in more close position with the naphthalene ring.

References

[1] Würthner, F., *Chem. Commun.* **2004**, 1564–1579.

[2] Oneil, M. P., Niemczyk, M. P., Svec,W. A., Gosztola, D., Gaines, G. L., Wasielewski, M. R., *Science*, **1992**, *257*, 63–65.

[3]Czerwinska, I., Sato, S., Juskowiak, B., Takenaka, S., *Bioorg. Med. Chem.,* **2014**, 22(9), 2593–2601.

[4]Saha, Ranajay, Rakshit, Surajit, Pal, Samir Kumar, *Journal of Molecular Recognition*, **2013**, *26*(11), 568–577.

[5]Suzuki, A., Kondo, K., Akita, M., Yoshizawa, M., *Ang. Chem. Int. Ed.*, **2013**, *52*(31), 8120–8123.

[6]Yang, C., Chen, Y., Wang, D., Zhao, L., Wang, M., *Org. Lett.* **2014**, *15*, 4414–4417.

[7]Lunazzi, L., Mazzanti, A., Minzoni, M., Anderson, J. E., *Org. Lett.*, 2005, 77, 1291–1294.

[8]Steele, M., Watkinson, M., Whiting, A., *J. Chem. Soc. Perkin Trans. 1*, **2001**, *6*, 588–598.

[9]Cohen, S., Thirumalaikumar, M., Pogodin, S., Agranat, I., *Struct. Chem.*, **2004**, *15,* 339–346.

[10] Okamoto, A., Yonezawa, N., *Chem. Lett.,* **2009**, *38*, 914.

[11] Okamoto, A, Mitsui, R., Yonezawa, N., *Chem. Lett.,* **2011**, *40*, 1283.

[12] Okamoto, A., Watanabe, S., Nakaema, K., Yonezawa, N., *Cryst. Str. Theo. Appl.,* **2012**, *1*,121–127.

[13] Okamoto, A., Ohisa, S., Yoshiwaka, S., Yonezawa, N., *Eur. Chem. Bull.*, **2015**, *4*(2), 67–73.

[14]Okamoto, A., Yoshiwaka, S., Mohri, S., Hijikata, D., Yonezawa, N., *Eur. Chem. Bull.*, **2014**, *3(8)*, 829–834.

[15] Nakaema, K., Noguchi, K., Okamoto, A., Yonezawa, N., *Acta Cryst.,* **2008**, *E64*, o2497.

[16] Sasagawa, K., Sakamoto, R., Hijikata, D., Yonezawa, N., Okamoto, A., *Acta Cryst.*, **2013**, *E69*, o651.

[17]Yoshiwaka, S.; Hijikata, D.; Sasagawa, K.; Okamoto, A.; Yonezawa, N.; *Acta Cryst.*, **2013**, *E69*, o242.

[18]Mohri, S., Ohisa, S., Noguchi, K., Yonezawa, N., Okamoto, A., *Acta Cryst.,* **2014**, *E70*, 138-141.

[19] Mitsui, R., Nagasawa, A., Noguchi, K., Okamoto, A., Yonezawa, N., *Acta Cryst.*, **2010**, *E66*, o1790.

[20] Sasagawa, R., Takeuchi, R., Kusakabe, T., Yonezawa, N., Okamoto, A., *Acta Cryst.*, **2013**, *E69*, o444–o445.

[21] Hijikata, D., Takada, T., Nagasawa, A., Okamoto, A., Yonezawa, N., *Acta Cryst.*, **2010,** *E66*, o2902–o2903.

[22] Yoshiwaka, S., Sasagawa, K., Noguchi, K., Okamoto, A., Yonezawa, N, *Acta Cryst.*, **2014**, *C70*, 1096–1100.

[23] Yoshiwaka, S., Ohisa, S., Yonezawa, N., Okamoto, A., *Eur. Chem. Bull.*, **2014**, *3(12)*, 1142–1147.

[24]Armarego, W. L. F., Perrin, D. D., "*Purification of Laboratory Chemicals*", Fourth edition, Reed Educational and Professional Publishing Ltd, Oxford, **1996**.

[25] Domasevitch, K. V., Solnsev, P. V., Krautscheid, H., Zhylenko, I. S., Rusanov, E. B., Chernega, A. N., *Chem. Commun.,* **2012**, *48*, 5847.

[26] Kuwano, R., Morioka, R., Kashiwabara, M., Kameyama, N., *Angew. Chem., Int. Ed*., **2012**, *51*, 4136.

SPATIAL ORGANIZATION OF BRIDGED *peri*-AROYLNAPHTHALENE COMPOUNDS HAVING 1,2- OR 1,3-BENZENEDIOXY-HINGE MOIETY IN SOLUTION

Sayaka Yoshiwaka[a], Daichi Hijikata[a], Noriyuki Yonezawa[a] and Akiko Okamoto[a]*

The bridged *peri*-aroylnaphthalene compounds having 1,3-benzendioxy-hinge units were newly synthesized and the spatial organization in solution was characterized in comparison with isomeric derivatives having 1,2-benzenedioxy-hinge unit and a non-bridged analogue. 1,2-Benzenedioxy and 1,3-benzenedioxy-hinge units, which connect the edge carbon atoms of aroyl groups, afford the distinct difference in rotation ability of benzene ring of aroyl groups. The sharpness/broadness and the non-equivalency of ^{1}H NMR signals of aromatic protons demonstrate the highly congested and hinge-depending spatial organization of these bridged *peri*-aroylnaphthalene molecules. Furthermore, the significant magnetic field deviation of the signals in ^{1}H NMR spectra proves the presence of effective induced magnetic field especially for the middle proton at the 2-position of the 1,3-benzenedioxy unit.

Corresponding Authors
    Fax: +81–42–388–7601
    E-Mail: aokamoto@cc.tuat.ac.jp
[a]   Department of Organic and Polymer Materials Chemistry, Tokyo University of Agriculture and Technology, 2–24–16 Naka-machi, Koganei, Tokyo 184–8588, Japan

Introduction

Macrocyclic compounds having unique π-conjugated structures have been investigated as promising framework for organic optoelectronic devices.[1–5] To bring forth the excellent semiconductive properties, such as electrical conductivity, luminescence and photo-harvesting behavior, organic chemists and material scientists have attempted to design and synthesize the candidate molecules, e.g., incorporating phenylene motif by various bonding modes.[6] Along with these synthetic aspects, structural studies on spatial organization of aromatic ring accumulation compounds in solid state/solution are also being carried currently.[7–9] To grasp the spatial situation and the dynamic behavior of the aromatic rings in the aromatic ring accumulation structures, non-coplanarly accumulated aromatic ring compounds should be suitable model compounds. Because their weak π-conjugate system might reveal normally hidden structure-governing factors other than π…π stacking interactions. Our group has been studying on the spatial organization in crystal/solution of *peri*-aroylnaphthalene compounds, where two aroyl groups are situated at 1- and 8-positions of the adjacent inner carbons of the 2,7-dialkoxynaphthalene core.[10–14] In crystal, these compounds display a unique spatial organization feature of non-coplanar accumulation of aromatic rings. In most cases of *peri*-aroylnaphthalene compounds, the two aroyl groups are aligned in an opposite direction (i.e., *anti*-orientation).[15–19] Recently, we observed that, in crystalline state, the phenoxybenzoyl groups at 1- and 8-positions of the naphthalene ring in 2,7-dimethoxy-1,8-bis(4-phenoxybenzoyl)naphthalene (**3a**) are aligned in same direction i.e., in *syn*-orientation.[20] This finding prompted us to attempt to elucidate of the determining factors for

orientations of two aroyl groups in *peri*-aroylnaphthalenes.[21] To achieve this aim, we have designed and synthesized bridged *peri*-aroylnaphthalene compounds having intramolecular connection between the terminal aromatic rings of the 1- and 8-benzoyl groups with catechol-hinge unit moiety (Figure 1, left).[22] The bridged compounds connected with suitable hinge at the edge carbons of the two aroyl groups plausibly have restricted conformation giving unique alignment of the molecular components including orientation and fixation of aroyl groups. Among the bridged homologous compounds with catechol ring-hinge, the analysis of the crystal structure of the catechol-bridged compounds (**1b**) was performed (Figure 2).
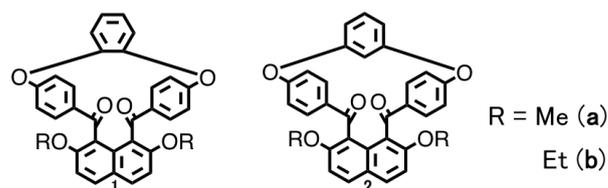

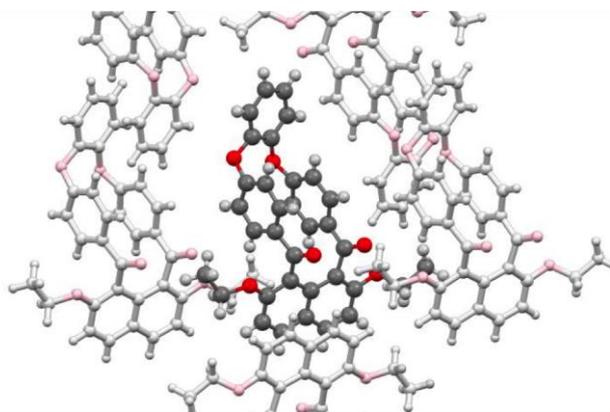**Figure 1.** Bridged *peri*-aroylnaphthalene compounds.

Figure 2. Crystal structure of bridged compound bearing catechol-hinge (**1b**).

Aromatic rings of the compound (**1b**) are accommodated non-coplanarly giving highly congested intramolecular circumstance. The plane of the catechol-hinge moiety almost parallels to the naphthalene ring. On the other hand, there are no strong interactions between aromatic rings within each molecule. The absence of effective intermolecular interaction means that conformation of the molecules of these compounds should be perturbed by addition of intramolecular/intermolecular interactions and possibly leads design of the analogues as synthetic unit. For application of these compounds as function-affording molecules in some practical material, understanding of the single molecular structure of the compound under non-crystalline state such as amorphous, liquid crystal, or solution is significantly important as well as that of the structural features in crystal. Based on such consideration, we have designed and synthesized another type of bridged compounds, which have resorcinol-hinge moiety at connecting 4,4'-position of aroyl groups instead of catechol unit for investigation of the spatial structure in solution (Figure 1, right).

In this paper, we report and discuss the characteristic features of molecular spatial organization of the bridged *peri*-aroylnaphthalene compounds in solution on the basis of comparison of their ^{1}H NMR spectra with those of non-bridged analogues.

Experimental

All reagents were of commercial quality and were used as received. Solvents were dried and purified using standard techniques.[23] 2,7-Dimethoxynaphthalene,[24] 2,7-diethoxy-naphthalene,[25] 2,7-diethoxy-1,8-bis(4-phenoxybenzoyl)-naphthalene (**3b**)[21] and the bridged *peri*-aroylnaphthalene compounds connected with 1,2-benzenedioxy moiety (**1**)[22] were prepared by reported methods.

Measurements

^{1}H NMR spectra were recorded on a JEOL JNM-AL300 spectrometer (300 MHz) and a JEOL ECX400 spectrometer (400 MHz). Chemical shifts are expressed in ppm relative to internal standard of Me_4Si (δ 0.00). ^{13}C NMR spectra were recorded on a JEOL JNM-AL300 spectrometer (75 MHz). Chemical shifts are expressed in ppm relative to internal standard of $CDCl_3$ (δ 77.0). IR spectra were recorded on a JASCO FT/IR-4100 spectrometer. High-resolution FAB mass spectra were recorded on a JEOL MStation (MS700) ion trap mass spectrometer in positive ion mode.

Synthesis of bridged *peri*-aroylnaphthalene (2)

To a solution of 1,8-bis(4-fluorobenzoyl)-2,7-dimethoxynaphthalene (0.3 mmol, 130.7 mg) in *N,N*-dimethylacetamide (DMAc, 7.5 mL), K_2CO_3 (1.5 mmol, 208.3 mg) and resorcinol (0.3 mmol, 34 mg) were added and the resulting solution was stirred at 423 K for 24 h. The reaction mixture was poured into aqueous 2 M HCl (75 mL) at room temperature (rt) resulting in formation of a pale yellow precipitate. The precipitate was collected by

filtration and dried in vacuo giving crude product (143 mg; conversion 50 %). The crude material was purified by column chromatography (silica gel, $CHCl_3$: AcOEt = 3 : 1) and recrystallized from AcOEt to give the target compound (**2a**) (isolated yield 36 %; m.p. 453.7–455.4 K).

Compound (**2b**) was prepared in essentially the same way as that of compound (**2a**). The crude material was purified by column chromatography (silica gel, $CHCl_3$: AcOEt = 3 : 1) and recrystallized from AcOEt (isolated yield 29 %; m.p. 464.3–465.7 K). The synthetic procedure of the bridged compounds (**2**) is summarized as following scheme.
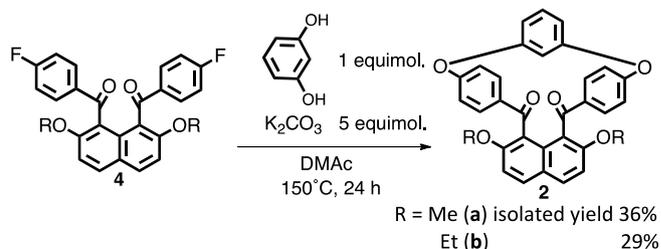
Scheme 1. Synthesis of the bridged compounds (**2**).

Spectral data

Compound (**2a**): ^{1}H NMR δ (300 MHz, $CDCl_3$): 8.14 (2H, dd, *J* = 8.7 Hz and 2.1 Hz), 8.00 (2H, d, *J* = 9.0 Hz), 7.26 (2H, d, *J* = 9.0 Hz), 7.23 (1H, t, *J* = 8.4 Hz), 7.18 (2H, dd, *J* = 8.7 Hz and 2.1 Hz), 6.94 (2H, dd, *J* = 8.7 Hz and 2.4 Hz), 6.74 (2H, dd, *J* = 8.4 Hz and 2.4 Hz), 6.62 (2H, dd, *J* = 8.7 Hz and 2.4 Hz), 4.01 (1H, t, *J* = 2.4 Hz), 3.76 (6H, s). ^{13}C NMR δ (75 MHz, $CDCl_3$): 56.79, 104.09, 109.17, 111.23, 121.05, 123.32, 124.22, 130.32, 130.42, 132.54, 133.28, 135.55, 156.66, 159.73, 161.76, 194.12 ppm. IR ν (KBr): 1677 (C=O), 1590, 1513, 1490 (Ar, naphthalene), 1497, 1609 (Ar, benzene), 1250 (C–O–C) cm^{-1}. HRMS (m/z): [M+H]$^+$ calcd. for $C_{32}H_{23}O_6$, 503.1489 found 503.1499.

Compound (**2b**): ^{1}H NMR δ (300 MHz, $CDCl_3$): 8.13 (2H, dd, *J* = 8.4 Hz and 2.4 Hz), 7.95 (2H, d, *J* = 8.7 Hz), 7.23 (1H, t, *J* = 8.4 Hz), 7.22 (2H, d, *J* = 8.7 Hz), 7.19 (2H, dd, *J* = 8.4 Hz and 2.4 Hz), 6.94 (2H, dd, *J* = 8.4 Hz and 2.4 Hz), 6.74 (2H, dd, *J* = 8.4 Hz and 2.4 Hz), 6.62 (2H, dd, *J* = 8.4 Hz and 2.4 Hz), 3.99–4.02 (1H, m), 3.94–4.16 (4H, m), 1.07 (6H, t, *J* = 7.2 Hz) ppm. ^{13}C NMR δ (75 MHz, $CDCl_3$): 14.66, 65.44, 104.10, 109.18, 112.50, 121.66, 123.16, 124.11, 130.20, 138.38, 132.33, 133.20, 135.73, 156.00, 159.60, 161.78, 194.09 ppm. IR ν (KBr): 1680 (C=O), 1590, 1512, 1490 (Ar, naphthalene), 1497, 1607 (Ar, benzene), 1250 (C–O–C) cm^{-1}. HRMS (m/z): [M+H]$^+$ calcd for $C_{34}H_{27}O_6$, 531.1808 found 531.1842.

Results and Discussion

The bridged compounds (**2**) were synthesized according to essentially the same synthetic method for bridged compounds (**1**), which was reported by us earlier.[22] In the previous paper, we reported the X-ray crystal structure of compound (**1b**) as displayed in Figure 2.[22] In this single crystal molecular structure there are no apparent effective intramolecular interactions either between aromatic rings of 1- and 8-benzoyl groups or between naphthalene ring and

catechol benzene ring. Furthermore, there are no strong intermolecular interactions also. These findings mean that the single molecular structure of compound (**1b**), in the crystal state is stabilized by weak van der Waals interactions. In other words, the stabilization factors of the single molecular structure originated from the spatial organization of the aromatic rings. In solution, where there are less intermolecular interactions, the structural features of the spatial organization might be more important. In view of this, we have investigated and compared the solution phase structure of bridged compounds (**1b**) and (**2b**) with that of non-bridged compound (**3b**) by ^{1}H NMR spectroscopy. The ^{1}H NMR spectra of bridged compounds (**1b**) and (**2b**) show four unique features, signal shapes of aromatic ring protons, non-equivalency of the symmetrically situated aromatic protons of the aroyl groups, deviation in characteristic chemical shifts of the signal assigned to the proton of the resorcinol, and the geminal protons in alkoxy groups at 2,7-positions of the naphthalene ring. First, in the aromatic region of ^{1}H NMR spectrum of non-bridged compound (**3b**), two signals attributed to the phenylene protons of the benzoyl groups appear at δ 7.68 and 6.88 ppm (Figure 3). While, in the ^{1}H NMR spectra of the bridged compounds, (**1b**) and (**2b**), four signals of the phenylene protons of the benzoyl groups appear with different chemical shifts for almost the same chemical structures with compound (**3b**), i.e., δ 7.80, 6.84, 6.54–6.74, and 6.20–6.40 ppm for compound (**1b**) (catechol-hinge derivative) and δ 8.14, 7.18, 6.94, and 6.62 ppm for compound (**2b**) (resorcinol-hinge derivative). The non-equivalency in aromatic H atoms and the significant deviation of chemical shifts are regarded as due to the unsymmetrical circumstance of magnetic field around macrocycle-forming accumulation of aromatic rings arising from restriction of the rotation of the benzoyl moieties of the compounds. Furthermore, the signal shapes of the aromatic protons are apparently different between catechol-hinge-bearing compound and resorcinol-hinge-bearing one. All four signals of the resorcinol-hinge-bearing compound are sharp, whereas two of four signals assigned as H(A3) and H(B3) protons in the catechol-hinge-bearing (**1b**) are broad.
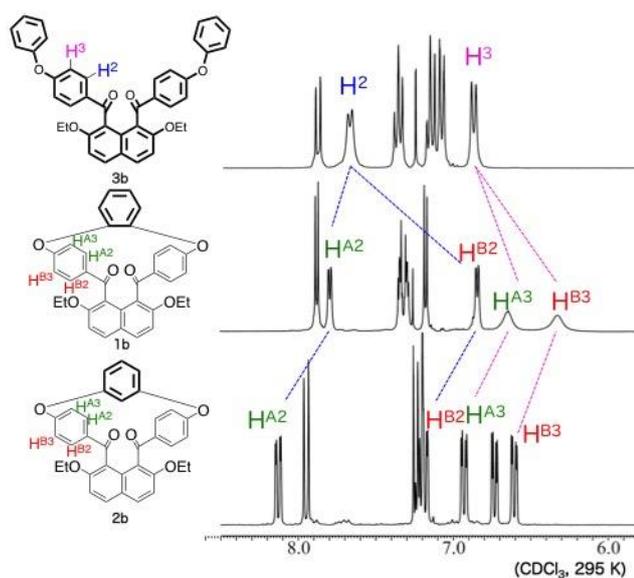
The unsymmetrical signal shapes on the same aromatic ring in the catechol-hinge-bearing compound strongly indicate that magnetic influence by catechol moiety is unequal against the aromatic protons of the benzoyl group.

The spatial structure in solution of the resorcinol-hinge type compound (**2a**) is further investigated by the [1]H–[1]H correlation spectroscopy (Figure 4). Correlation spectra between δ 3.25–4.75 ppm and δ 6.50–8.25 ppm regions show characteristic crossing feature. The signal of the H atom at 2-position of the resorcinol moiety drastically shifts from the general value of aromatic region to δ 4.00 ppm in the resorcinol-hinge-bearing compound (**2a**).
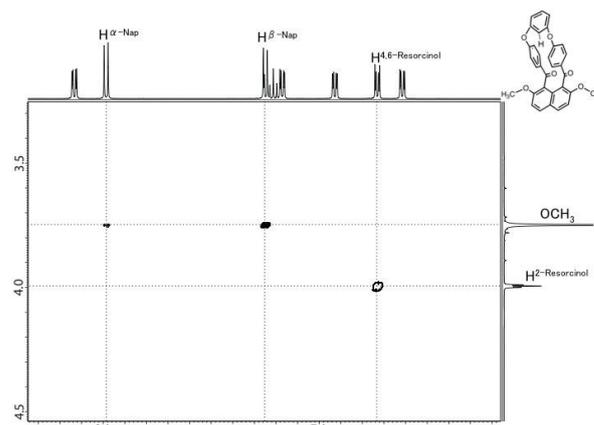

Figure 4. ^{1}H–^{1}H COSY spectrum of compound (**2a**), 500 MHz, at 293 K compound (**2a**) (*ca*. 0.02 mmol) was dissolved in CDCl₃ (0.5 mL).

This higher magnetic field deviation clearly displays the presence of significant and specific magnetic field effect. This is interpreted as caused by the rather fixed conformation, in which the H atom of resorcinol moiety is situated upon both of two benzene rings of the aroyl groups, i.e., being sandwiched among two aromatic π-systems resulting in doubly efficient shielding effect.

The signals of the methoxy groups at 2- and 7-positions of the naphthalene rings of bridged compounds (**1a**) and (**2a**) are observed as singlet in ordinary alkoxy region of the ^{1}H NMR spectra at about δ 3.5 to 4.5 ppm (Figure 5). The geminal protons of methyleneoxy group of ethoxy groups at 2- and 7-positions in non-bridged compound (**3b**) also show equivalency. On the other hand, in the ^{1}H NMR spectra of the bridged compounds (**1b**) and (**2b**), geminal non-equivalent signals appear. The ethoxy groups at 2- and 7-positions of the naphthalene rings are plausibly bulky enough to be restricted in rotation by the spatial hindrance of the fixed benzoyl groups. So the signals of –CH₂O– are distinguished as geminally non-equivalent.

By connecting the two benzoyl groups of *peri*-aroylnaphthalene compounds, the rotation ability of the aromatic rings in the benzoyl moieties is reduced. On the other hand, the different shapes of signals between catechol-hinge-bearing bridged compound and resorcinol-hinge homologue reflect the difference in spatial arrangement and flexibility regulated by the substitution positions of the benzene ring connecting to the benzoyl groups to a greater or lesser degree (Figure 6).

Figure 3. ^{1}H NMR study of compounds **3b**, **1b**, and **2b** in CDCl₃ (aromatic region).

We consider that the resorcinol-hinge moiety has relatively fixed conformation and the rotation of aromatic rings is strictly regulated in solution at room temperature. The spatial structure in solution may be closed to that in crystal state but the crystal structure has not been established so far. The rather flexible catechol-hinge-bearing molecule probably transforms the connected catechol moiety from standing up formation to lying down one repeatedly.
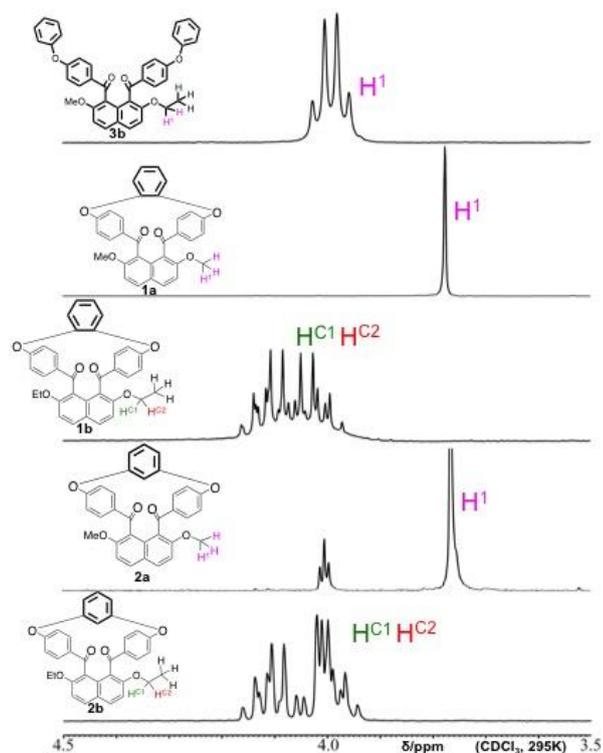

Figure 5. ¹H NMR study of compounds **3b**, **1a**, **1b**, **2a**, and **2b** in CDCl₃ (δ 3.5–4.5 ppm).
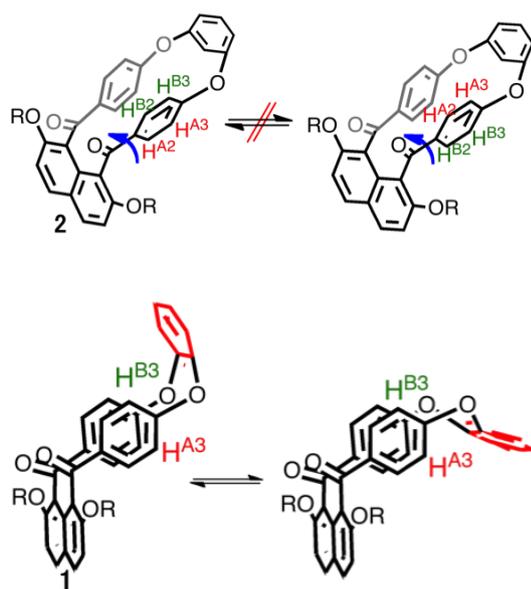

Figure 6. Plausible motions of bridged compounds **2** and **1** in solution.

Conclusion

We have studied the characteristic features of the spatial organization of bridged compounds (**1**) and (**2**) in solution by the aid of ¹H NMR spectroscopy. Signals of H atoms of the benzoyl groups appear with distinct shift values and different broadness. The observation is in accordance with the proposed structure in solution phase having restricted rotation for the benzene rings of benzoyl groups. There is a rather large differentiating feature between catechol-hinge compound and resorcinol-hinge one. A much higher magnetic field deviation of the signal of the proton at 2-position of resorcinol moiety in compound (**2**) indicates that the H atom is sandwiched and fixed between the π-systems of two benzoyl moieties. The bridged compound (**1**) also has a restricted rotation of the aromatic rings in the benzoyl moieties, whereas there is a free movement in the catechol-hinge-moiety. Furthermore, the rotation ability of the alkoxy groups in 2- and 7-positions in the naphthalene ring is proved to be reduced significantly. The molecular spatial organization of bridged *peri*-aroylnaphthalene compounds are shown to be highly congested. The tight arrangement of the aromatic rings in these compounds is crucial enough to be detected as deviation of chemical shift, shape of the signals of aromatic ring H atoms, and geminal non-equivalency in the adjacent alkoxy groups by ¹H NMR spectroscopy.

References

[1]Liu J, Lam, J. W. Y., Tang, B. Z.; *Chem. Rev.,* **2009**, *109*, 5799-5867.

[2]Masuda,T., *J. Polym. Sci., Part A Polym. Chem.,* **2007**, *45*, 165-180.

[3] Hoven, C. V., Garcia, A., Bazan, G. C., Nguyen, T. Q., *Adv. Mater.,* **2008***, 20*, 3793-3810.

[4]Bunz, U. H. F., Menning, S., Martin, N., *Angew. Chem. Int. Ed.*, **2012**, *51*, 7094–7101.

[5]Kayahara, E.; Patel, V. K.; Yamago, S., *J. Am. Chem. Soc.*, **2014**, *136*, 2284-2287.

[6]Pawlicki,M., Garbicz, M., Szterenberg, L., Latos-Grazynski, L., *Angew. Chem. Int. Ed.,* **2014**, *53*, 1-5.

[7]Cougnon, F. B. L., Ponnuswamy, N., Pantos, G. D., Sanders, J. K. M., *Org. Biomol. Chem.,* **2015**, in press

[8]Cohen, S., Thirumalaikumar, M., Pogodin, S., Agranat, I., *Struct. Chem.*, **2004**, *15*, 339-346.

[9]Jing, L.-H., Qin, D.-B., He, L., Gu, S.-J., Zhang, H.-X., Lei, G., *Acta Cryst.,* **2005**, *E61*, o3595–o3596.

[10]Okamoto, A., Yonezawa, N., *Chem. Lett.,* **2009**, *38*, 914.

[11]Okamoto, A, Mitsui, R., Yonezawa, N., *Chem. Lett.,* **2011**, *40*, 1283.

[12]Okamoto, A.; Watanabe, S.; Nakaema, K.; Yonezawa, N.; *Cryst. Str. Theo. Appl.,* **2012**, *1*,121-127.

[13]Okamoto, A., Yoshiwaka, S.; Mohri, S.; Hijikata, D.; Yonezawa, N.; *Eur. Chem. Bull.,* **2014**, *3(8)*, 829–834.

[14]Nakaema, K.; Noguchi, K., Okamoto, A., Yonezawa, N., *Acta Cryst.,* **2008**, *E64*, o2497.

[15]Sasagawa, K., Sakamoto, R., Kusakabe, T., Okamoto, A., Yonezawa, N., *Acta Cryst.*, **2013,** *E69*, o146.

[16]Sasagawa, K., Sakamoto, R., Takeuchi, R., Yonezawa, N., Okamoto, A., *Acta Cryst.*, **2013,** *E69,* o395–o396.

[17]Sasagawa, K., Sakamoto, R., Hijikata, D., Yonezawa, N., Okamoto, A., *Acta Cryst.*, **2013,** *E69,* o651.

[18]Yoshiwaka, S., Hijikata, D., Sasagawa, K., Okamoto, A., Yonezawa, N., *Acta Cryst.*, **2013**, *E69*, o242.

[19]Mohri, S., Ohisa, S., Noguchi, K., Yonezawa, N., Okamoto, A., *Acta Cryst.,* **2014,** *E70*, 138-141.

[20]Hijikata, D., Takada, T., Nagasawa, A., Okamoto, A., Yonezawa, N., *Acta Cryst.*, **2010,** *E66*, o2902–o2903.

[21]Yoshiwaka, S., Sasagawa, K., Noguchi, K., Okamoto, A., Yonezawa, N. *Acta Cryst.*, **2014**, *C70*, 1096–1100.

[22]Yoshiwaka, S., Ohisa, S., Yonezawa, N., Okamoto, A., *Eur. Chem. Bull.,* **2014**, *3(12)*, 1142–1147.

[23]Armarego, W.L. F., Perrin, D. D., "*Purification of Laboratory Chemicals",* Fourth edition, Reed Educational and Professional Publishing Ltd, Oxford, **1996**.

[24]Domasevitch, K. V., Solnsev, P. V., Krautscheid, H., Zhylenko, I. S., Rusanov, E. B., Chernega, A. N., *Chem. Commun.,* **2012**, *48*, 5847.

[25]Kuwano, R., Morioka, R., Kashiwabara, M., Kameyama, N., *Angew. Chem., Int. Ed*., **2012**, *51*, 4136.

SYNTHESIS AND CHARACTERIZATION OF SOME NEW γ-LACTAM COMPOUNDS

S. Awadh Gatea[a] and M. Shakir Magtoof [a]*

This study is concerned with the synthesis and characterization of γ-lactams **3a-3h**. These compounds were prepared by reacting phenylsuccinic anhydride with the appropriate Schiff bases (imines) **2a-2h** by heating at 51-61 °C in chloroform with moderate yields (70-92 **%**). The structures of these γ-lactams were established on the basis of the spectral studies using IR, ^{1}H-NMR,^{13}C-NMR, HSQC ^{1}H-^{13}C-NMR, and MS.

*Corresponding Authors
    Tel: 009647813199256
    E-Mail: Mahmood672000@yahoo.com
[a] Department of Chemistry, Science, College, Thiqar
     University, Thiqar, Nashyria, Iraq.

Introduction

Five-membered ring lactams, which are known as γ-lactams or 2-oxopyrrolidines (Figure 1), are important structural motifs in biologically active natural products and are used in medicines and approved drugs.[1]
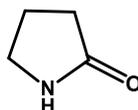

Figure 1. γ-Lactam ring

γ -Lactams have attracted great attention in recent years because they are valuable building blocks in synthesis, and due to the presence of a γ-lactam core are present in the structure of several biologically active molecules.[2] Substituted γ-lactams, in particular, have potential application in drug synthesis, but the development of stereoselective synthesis of chiral γ-lactams remains a challenge.[3,4]

Developing effective and simple synthetic methods is important so that the drug candidates can be screened. A stereoselective addition to a γ-lactam skeleton provides a direct and efficient method for synthesizing various γ-lactam derivatives. However, the most commonly used methods for synthesizing chiral γ-lactams are based on the cyclization or cycloaddition of N-containing precursors, which are synthesized stereoselectively, and there are limited studies on the stereoselective additions to γ-lactam skeletons.[5-7]

Experimental part

All solvents were distilled/dried prior to use, whenever this seemed necessary, by standard methods. All solvent extracts were dried over anhydrous sodium sulphate unless other wise specified.

The ^{1}H-NMR spectra were recorded using VARIAN spectrophotometer (300 MHz), the ^{13}C-NMR spectra were recorded using VARIAN spectrophotometer (75 MHz), and the HSQC ^{1}H-^{13}C-NMR spectra were recorded using VARIAN spectrophotometer (600 MHz, 150 MHz). The chemical shift values are expressed in δ (ppm), using tetramethylsilane (TMS) as internal standard and d_6-DMSO as solvent. The mass spectra were recorded at (3 kV) and (4 kV) using HPLC-LCQ Fleet/Thermo Scientific spectrophotometer. The IR spectra were recorded using Shimadzu FT-IR affinity spectrophotometers as KBr disks. Only principal absorption bands of interest are reported and expressed in cm^{-1}.

General Procedure for the preparation of imines 2a-2h [27-29]

Preparation of mono-imines 2a-2d.

In general, the mono-imines **2a-2d** were prepared by reacting the mixture of 0.01 mol amine with 0.01 mol aldehyde in 20 ml of chloroform and 4-6 drops of glacial acetic acid under heating in water bath at 51-61 °C. The reaction mixture was refluxed for 2-20 h with stirring. The progress of the reaction was followed by TLC. After completion, the solvent was evaporated and the residue was recrystallized from a suitable solvent.

N-(2-Chlorobenzylidene)-4-chloro-aniline 2a

The compound was prepared by reacting 1.27 g (0.01 mol) of 4-chloroaniline and 1.40 g (0.01 mol) of 2-chloro-benzaldehyde. Yield = 77 %, m.p. = 64-65 °C, IR (KBr disk) 1620 cm^{-1} (C=N).

N-(2-Bromobenzylidene)-4-chloro-aniline, 2b

The compound was prepared by reacting 1.27 g (0.01 mol) of 4-chloroaniline with 1.85 g (0.01 mol) of 2-bromobenzaldehyde. Yield = 83 %, m.p. = 74-75 °C, IR (KBr disk): 1616 cm^{-1} (C=N).

N-(2-Bromobenzylidene)-4-methyl-aniline, 2c

The compound was prepared by reacting 1.07 g, (0.01 mol) of 4-methylaniline with 1.85 g (0.01 mol) of 2-bromobenzaldehyde. Yield = 80 %, m.p. = 43-44 °C, IR (KBr disk): 1616 cm^{-1} (C=N).

N-(2-Fluorobenzylidene)-4-methyl-aniline, 2d

The compound was prepared by reacting 1.07 g (0.01 mol) of 4-methylaniline with 1.24 g (0.01 mol) of 2-fluorobenzaldehyde. Yield = 90 %, m.p = 44-45 °C, IR (KBr disk): 1624 cm^{-1} (C=N).

Preparation of bis-imines, 2e-2h .

In general, the bis-imines **2e-2h** were prepared by reacting the mixture of 0.01 mol amine with 0.02 mol of aldehyde in 20 mL of chloroform and 4-6 drops of glacial acetic acid under heating in water bath at 51-61°C, The reaction mixture was refluxed for 2-20 h with stirring. The progress of the reaction was followed by TLC. After completion, the solvent was evaporated and the residue was recrystallized from a suitable solvent.

N^1,N^4-Bis(2-chlorobenzylidene)benzene-1,4-diamine, 2e

The compound was prepared by reacting 1.08 g (0.01 mol) of *p*-phenylenediamine with 2.80 g (0.02 mol) of 2-chlorobenzaldehyde. Yield = 88 %, m.p = 150-151 °C, IR (KBr disk): 1612 cm^{-1} (C=N).

N^1,N^4-Bis(2-fluorobenzylidene)benzene-1,4-diamine, 2f

The compound was prepared by reacting 1.08 g (0.01 mol) of *p*-phenylenediamine with 2.48 g (0.02 mol) of 2-fluorobenzaldehyde. Yield = 60 %, m.p = 94-96 °C, IR (KBr): 1612 cm^{-1} (C=N).

N^1,N^5-Bis(2-chlorobenzylidene)naphthalene-1,5-diamine, 2g

The compound was prepared by reacting 1.58 g (0.01 mol) of 1,5-diaminonaphthalene with 2.80 g (0.02 mol) of 2-chlorobenzaldehyde. Yield = 89 %, m. p. =240-241 °C, IR (KBr disk): 1612 cm^{-1} (C=N).

N^1,N^5-Bis(4-methoxybenzylidene)naphthalene-1,5-diamine, 2h

The compound was prepared by reacting 1.58 g (0.01 mol) of 1,5-diaminonaphthalene with 2.72 g (0.02 mol) of 4-methoxybenzaldehyde. Yield = 85 %, m.p =180-182 °C, IR (KBr disk): 1620 cm^{-1} (C=N).

General procedure for the preparation of γ-lactams 3a-3h [30,31]

Preparation of mono-γ-lactams 3a-d

In general, the mono-γ- lactams **3a-3d** were prepared by reacting the mixture of 0.01 mol of mono-imine **2a-2d** with 0.01 mol of phenylsuccinic anhydride in 20 ml of chloroform and heating the mixture in water bath at 51-61 °C. The reaction mixture was refluxed for 12-16 h with stirring. The progress of the reaction was followed by TLC. After completion, the solvent was evaporated, and the residue was recrystallized from a suitable solvent.

(E,Z)-2-(2-Chlorophenyl)-1-(4-chlorophenyl)-5-oxo-3-phenyl-pyrrolidine-3-carboxylic acid, 3a

The compound was prepared by reacting 2.50 g (0.01 mol) of N-(2-chlorobenzylidene) 4-chloroaniline (**2a**) with 1.76 g (0.01 mol) of phenylsuccinic anhydride. Yield = 78 %, m.p = 153-154 ºC, IR (KBr): 1658 cm^{-1} (HO–C=O), 1705 cm^{-1} (–N–C=O). **For major isomer (Z-isomer):** yield = 55 %, ^{1}H-NMR (300 MHz, DMSO) data: δ 2.64-2.72 ppm (*dd*, *J* = 6, 6 Hz, 1H), 3.04-3.13 ppm (*dd*, *J* = 9, 12 Hz, 2H), 4.00-4.05 ppm (*dd*, *J* = 6, 6 Hz, 1H), 7.61-7.24 ppm (*m*, 13H), 10.11 ppm (*s*, 1H), ^{13}C-NMR (75 MHz, DMSO) data : δ. 39.60 ppm, 46.77 ppm, 120.42 ppm, 120.47 ppm, 126.51 ppm, 126.64 ppm, 127.10 ppm, 127.11 ppm, 127.53 ppm, 127.70 ppm, 128.56 ppm, 128.59 ppm, 138.05 ppm, 138.93 ppm, 139.32 ppm , 169.27 ppm, 174.12 ppm. **For minor isomer (E-isomer):** yield = 45 %; ^{1}H-NMR (300 MHz, DMSO) data, δ: 2.55-2.62 ppm (*dd*, *J* =3, 6 Hz, 1H), 3.04-3.13 ppm (*dd*, *J*=9, 12Hz, 2H), 4.07-4.12 ppm (*dd*, *J*=3, 6 Hz, 1H), 7.24-7.61 ppm (*m*, 13H); 10.29 ppm (*s*, 1H), ^{13}C-NMR (75 MHz, DMSO) data: δ: 37.33 ppm, 47.97 ppm, 120.42 ppm, 120.47 ppm, 126.51 ppm, 126.64 ppm, 127.10 ppm, 127.11 ppm, 127.53 ppm, 127.70 ppm, 128.56 ppm, 128.59 ppm, 138.05 ppm, 138.93 ppm, 139.32 ppm, 171.03 ppm, 172.74 ppm.

(E,Z)-2-(2-Bromophenyl)-1-(4-chlorophenyl)-5-oxo-3-phenyl-pyrrolidine-3-carboxylic acid, 3b

The compound was prepared by reacting 2.94 g (0.01 mol) of N-(2-bromobenzylidene)-4-chloroaniline (**2b**) with 1.76 g (0.01 mol) of phenylsuccinic anhydride. Yield = 70 %, m.p. = 160-161 ºC, IR (KBr disk): 1658 cm^{-1} (HO–C=O), 1705 cm^{-1} (–N–C=O). For **major isomer (Z-isomer)**: Yield = 66 %, ^{1}H-NMR (300 MHz, DMSO) : δ 2.64-2.71 ppm (*dd*, *J* = 6, 6 Hz, 1H), 3.04-3.13 ppm (*dd*, *J* = 9, 12 Hz, 2H); 3.99-4.05 ppm (*dd*, *J* = 6, 6 Hz, 1H; 7.61-7.24 ppm (*m*, 13H), 10.12 ppm (*s*, 1H); ^{13}C-NMR (75 MHz, DMSO) data: δ: 39.60 ppm, 46.78 ppm, 120.41 ppm, 120.46 ppm, 126.50 ppm, 126.63 ppm, 127.11 ppm, 127.53 ppm, 127.70 ppm, 128.58 ppm, 138.05 ppm, 138.18 ppm, 138.94 ppm, 139.32 ppm, 169.27 ppm, 174.11 ppm. For **minor isomer (E-isomer):** yield = 34 %, ^{1}H-NMR (300 MHz, DMSO): δ: 2.55- 2.62 ppm (*dd*, *J* = 3, 6 Hz, 1H), 3.04-3.13 ppm (*dd*, *J* = 9, 12 Hz, 2H), 4.06-4.11 ppm (*dd*, *J*=6, 3 Hz, 1H); 7.24-7.61 ppm (*m*, 13H); 10.29 ppm (*s*, 1H), ^{13}C-NMR (75 MHz, DMSO): δ 37.33 ppm; 47.97 ppm; 120.41 ppm, 120.46 ppm, 126.50 ppm, 126.63 ppm, 127.11 ppm, 127.53 ppm, 127.70 ppm, 128.58 ppm, 138.05 ppm, 138.18 ppm, 138.94 ppm, 139.32 ppm, 172.74 ppm, 171.02 ppm.

(E)-2-(2-Bromophenyl)-5-oxo-3-phenyl-1-(p-tolyl)pyrrolidine-3-carboxylic acid, 3c

The compound was prepared by reacting 2.74 g (0.01 mol) N-(2-bromobenzylidene)-4-methylaniline (**2c**) with 1.76 g (0.01 mol) phenylsuccinic anhydride. Yield = 88 %, m.p = 159-160ºC, IR (KBr disk): 1651 cm^{-1} (HO–C=O), 1701 cm^{-1} (–N–C=O). ^{1}H-NMR (300 MHz, DMSO) data: δ: 2.22 ppm (*s*, 3H), 2.54-2.61 ppm (*dd, J* = 6, 3 Hz, 1H); 3.04-3.13 ppm (dd, J= 9, 12 Hz, 2H), 4.07-4.12 ppm (*dd, J* = 3, 6 Hz, 1H), (7.05–7.46) ppm, (*m*, 13H), 10.05 ppm (*s*, 1H), ^{13}C-NMR (75 MHz, DMSO) data : δ^{13}C 20.20 ppm, 37.15 ppm, 47.67 ppm, 118.73 ppm, 126.80 ppm, 127.34 ppm, 128.30 ppm, 128.82 ppm, 131.77 ppm, 136.59 ppm, 139.48 ppm, 170.36 ppm, 172.57 ppm.

(E)-2-(2-Fluorophenyl)-5-oxo-3-phenyl-1-(p-tolyl)pyrrolidine-3-carboxylic acid, 3d

The compound was prepared by reacting 2.13 g (0.01 mol) N-(2-fluorobenzylidene)-4-methylaniline (**2d**) with 1.76 g (0.01 mol) of phenylsuccinic anhydride. Yield = 90 %, m.p = 204-205 ºC, IR (KBr disk): 1651 cm^{-1} (HO-C=O), 1701 cm^{-1} (–N–C=O). ^{1}H-NMR (300 MHz, DMSO) data : δ 2.22 ppm (*s*, 3H), 2.54-2.61 ppm (*dd, J*=6, 3 Hz, 1H), 3.03-3.12 ppm (*dd*, J = 9, 12 Hz, 2H), 4.06-4.11 ppm (*dd, J*=3, 6 Hz, 1H), 6.82-7.46 ppm (m, 13H), 10.04 ppm (s, 1H), ^{13}C-NMR (75 MHz, DMSO) data : δ: 20.22 ppm, 37.15 ppm, 47.68 ppm, 118.74 ppm, 126.80 ppm, 127.35 ppm, 128.30 ppm, 128.82 ppm, 131.77 ppm, 136.59 ppm, 139.48 ppm, 170.36 ppm; 172.56 ppm.

Preparation of bis-γ-lactams 3e-3h

In general, the bis-γ-lactams **3e-3h** were prepared by reacting 0.01 mol bis-imines **2e-2h** with 0.02 mol of phenylsuccinic anhydride in 20 ml of chloroform under heating in water bath at 51-61 ˚C. The reaction mixture was refluxed for 12-16 h with stirring. The progress of the reaction was followed by TLC. After completion, the solvent was evaporated and the residue was recrystallized from a suitable solvent.

(E,Z)-1-(4-(3-Carboxy-2-(2-chlorophenyl)-5-oxo-3-phenylpyr-rolidin-1-yl)phenyl)-2-(2-chlorophenyl)-5-oxo-3-phenylpyrro-lidine-3-carboxylic acid, 3e

The compound was prepared by reacting 3.53 g (0.01 mol) N^1,N^4-bis(2-fluorobenzylidene)benzene-1,4-diamine (**2e**) with 3.52 g, (0.02 mol) of phenylsuccinic anhydride. Yield = 71 %, m.p = 180-181 ºC, IR (KBr): 1658 cm^{-1} (HO–C=O), 1701 cm^{-1} (–N–C=O). **For major isomer (Z-isomer):** yield = 69 **%**, ^{1}H-NMR (300 MHz, DMSO) data: δ 2.61-2.69 ppm (*dd, J* = 6, 6 Hz, 2H); 3.02-3.10 ppm (*dd, J* = 9, 12 Hz, 4H); 3.99-4.04 ppm (*dd, J* = 6, 6 Hz, 2H), 7.23-7.49 ppm (*m*, 22H), 9.90 ppm (*s*, 2H), ^{13}C-NMR (75 MHz , DMSO) data: δ 39.65 ppm; 46.86 ppm, 119.18 ppm, 119.24 ppm, 126.95 ppm, 127.03 ppm, 127.50 ppm, 127.69 ppm, 128.45 ppm, 134.40 ppm, 134.49 ppm, 134.52 ppm, 139.05 ppm, 139.64 ppm, 168.69 ppm, 174.15 ppm. **For minor isomer (E-isomer):** yield 31 %, ^{1}H-NMR (300 MHz, DMSO) data : δ: 2.54-2.61 ppm (*dd, J* = 3, 6 Hz, 2H), 3.02-3.10 ppm (dd, J =

9, 12 Hz, 4H), 4.05-4.11 ppm (*dd, J* = 6, 3 Hz, 2H), 7.23-7.49 ppm (*m*, 22H), 10.08 ppm (*s*, 2H), ^{13}C-NMR (75 MHz, DMSO) data : δ: 37.33 ppm, 47.81 ppm, 119.18 ppm, 119.24 ppm, 126.95 ppm, 127.03 ppm, 127.50 ppm, 127.69 ppm, 128.45 ppm, 134.40 ppm, 134.49 ppm, 134.52 ppm, 139.05 ppm, 170.43 ppm, 172.75 ppm.

(E,Z)-1-(4-(3-Carboxy-2-(2-fluorophenyl)-5-oxo-3-phenylpyr-rolidin-1-yl)phenyl)-2-(2-fluorophenyl)-5-oxo-3-phenylpyrro-lidin-3-carboxylic acid, 3f

The compound was prepared by reacting 3.20 g (0.01 mol) N^1,N^4-bis(2-fluorobenzylidene)benzene-1,4-diamine (**2f**) with 3.52 g (0.02 mol) phenylsuccinic anhydride. Yield = 90 %, m.p = 185-186º C, IR (KBr disk): 1658 cm^{-1} (HO–C=O), 1701 cm^{-1} (–N–C=O). **For major isomer (Z-isomer):** yield = 76%, ^{1}H-NMR (300 MHz, DMSO) data : δ 2.61-2.68 ppm (*dd, J* = 6, 6 Hz, 2H); 3.01-3.10 ppm (*dd, J*=9, 12 Hz, 4H); 3.99-4.04 ppm (*dd, J* = 6, 6 Hz, 2H); 7.23-7.64 ppm (*m*, 22H), 9.90 ppm (*s*, 2H), ^{13}C-NMR (75 MHz, DMSO) data : δ: 39.69 ppm, 46.90 ppm, 119.26 ppm, 126.97 ppm, 127.05 ppm, 127.53 ppm, 127.71 ppm, 128.48 ppm, 128.55 ppm, 134.43 ppm, 134.51 ppm, 139.08 ppm, 139.67 ppm, 168.72 ppm, 174.18 ppm. HSQC ^{1}H-^{13}C NMR (600 MHz, 150 MHz, DMSO) data: (2.67, 39.40) ppm, (3.06, 39.40) ppm, (4.02, 46.61) ppm, {(7.26, 126.83), (7.27, 128.24), (7.32, 128.10), (7.34, 128.30), (7.38, 127.33), (7.43, 118.94), (7.45, 119.00), (7.46, 119.01)} ppm. **For minor isomer (E-isomer):** yield 24 %, ^{1}H-NMR (300 MHz, DMSO) data δ: 2.53-2.61 ppm (*dd, J* = 3, 6 Hz, 2H), 3.01-3.10 ppm (*dd, J* = 9, 12 Hz, 4H), 4.05-4.10 ppm (*dd, J* = 6, 3 Hz, 2H), 7.23-7.64 ppm (*m*, 22H), 10.08 ppm (*s*, 2H), ^{13}C-NMR (75 MHz, DMSO) data: δ 37.37 ppm, 47.84 ppm,119.26 ppm, 126.97 ppm, 127.05 ppm, 127.53 ppm, 127.71 ppm, 128.48 ppm, 128.55 ppm, 134.43 ppm, 134.51 ppm, 139.08 ppm, 139.67 ppm, 170.46 ppm, 172.77 ppm. HSQC ^{1}H-^{13}C NMR (600 MHz, 150 MHz, DMSO) data: (2.56, 37.08) ppm, (3.07, 37.09) ppm, (4.08, 47.55) ppm, {(7.26, 126.83), (7.27, 128.24), (7.32, 128.10), (7.34, 128.30), (7.38, 127.33), (7.43, 118.94), (7.45, 119.00), (7.46, 119.01)} ppm.

(E,Z)-1-(5-(-3-Carboxy-2-(2-chlorophenyl)-5-oxo-3-phenylpyr-rolidin-1-yl)naphthalen-1-yl)-2-(2-chlorophenyl)-5-oxo-3-phe-nylpyrrolidine-3-carboxylic acid, 3g

The compound was prepared by reacting (4.03 g, 0.01 mol) N^1,N^5-bis(2-chlorobenzylidene)-1,5-diaminonaphth-alene (**2g**) with (3.52 g, 0.02 mol) of phenylsuccinic anhydride. Yield = 84 %, m.p = 244-245 ºC, IR (KBr disk) 1654 cm^{-1} (HO–C=O), 1705 cm^{-1} (–N–C=O). ^{1}H-NMR (300 MHz, DMSO) data: **For major isomer (Z-isomer):** yield=81 %; δ 2.84-2.92 ppm (*dd, J* = 6, 6 Hz, 2H); 3.18-3.27 ppm (*dd, J* = 12, 9 Hz, 4H), 4.05 -4.10 ppm (*t, J* = 6, 9 Hz, 2H), 7.08-8.38 ppm (*m*, 24H), 9.96 ppm (*s*, 2H), ^{13}C-NMR (75 MHz, DMSO) data : δ: 39.36 ppm; 47.20 ppm; 120.27 ppm, 121.97 ppm, 125.11 ppm, 127.09 ppm, 127.58 ppm, 127.84 ppm, 128.53 ppm, 128.67 ppm, 128.91 ppm, 133.57 ppm, 138.93 ppm, 169.62 ppm, 174.17 ppm. **For minor isomer (E-isomer):** yield=19 %, δ: 2.62- 2.69 ppm (*dd, J* = 3, 6 Hz, 2H); 3.18-3.27 ppm (*dd, J* = 12, 9 Hz, 4H), 4.34-4.39 ppm (*dd, J* = 3, 6 Hz, 2H), 7.08-8.38 ppm (*m*,

24H); 10.16 ppm (*s*, 2H), ^{13}C-NMR (75 MHz, DMSO) data :
δ: 37.33 ppm, 47.31 ppm, 119.18 ppm, 119.24 ppm, 126.95 ppm, 127.03 ppm, 127.50 ppm, 127.69 ppm, 128.45 ppm, 134.40 ppm, 134.49 ppm, 134.52 ppm, 139.05 ppm, 139.64 ppm, 171.62 ppm, 172.86 ppm.

(*E*,*Z*)-1-(5-(-3-Carboxy-2-(4-methoxyphenyl)-5-oxo-3-phenyl-pyrrolidin-1-yl)naphthalene-1-yl)-2-(4-methoxyphenyl)-5-oxo-3-phenyl-pyrrolidine-3-carboxylic acid, 3h

The compound was prepared by reacting 3.94 g (0.01 mol) N^1,N^5-bis(4-methoxybenzylidene)-1,5-diamino-naphthalene **(2h)** with 3.52 g (0.02 mol) phenylsuccinic anhydride. Yield = 85 %, m.p = 214-216 ℃, IR (KBr disk): 1654 cm^{-1} (HO–C=O), 1708 cm^{-1} (–N–C=O). **For major isomer (*Z*-isomer):** yield = 70 %, ^{1}H-NMR (300 MHz, DMSO) data: δ: 2.85-2.94 ppm (*q, J* = 6, 6, 9, 6 Hz, 2H); 3.10-3.29 ppm (*m, J* = 9, 12, 9, 6 Hz, 4H); 3.86 ppm (*s*, 6H); 4.05-4.12 ppm (*dd, J* = 6, 6 Hz, 2H); 7.11-8.61 ppm (*m*, 24H); 9.95 ppm (*s*, 2H), ^{13}C-NMR (75 MHz, DMSO) data: δ: 39.34 ppm, 47.18 ppm, 55.45 ppm, 114.42 ppm, 114.54 ppm, 120.20 ppm, 121.99 ppm, 122.24 ppm, 125.13 ppm, 127.11 ppm, 127.60 ppm, 127.85 ppm, 128.49 ppm, 128.55 ppm, 128.93 ppm, 129.04 ppm, 129.09 ppm, 130.69 ppm, 131.76 ppm, 133.36 ppm, 133.59 ppm, 138.91 ppm, 139.74 ppm, 144.38 ppm, 169.73 ppm, 174.17 ppm. **For minor isomer (*E*-isome**r): yield=30 %, 1H-NMR (300 MHz , DMSO) data: δ 2.62- 2.69 ppm (*dd, J* = 3, 3 Hz, 2H), 3.10-3.29 ppm (*m, J* = 9, 12, 9, 6 Hz, 4H); 3.86 ppm (*s*, 6H), 4.34-4.39 ppm (*dd, J* = 6, 6 Hz, 2H), 7.11-8.61 ppm (*m*, 24H), 10.16 ppm (*s*, 2H); ^{13}C -NMR (75 MHz, DMSO) data: δ: 37.33 ppm; 47.32 ppm, 55.65 ppm, 114.42 ppm, 114.54 ppm, 120.20 ppm, 121.99 ppm, 122.24 ppm, 125.13 ppm, 127.11 ppm, 127.60 ppm, 127.85 ppm, 128.49 ppm, 128.55 ppm, 128.93 ppm, 129.04 ppm, 129.09 ppm, 130.69 ppm, 131.76 ppm, 133.36 ppm, 133.59 ppm, 138.91 ppm, 139.74 ppm, 144.38 ppm, 171.63 ppm, 172.85 ppm.

RESULTS AND DISCUSSION

γ-Lactams represent important substructures for the synthesis of natural products,[8-12] and biologically important compounds in drug discovery [13-16]. The prevalence of these structures has resulted in the development of many efficient syntheses [17–22], which have led to the production of diverse libraries of small molecules for biological evaluation [16,23,24]. γ-lactams **3a-3h** are obtained from reaction of imines with phenylsuccinic anhydride.

3a   **3b**

3c   **3d**

3e

3f

3g   **3h**
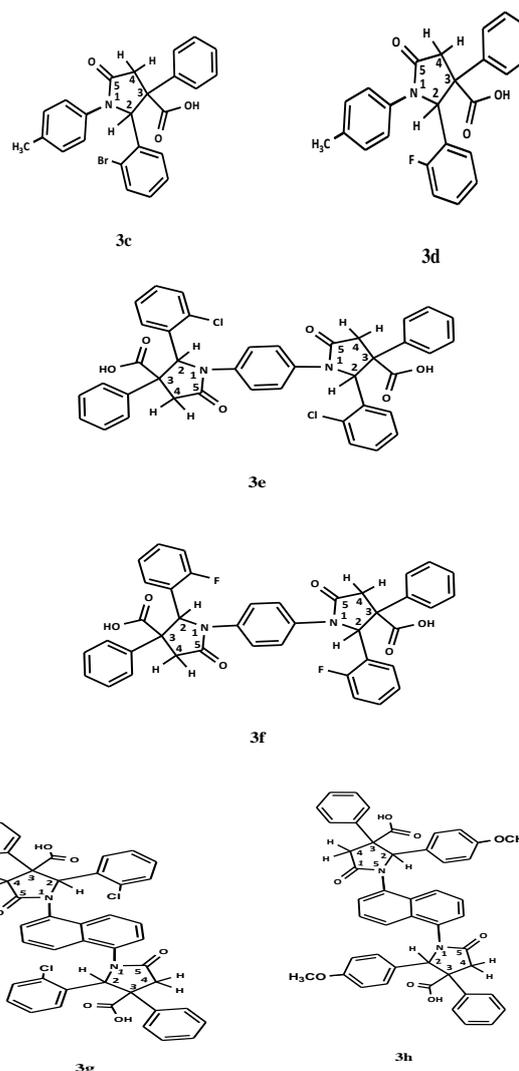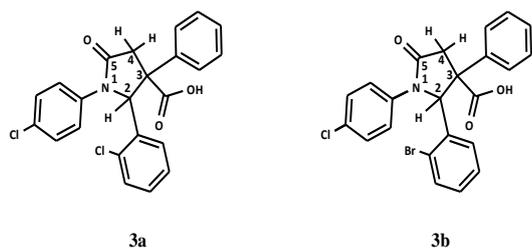
The general reaction of mono-γ-lactams **3a-3d** is outlined in Scheme 1. It is the reaction between phenylsuccinic anhydride with mono-imines **2a-2d** in chloroform solvent to yield the products mono-γ-lactams **3a-3d**, and these are shown in Table 1.
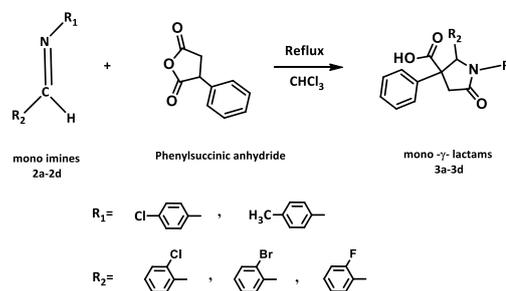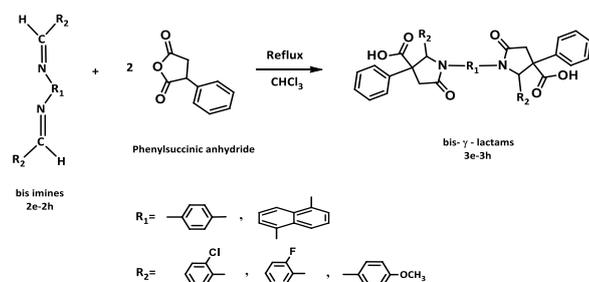

Scheme 1.

The general reaction of bis-γ-lactams **3e-3h** is outlined in Scheme 2. It is the reaction between phenylsuccinic anhydride with bis-imines **2e-2h** in chloroform solvent to yield the products bis-γ-lactams **3e-3h** as shown in Table 2**.**
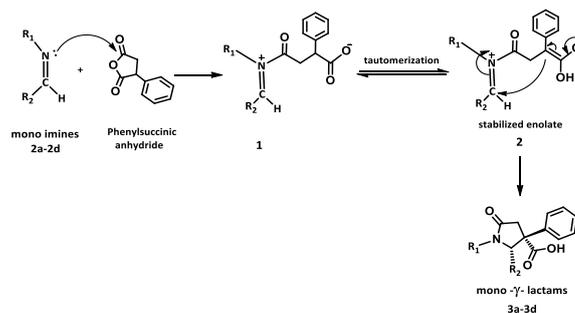
Scheme 2.

Scheme 3.

Table 1. Mono-γ-lactam **3a-3d** compounds and its imines **2a-2d**

| Imines	Mono-γ-lactams	R^1	R^2
2a	3a	Cl	Cl
2b	3b	Cl	Br
2c	3c	H$_3$C	Br
2d	3d	H$_3$C	F

Scheme 4

The general mechanism [25,26] of these reactions involve formation of a zwitterionic enolate intermediate **1,3** from a phenylsuccinic anhydride, and the formation of enolate **2,4** is favored by delocalization of negative charge into the electron deficient aromatic ring if one is suitably positioned. This is how the lactam ring is formed.

Table 2 . bis-γ-lactam **3e-3h** compounds and its imines **2e-2h**

Imines	Bis-γ-lactams	R^1	R^2
2e	3e		Cl
2f	3f		F
2g	3g		Cl
2h	3h		OCH$_3$
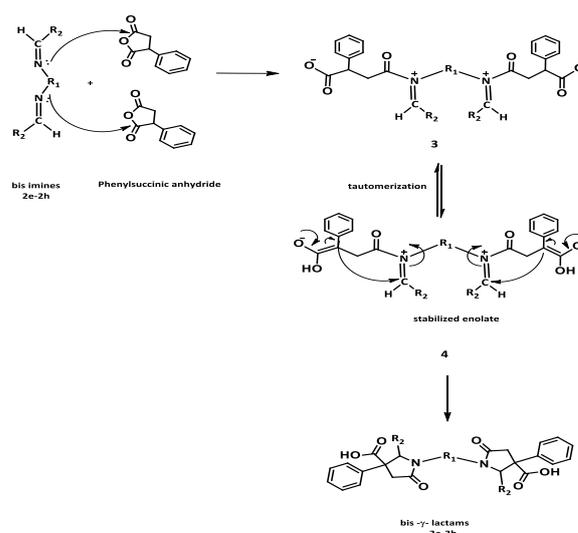
Infrared (IR) spectral analysis

The **IR** spectra of mono-γ-lactam **3a-3d)** and bis-γ-lactam **3e-3h)** are characterized by the six bands corresponding to the stretching vibration of the aromatic C-H, aliphatic C-H, carbonyl carboxylic group, carbonyl amide group, aromatic C=C and substituted ring which occurs within the ranges 3025-3082, 2735-2958, 1651-1658, 1701-1708, 1512-1612 and 817-983 cm^{-1} respectively.

^{1}H-NMR spectral analysis

The ^{1}H-NMR spectra of 2-(2-chlorophenyl)-1-(4-chlorophenyl)-5-oxo-3-phenylpyrrolidine-3-carboxylic acid **3a**, shows the presence of **syn (Z) isomer (major isomer)**: in pyrrolidine-2-one ring double doublet signal at δ (2.64-2.72) ppm with *J* = 6 Hz, 6 Hz for one proton (*dd*, 1H, C$_4$-H), and for **anti (E) isomer (minor isomer)** : in pyrrolidine-2-one ring double doublet signal at δ (2.55-2.62) ppm with *J* = 6 Hz, 3 Hz for one proton (*dd*, 1H, C$_4$-H), Fig. 2. and double doublet signal at δ (3.04-3.13) ppm with *J* = 9 Hz, 12 Hz for two protons (dd, 2H, C$_4$-H) of **syn isomer** and **anti isomer**, Fig. 3.
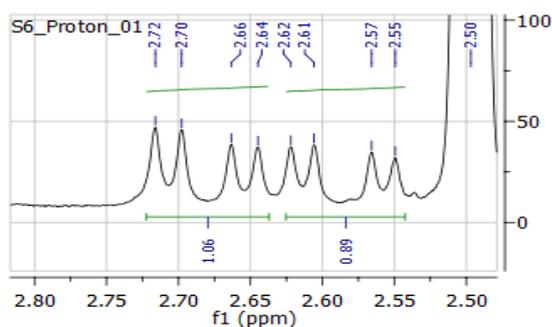
Figure 2. Selected ^{1}H NMR signals of the **syn-3a** isomer
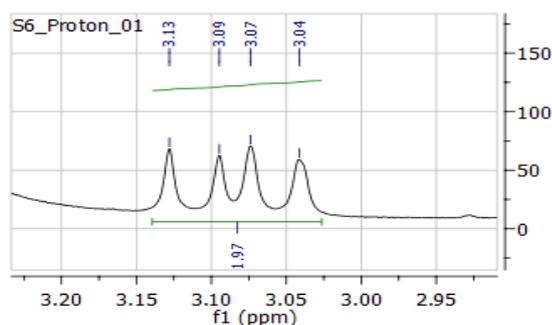
Figure 3. Selected ^{1}H NMR signals of the **anti-3a** isomer

A double doublet signal at δ 4.00-4.05 ppm with J = 6 Hz, 6 Hz for one protons (*dd* , H, C_2-H) of **syn isomer**, and a double doublet signal at δ 4.07-4.12 ppm with J = 3 Hz, 6 Hz for one proton (*dd*, 2H, C_2-H) of **anti isomer can be seen in** Fig 4.
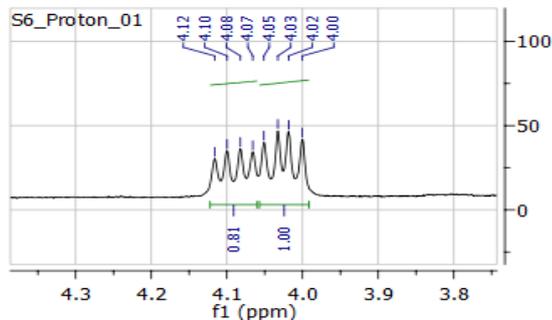
Figure 4. Selected ^{1}H NMR signals of the **anti-3a** and the **syn-3a** isomer**s**

The ^{1}H-NMR spectra of **3a** shows multiplet signal at δ 7.4-7.61 ppm for thirteen aromatic protons (*m*, 13H, aromatic protons) of **syn isomer** and **anti isomer** can be seen in Fig. 5.
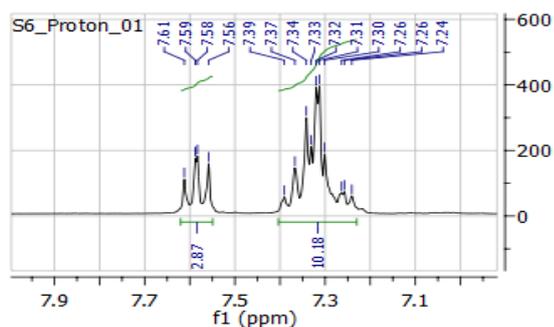
Figure 5. Aromatic ^{1}H NMR signals of the **syn-3a** and the **anti-3a** isomers

A singlet signal at δ 10.11 ppm for one proton of carboxylic group (*s*, 1H, COO-H) of **syn** isomer and the singlet signal at δ 10.29 ppm is for one proton of carboxylic group (*s*, H, COO-H) of **anti** isomer as is shown in Fig. 6.
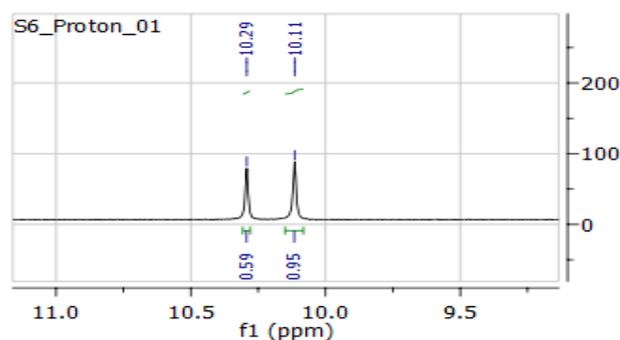
Figure 6. Carboxylic ^{1}H NMR signals of **the syn-3a** and the **anti-3a** isomers

Syn isomer (Major)

Anti isomer (Minor)
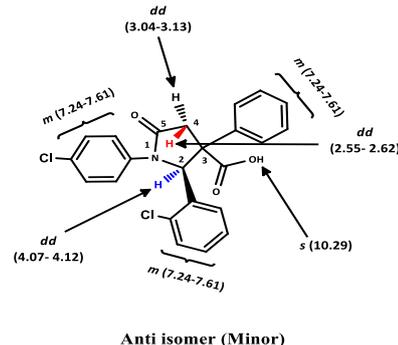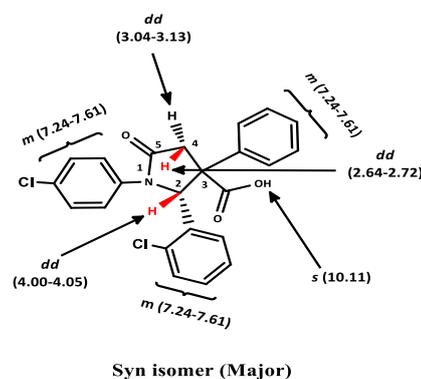
^{13}C-NMR spectral analysis

The ^{13}C-NMR spectra of the 2-(2-chlorophenyl)-1-(4-chlorophenyl)-5-oxo-3-phenylpyrrolidine-3-carboxylic acid **3a**, are shown in pyrrolidine-2-one ring: for syn (Z) isomer (major isomer) singlet signal at δ 39.60 ppm of one carbon (C_4-H_2), and for anti (E) isomer (minor isomer) singlet signal at δ 37.33 ppm of one carbon (C_4-H_2), Figure 7.

212
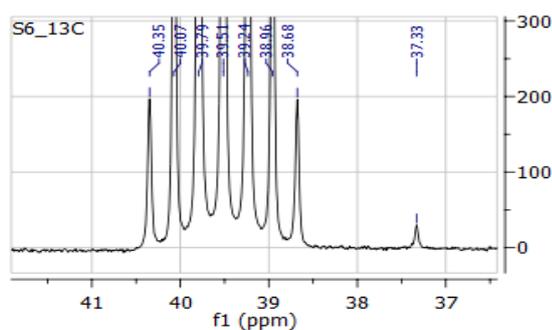
Figure 7. Pyrrolidine-2-one ring ^{13}C NMR signals of the **syn-3a** and **the anti-3a**

A singlet signal at δ 46.77 ppm is for one carbon (C$_2$-H) for **syn isomer**, and singlet signal at δ 47.97 ppm of one carbon (C$_2$-H) is for the anti isomer. The spectrum can be seen in Figure 8.

The ^{13}C-NMR spectra of the **3a** shows signals of aromatic carbons at δ 120.42, 120.47, 127.10, 127.11, 127.53, 127.70, 128.56, 128.59, 138.05, 138.19, 138.93 and 139.32 ppm for the **syn isomer** and the **anti isomer**. The spectrum can be seen in Figure 9.

Figure 8. C$_2$-H type ^{13}C NMR signals of the **syn-3a** and **the anti-3a**
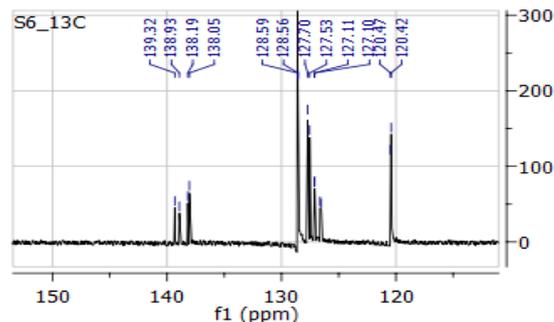
Figure 9. Aromatic ^{13}C NMR signals of the **syn-3a** and **the anti-3a**

Table 3 . ^{1}H-NMR spectral analysis of the mono-γ-lactams **3a-3d**

Mono-γ-lactams	C$_4$-H,ring, *J* Hz	C$_2$-H, ring, *J* Hz	COOH	C$_4$-H ring, *J* Hz	C$_2$-H,ring, *J* Hz	COOH
C$_{23}$H$_{17}$Cl$_2$NO$_3$	(syn isomer) Major(55 % yield)			(anti isomer) Minor (45 % yield)		
3a	2.64-2.72 (*dd*), J=6, 6, 1H	4.00-4.05, (*dd*), J=6, 6, 1H	10.11 (*s*), 1H	2.55-2.62, (*dd*), J =6, 3, 1H	4.07-4.12, (*dd*), J=3, 6, 1H	10.29 (*s*), 1H
C$_{23}$H$_{17}$BrClNO$_3$	(syn isomer) Major (66 % yield)			(anti isomer) Minor (34 % yield)		
3b	2.64-2.71, (*dd*), J=6, 6, 1H	3.99-4.05, (*dd*), J=6, 6, 1H	10.12 (*s*), 1H	2.55-2.62, (*dd*), J =3, 6, 1H	4.06-4.11, (*dd*), J=6, 3, 1H	10.29 (*s*), 1H

Mono-γ-lactams	C$_4$-H$_2$ ring, *J* Hz	C$_2$-H ring, *J* Hz	COOH
C$_{24}$H$_{20}$BrNO$_3$ anti-3c	2.54-2.61 (*dd*), J = 6, 3, 1H	4.07-4.12 (*dd*), J=3, 6, 1H	10.05 (*s*)1H
C$_{24}$H$_{20}$FNO$_3$ anti-3d	2.54-2.61 (*dd*), J=6, 3, 1H	4.06-4.11 (*dd*), J=3, 6, 1H	10.04 (*s*)1H

213

Table 4. ^{1}H-NMR spectral analysis of the bis-γ-lactams **3e-3h**

Bis-γ-lactams	C$_4$-H ring, *J* Hz	C$_2$-H ring, *J* Hz	COOH	C$_4$-H ring, *J* Hz	C$_2$-H ring, *J* Hz	COOH
C$_{40}$H$_{30}$Cl$_2$N$_2$O$_6$ **3e**	(syn isomer) Major (69% yield)			(anti isomer) Minor (31% yield)		
	2.61-2.69 (*dd*), *J*=6, 6(2H)	3.99-4.05 (*dd*), *J*=6, 6 (2H)	9.90 (*s*) 2H	2.54-2.61 (*dd*), *J* =3, 6(2H)	4.05-4.10 (*dd*) *J*=6, 3 2H	10.08 (*s*), 2H
C$_{40}$H$_{30}$F$_2$N$_2$O$_6$ **3f**	(syn isomer) Major(76% yield)			(anti isomer) Minor(24% yield)		
	2.61-2.68 (*dd*), *J*=6, 6 (2H)	3.99-4.04 (*dd*) *J*=6, 6 (2H)	9.90 (*s*), 2H	2.53-2.61 (*dd*), *J* =3, 6 (2H)	4.07-4.10 (*t*), *J*=6, 3 (2H)	10.08 (*s*), 2H
C$_{44}$H$_{32}$Cl$_2$N$_2$O$_6$ **3g**	(syn isomer) Major (81% yield)			(anti isomer) Minor(19% yield)		
	2.84-2.92 (*dd*), *J*=6, 6 (2H)	4.05-4.10 (*dd*), *J*=6, 9 (2H)	9.96(*s*), 2H	2.62-2.62 (*dd*), *J* = 3, 6 (2H)	4.07-4.12 (*dd*), *J*=3, 6 (2H)	10.16 (*s*), 2H
C$_{46}$H$_{38}$N$_2$O$_8$ **3h**	(syn isomer) Major (70% yield)			(anti isomer) Minor (30% yield)		
	2.85-2.94, *q*, *J*=6, 6, 9, 9 (2H)	4.05-4.12, (*dd*), *J*=6, 6 (2H)	9.95(*s*), 2H	2.62-2.69, (*dd*), *J* =3, 3 (2H)	4.34-4.39, (*dd*), *J*=6, 6 (2H)	10.16, (*s*), 2H

Table 5. ^{13}C-NMR spectral analysis of the mono-γ-lactams **3a-3d**

Mono-γ-lactams	C$_4$-ring, ppm	C$_2$-ring, ppm	HOC=O, ppm	-N-C=O, ppm	C$_4$-ring, ppm	C$_2$-ring, ppm	HOC=O, ppm	-N-C=O, ppm
C$_{23}$H$_{17}$Cl$_2$NO$_3$ **3a**	(syn isomer) Major (69 % yield)				(anti isomer) Minor (31 % yield)			
	39.60	46.77	169.27	171.03	37.33	47.97	172.74	174.12
C$_{23}$H$_{17}$BrClNO$_3$ **3b**	(syn isomer) Major (66 % yield)				(anti isomer) Minor (34 % yield)			
	39.60	46.78	169.27	171.02	37.33	47.97	172.74	174.11

Mono-γ-lactams	C$_4$- ring, ppm	C$_2$-ring, ppm	HO-C=O, ppm	-N-C=O, ppm
Anti, 3c C$_{24}$H$_{20}$BrNO$_3$	37.15	47.67	170.36	172.57
Anti, 3d C$_{24}$H$_{20}$FNO$_3$	37.15	47.68	170.36	172.56

Table 6. ^{13}C-NMR spectral analysis of the bis- γ-lactams **3e-3h**

Bis-γ-lactams	C$_4$-ring, ppm	C$_2$-ring, ppm	HOC=O,ppm	-N-C=O, ppm	C$_4$-ring, Ppm	C$_2$-ring, ppm	HOC=O, ppm	-N-C=O, ppm
C$_{40}$H$_{30}$Cl$_2$N$_2$O$_6$ **3e**	syn isomer (69 % yield)				anti isomer (31 % yield)			
	39.65	46.86	168.69	170.75	37.33	47.81	172.75	174.15
C$_{40}$H$_{30}$F$_2$N$_2$O$_6$ **3f**	syn isomer (76 % yield)				anti isomer (24 % yield)			
	39.69	46.90	168.72	170.46	37.33	47.84	172.77	174.18
C$_{44}$H$_{32}$Cl$_2$N$_2$O$_6$ **3g**	syn isomer (81 % yield)				anti isomer (19 % yield)			
	39.36	47.20	169.73	171.62	37.33	47.31	172.86	174.17
C$_{46}$H$_{38}$N$_2$O$_8$ **3h**	syn isomer (70 % yield)				anti isomer (30 % yield)			
	39.34	47.18	169.73	171.63	37.33	47.32	172.85	174.17

The spectrum shows a singlet signal of the carboxylic carbonyl group at δ 169.27 ppm**,** and an other singlet signal of the amide carbonyl group for the **syn isomer** at 171.03 ppm and a singlet signal of the carboxylic carbonyl group at δ 172.74 ppm, and an other singlet signal of the amidecarbonyl group carbon at 174.12 ppm (equivalent carbon).
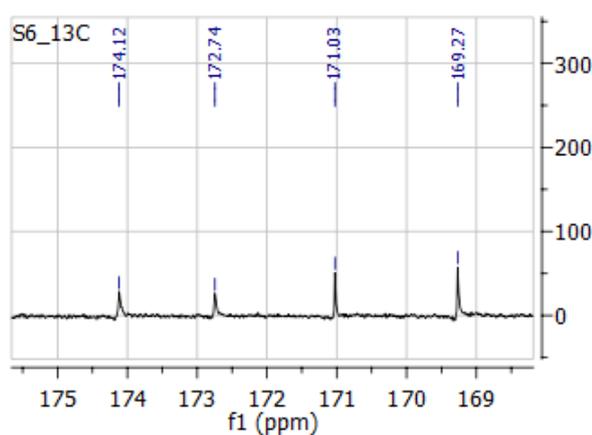
Figure 10. Selected ^{13}C NMR signals of syn-3a and anti-3a

HSQC ^{1}H-^{13}C-NMR spectral analysis

The **HSQC ^{1}H-^{13}C-NMR** spectra of **3f**, showed pyrrolidine-2-one ring: for syn (Z) isomer (major isomer), the correlation of protons signals for -CH$_2$- group at δ 2.67 ppm and δ 3.06 ppm with carbon signal at δ 39.40 ppm of same group led to the assignment of this signal to methylene group, and proton signal 4.02 ppm for -CH- group with

carbon signal of same group at 46.61 ppm, which lead to the assignment of this signal to -CH- group, and in pyrrolidine-2-one ring for anti *(E)* isomer (minor isomer): the correlation of protons signals for -CH$_2$- group,.and showed in pyrrolidine-2-one ring for anti *(E)* isomer (minor isomer): the correlation of protons signals for -CH$_2$- group at δ 2.56 ppm and δ 3.07 ppm with carbon signal at δ 37.08 ppm of same group which lead to the assignment of this signal to methylene group, and proton signal 4.08 ppm for -CH- group with carbon signal of same group at 47.55 ppm, which led to the assignment of this signal to -CH- group, (Digure 11). The HSQC ^{1}H-^{13}C-NMR spectra of the **3f** showed for syn isomer and anti isomer, the aromatic protons signals at δ 7.26, 7.27, 7.32, 7.34, 7.38, 7.43, 7.45 and 7.46 ppm correlation with carbon aromatic signals at 126.83, 128.24, 128.10, 128.30, 127.33, 118.94, 119.00 and 119.01 ppm respectively, (Figure 12).
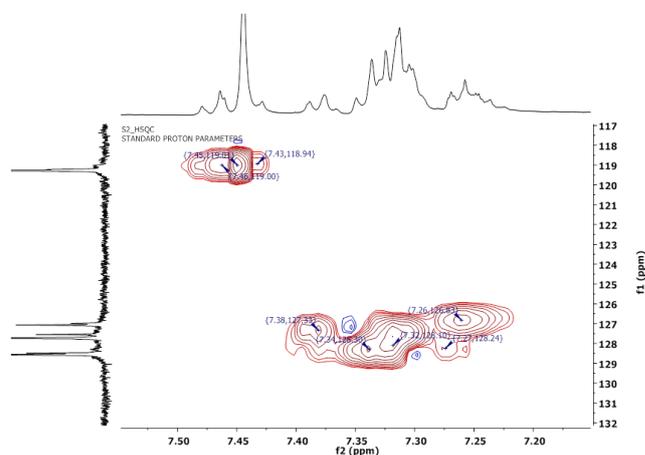
Figure 11. Selected **HSQC ^{1}H-^{13}C-NMR** spectra of the **3f**

Figure 12. Aromatic HSQC ^{1}H-^{13}C-NMR spectra of the **3f**

Mass spectral analysis

The Mass spectra of 3b, showed the molecular ion peak $[M+H]^+ = 470$, $[2M+H]^+ = 939$ and showed the important fragmentation peaks in m/z = 304 m/z = 386, m/z = 393, m/z =326, m/z =315, m/z =474, m/z = 486, m/z =607, m/z =645, m/z = 629.

The Mass spectra of 3c, showed the molecular ion peak $[M+H]^+ = 685$, $[M+Na]^+ = 450$, $[2M+H]^+ = 899$, and showed the important fragmentation peaks in m/z = 284 , m/z = 266, m/z = 238, m/z = 567, m/z = 477, m/z = 589, m/z = 605.
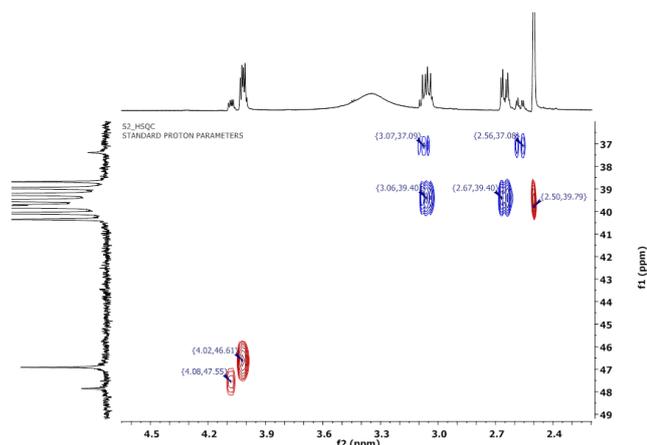
The Mass spectra of 3d (fig. 9) and (fig. 10), showed the molecular ion peak $[M+H]^+ = 390$, $[2M+H]^+ = 779$, and showed the important fragmentation peaks in m/z = 255, m/z = 371, m/z = 629, m/z = 585, m/z = 429, m/z = 412.

The Mass spectra of 3e, showed the molecular ion peak $[M+H]^+ = 705$, and showed the important fragmentation peaks in m/z = 285, m/z = 300, m/z = 341, m/z = 383, m/z = 391, m/z = 443, m/z = 461, m/z = 579.

The Mass spectra of 3h, showed the molecular ion peak $[M+H]^+ = 747$, $[2M+H]^+ = 1493$, and showed the important fragmentation peaks in m/z = 453, m/z = 533, m/z =689, m/z = 453, m/z = 905, m/z = 985, m/z = 963, m/z = 845, m/z = 809.

Acknowledgements

References

[1]Younai, A., Chin, G. F., Fettinger, J. C. and Shaw, J. T., *J. Org. Chem.*, **2010,** *75*, 8337.

[2]Nöth, J., Frankowski, K. J., Neuenswander, B., Aubé, J. and Reiser, O., *J. Comb. Chem.,* **2008,** *10*, 456.

[3]Zhao, X., DiRocco, D. A. and Rovis, T., *J. Am. Chem. Soc.,* **2011,** *133*, 12466-12469.

[4]Comesse, S., Sanselme, M. and Daïch, A., *J. Org. Chem.*, **2008,** *73*, 5566-5569.

[5]Zhang,Y., Shao, Y. -L., Xu, H. -S. and Wang, W., *J. Org. Chem.*, **2011,** *76*, 1472-1474.

[6]Shao, C., Yu, H. -J., Wu, N. -Y., Tian, P., Wang, R., Feng, C. -G. and Lin, G. -Q*., Org. Lett*., **2011,** *13*, 788-791.

[7]Lin, L., Zhang, J., Ma, X., Fu, X. and Wang, R., *Org .Lett*., **2011,** *13*, 6410-6413.

[8]Mori,T., Takahashi, K., Kashiwabara, M., Uemura, D., Katayama, C., Iwadare, S., Shizuri,Y., Mitomo, R., Nakano, F. and Matsuzaki, A., *Tetrahedron. Lett*., **1985,** *26*, 1073-1076.

[9]Feling, R. H., Buchanan, G. O., Mincer, T. J., Kauffman, C.A., Jensen, P. R. and Fenical, W., *Angew. Chem. Int. Ed*., **2003,** *42,* 355-357.

[10]Guntern, A., Ioset, J. R., Queiroz, E. F., Sandor, P., Foggin, C. M. and Hostettmann, K., *J. Nat. Prod*., **2003,** *66*, 1550-1553.

[11]Manam, R. R., Teisan, S., White, D. J., Nicholson, B., Grodberg, J., Neuteboom, S. T. C., Lam, K. S., Mosca, D. A., Lloyd, G. K. and Potts, B. C. M., *J. Nat. Prod.*, **2005,** *68*, 240-243.

[12]Okazaki,Y., Ishizuka, A., Ishihara, A., Nishioka ,T. and Iwamura ,H*., J. Org. Chem*., **2007,** *72*, 3830-3839.

[13]Stuk, T. L., Assink, B. K., Bates, R. C., Erdman, D. T., Fedij, V., Jennings, S. M., Lassig, J. A., Smith, R. J. and Smith, T. L*., Org. Proces. Res. Dev,.* **2003,** *7*, 851-855.

[14]Masse, C. E., Morgan ,A. J., Adams, J. and Panek, J. S., *Eur. J Org. Chem*., **2000,** 2513-2528.

[15]Fenical, W., Jensen, P. R., Palladino, M. A., Lam, K. S., Lloyd, G. K. and Potts, B.C., *Bioorg. Med. Chem.,* **2009,** *17*, 2175-2180.

[16]Ng, P. Y., Tang,Y., Knosp, W. M., Stadler, H. S. and Shaw, J. T., *Angew. Chem. Int. Ed.,* **2007,** *46*, 5352-5355.

[17]Ng, P. Y., Masse, C. E. and Shaw, J. T., *Org Lett*. **2006,** *8,* 3999-4002.

[18]Wei, J. Q. and Shaw, J. T., Org. Lett., **2007,** *9*, 4077-4080.

[19]Tan, D. Q., Martin, K. S., Fettinger, J. C. and Shaw, J. T., *Proc Natl. Acad. Sci. USA*., **2011,** *108,* 6781-6786.

[20]Lettan, R. B., Galliford, C.V., Woodward, C. C. and Scheidt, K. A., *J. Am. Chem. Soc*., **2009,** *131*, 8805-8814.

[21]Raup, D. E. A., Cardinal-David, B., Holte, D. and Scheidt, K. A., *Nat. Chem.* **2010,** *2,* 766-771.

[22]Zhao, X., DiRocco, D. A. and Rovis, T., *J. Am. Chem. Soc*., **2011,** *133,* 12466-12469.

[23]Galliford, C. V. and Scheidt, K. A., *Angew. Chem. Int. Ed.* **2007,** *46,* 8748-8758.

[24]Marti, C. and Carreira, E. M., *Eur. J. Org. Chem*., **2003,** 2209-2219.

[25]Lopez, M. G. and Shaw, J. T., *Chem. Rev*., **2009,** *109,* 164-189.

[26]Masse, C. E., Ng, P. Y., Fukase,Y., Sanachez-Rosello, M. and Shaw, J. T., *J. Comb. Chem.*, **2006,** *8*, 293-296.

[27]Hello, K .M ., *Iraqi. J. Chem*., **2000,** *24,* 266.

[28]Krishnaswamy, D., *Tetrahedron.*, **2002,** *34,* 4567.

[29]Abdulrhman, Y. K., Mahmood, S. M., *Best Journal.,* **2014,** *2, (5)*, 37-48.

[30]Burdzhiev, N. T. and Stanoeva, E. R., *Z. Naturforsch.*, **2008,** *63b*, 313-320.

[31]Majeed, N. N., Esaa, A. H. and Turki, A. A., *Pharm. Chem.*, **2014,** *6(2),* 288-293.

HETEROGENEOUS PHOTO-FENTON-LIKE DEGRADATION

OF EVANS BLUE USING Cu₃V₂(OH)₂O₇·2H₂O

Sangeeta Kalal[a], Arpita Pandey[a], Chetna Ameta[a], Rakshit Ameta[b] and Pinki Bala Punjabi[a]*

Degradation of a non-biodegradable azo-dye (Evans blue) has been carried out by the heterogeneous photo-Fenton like processes using copper pyrovanadate (Cu₃V₂(OH)₂O₇·2H₂O) as a catalyst. This catalyst was prepared by wet chemical method. These catalysts were characterized by different techniques such as scanning electron microscopy (SEM), X-ray diffraction (XRD), Fourier transform infrared spectroscopy (FTIR), and Brunauer–Emmett–Teller (BET) surface area analysis. The effect of various parameters such as initial pH, concentration of dye, amount of catalyst, amount of H_2O_2 and light intensity on the reaction rate has also been studied. The various parameters like chemical oxygen demand (COD), conductance, pH, TDS, salinity and dissolved oxygen (DO) in the reaction mixture has been determined before and after treatment. The rate of photo-Fenton degradation of this dye followed pseudo-first order kinetics. A tentative mechanism involving $^{\bullet}OH$ radicals as an oxidant for degradation of dye has been proposed.

* Corresponding Authors
    Fax: +91- 294 2464839
    E-Mail: pb_punjabi@yahoo.com
[a]   Photochemistry Laboratory, Department of Chemistry, M. L. Sukhadia University, Udaipur –313001, Rajasthan, INDIA
[b]   Department of Chemistry, Pacific College of Basic & Applied Sciences, PAHER University, Udaipur – 313003, Rajasthan, INDIA

Introduction

Azo dyes, characterized by the presence of one or more azo groups (-N=N-) bound to aromatic rings, are the largest and most important class of synthetic organic dyes. It has been estimated that more than 50 % of all dyes in common use are azo dyes because of their chemical stability and versatility.[1] About 10-15 % of the synthetic textile dyes used are lost in waste streams during manufacturing or processing operations.[2] Azo dyes are not biodegradable by aerobic treatment processes.[3] In addition, under anaerobic condition, they give potentially carcinogenic aromatic amines, which cause long term health concerns.[4]
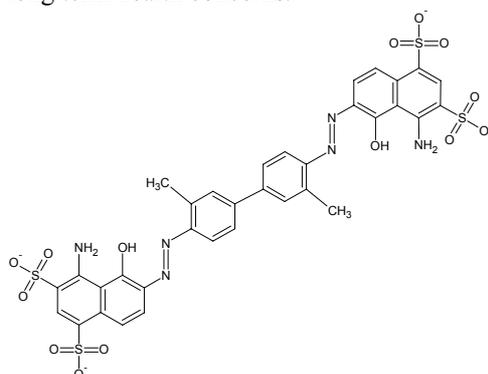
Figure 1. Structure of Evans blue

Evans Blue or T-1824, is an azo dye (Figure 1), which has a very high affinity for serum albumin. Because of this, it can be useful in physiology in estimating the proportion of body water contained in blood plasma.

Several methods have been tried from time to time for the treatment of effluents from dyeing industries, out of which, most common are chemical precipitation and biological methods. In order to develop an efficient method for converting such dyestuffs into harmless products, advanced oxidation processes (AOPs) have been widely applied in recent years, which are characterized by the generation of highly oxidative hydroxyl radicals ($^{\bullet}OH$) in the homogeneous or heterogeneous phase.[5]

Heterogeneous Fenton-like catalysts, such as iron oxides[6,7] and transition metal oxides,[8-10] have recently been reported. Costa et al.[11] introduced Co, Mn, and Ni into the magnetite structure to prepare some two-metal composite heterogeneous Fenton like catalysts $Fe_{3-x}Mn_xO_4$, $Fe_{3-x}Co_xO_4$ and $Fe_{3-x}Ni_xO_4$. It was found that the Co and Mn, but not Ni, resulted in a significant increase in the degradation of the organic pollutants. This enhanced activity was attributed to the coupling of the redox pairs of Fe^{3+}/Fe^{2+} and $Co^{2+}/Co^{3+}(Mn^{2+}/Mn^{3+})$, which resulted in more efficient regeneration of the Fenton active species Fe^{2+}.

Mixed vanadium–chromium oxides present a wide range of interesting properties like excellent catalytic properties,[12-20] potential candidates for anodes in lithium-ion batteries,[21] etc. Zinc pyrovanadate ($Zn_3(OH)_2V_2O_7·2H_2O$)[22] and copper pyrovanadate ($Cu_3V_2(OH)_2O_7·2H_2O$)[23] have been prepared by hydrothermal[24] and the coprecipitation techniques.[25] But till date copper pyrovanadate ($Cu_3V_2(OH)_2O_7·2H_2O$) has not been used quite commonly as heterogeneous photo-Fenton like catalyst.

Hence, in the present study, the focus was on the optimization of the degradation of an azo dye, Evans blue, in presence of copper pyrovanadate ($Cu_3V_2(OH)_2O_7 \cdot 2H_2O$) as heterogeneous photo-Fenton like catalyst.

Experimental

Synthesis of Catalyst

($Cu_3V_2(OH)_2O_7 \cdot 2H_2O$) was prepared by wet chemical process.[26] Copper nitrate aqueous solution (0.1 M L^{-1}) was quickly poured into an aqueous solution of NH_4VO_3 (0.2 M L^{-1}) maintained at 75 °C under continuous stirring.

A yellow precipitate was formed. On further stirring for 1 h, the color of the precipitate was changed to green. It was then separated by filtration, washed several times with pure water and methanol and dried at room temperature overnight.

Characterization

X-ray powder diffraction (XRD) measurements were performed on a BrukerD8 Advance X-ray diffractometer using Cu Kα radiation (λ = 0.154 nm). Infrared (IR) spectra were recorded using a Perkin-Elmer FTIR-1730 spectrometer with KBr disks at room temperature in the range of 4000–400 cm^{-1}. Scanning electron microscopy (SEM) studies were performed using a Bruker AXS microscope equipped with energy dispersive X-ray (EDX) fluorescence spectral analysis for element composition and Robinson secondary electron (SE) and backscattered electron (BSE) detectors for imaging. The surface area of the sample was determined by nitrogen adsorption/desorption analysis. The instrument utilized for nitrogen sorption analysis was a Micromeritics (Gemini 2370), USA Surface Area Analyzer. Stability of the catalyst was checked by atomic absorption spectroscopy using ETCL4129A atomic absorption spectrophotometer.

Procedure

For the photo-Fenton degradation, stock solution of dye (10^{-3} M) was prepared. A reaction mixture containing dye (≈ 10^{-5} *M*), catalyst and hydrogen peroxide, was exposed to light for a certain period of time. A 200 W tungsten lamp (Philips) was used for irradiation purpose. The intensity of light at various distances was measured by "Suryamapi" (CEL Model 201). A water filter was used to cut off thermal radiations. *p*H of the solution was measured by a digital *p*H meter (Systronics Model 335) and it was adjusted by using standard 0.1 *N* sulphuric acid and 0.1 *N* sodium hydroxide solutions. The progress of the degradation was monitored by measuring the absorbance of the reaction mixture at regular time intervals using UV visible spectrophotometer (Systronics Model 106).

It was observed that the absorbance of the solution decreases with increasing time intervals, which indicates that the concentration of Evans blue dye decreases with increasing time of exposure. A plot of 2 + log A versus time was linear following pseudo-first order kinetics.

The rate constant was measured using following expression:

$$k = 2.303 \times \text{Slope} \quad \dots \quad (1)$$

A typical run has been presented (Figure 2)
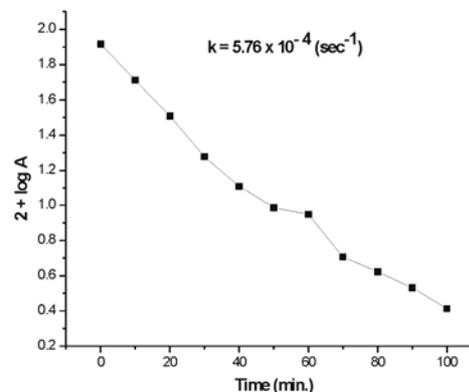
Figure 2. Typical run

The chemical oxygen demand of reaction mixture before and after treatment has been determined by redox method using ferrous ammonium sulphate and $KMnO_4$. The photodegradation efficiency of the catalyst was calculated from the following expression:

$$\eta = \frac{COD_{before} - COD_{after}}{COD_{before}} \times 100 \quad (2)$$

where

η = photodegradation efficiency (%),

COD_{before} = COD of dye solution before illumination, and

COD_{after} = COD of dye solution after illumination

Other quality parameters i.e. dissolved oxygen, conductivity, salinity and total dissolved solids were measured using water analyzer (Systronics Model 371).

Results and discussion

Characterization results

Scanning electron microscopy (SEM) image of ($Cu_3V_2(OH)_2O_7 \cdot 2H_2O$) has been shown in Figure 3. The basic structure of catalyst (volborthite) is a sheet-like structure with copper oxide/hydroxide layers held together by the pyrovanadate groups. These layers are stacked by layers of water. It can also be seen from the SEM result that in addition to the larger particles, the surface contains some smaller particles as small as 20 μm or even smaller.

Figure 3. SEM image of catalyst

The specific surface area of the catalyst was measured by means of conventional BET method. Results showed that the average specific surface area of $(Cu_3V_2(OH)_2O_7 \cdot 2H_2O)$ particle was 17.6 $m^2 g^{-1}$ at 105 °C.

In FT-IR (Figure 4), the band at 1508 cm^{-1} was assigned to the bending vibration of adsorbed water. The wide band at 3500-3600 cm^{-1} was attributed to the stretching of OH groups of chemisorbed water. This fact suggested that after loss of the water adsorbed on the surface, the catalyst did not suffer any obvious decomposition and had some favorable thermal stability in the temperature range investigated. Cu-O bonding has been confirmed by a band at 592 cm^{-1}. The absorption band with the maxima at 896 cm^{-1} corresponds to the V-O stretching bond.[27,28] Band at 798 cm^{-1} corresponds to the V-O-V stretching bond.

Figure 4. FT-IR spectrum of catalyst

Stability of the catalyst was checked by atomic absorption spectroscopy using ECTL 4129A atomic absorption spectrophotometer. Even after one month, leaching of copper or vanadium ions from the catalyst was found to be negligible. Thus, catalyst was found to possess good stability for its use as heterogeneous photo-Fenton like reagents under visible range.

XRD diffraction pattern of the sample was recorded on 18 KW X-Ray diffractometer using Cu Kα radiation. Diffraction pattern was recorded over the 2θ range from 10º to 90º with a step size of 0.05º. Figure 5 shows the XRD pattern of the copper pyrovanadate $(Cu_3V_2(OH)_2O_7 \cdot 2H_2O)$. All the peaks in pattern can be indexed to a pure monoclinic $(Cu_3V_2(OH)_2O_7 \cdot 2H_2O)$ phase, in good agreement with the report of Lafontaine et al.[29] and the JCPDS card No. 46-1443. The crystallite size (t) of the peak can be calculated by using Scherrer's formula: $t = 0.9 \ \lambda / \beta \cos \theta$ where λ is the wavelength of X-rays used (1.5406 Å), β is the full width at half maximum (FWHM) and θ is the angle of diffraction.

Figure 5. XRD pattern of copper pyrovanadate

Effect of various parameters

The effect of pH on the rate of photo-Fenton degradation has been investigated in pH range 5.0 – 8.5 (Figure 6). It has been observed that with an increase in pH, rate of reaction increases and after attaining the maximum value at pH 6.0, the rate decreases with further increase in pH.

Figure 6. Effect of initial pH

It can be anticipated that changes in pH will influence the degradation of the dye in two ways (a) direct involvement of H^+ in the reaction at lower pH (b) mass transport limitations imposed by the precipitation of a passive film on the metal surface at higher pH.

(a) The hydroxyl radicals are generated by two steps:

(i) by the reaction between Cu^+ and V^{4+} ions with hydrogen peroxide,

(ii) by the photochemical reaction of Cu^{2+} and V^{5+} ions and water.

The increase in pH of the medium favours the step (ii) where H^+ ions are formed along with hydroxyl radicals, whereas ^-OH are generated in step (i). Thus, it may be concluded that the step (ii) dominates over step (i) at pH below 6.0. At pH 6.0, both these steps are favoured equally so that the rate of reaction becomes maximum. However, the retardation of the reaction above pH 6.0 suggests the dominance of step (i) over step (ii).

(b) Alternatively, another explanation is also possible. It was observed that the rate of reaction increases on increase in pH of the medium and it was based on the fact that relative number of ^-OH ions increases with increasing pH. As a consequence, the number of $^\bullet OH$ radicals will also increase, resulting in higher rate of degradation of dye. But on increasing the pH beyond 6.0, the number of ^-OH ions also increase and get adsorbed on the catalyst surface making it negatively charged. The approach of the anionic dye molecule towards catalyst surface becomes difficult due to electrostatic repulsion. As a result, the rate of degradation decreases.

The effect of variation of dye concentration on the rate of photo-Fenton degradation has been observed in the range from 0.40×10^{-5} M to 1.8×10^{-5} M (Figure 7). It has been observed that the rate of degradation increases with increase in concentration of Evans blue up to 1.0×10^{-5} M.
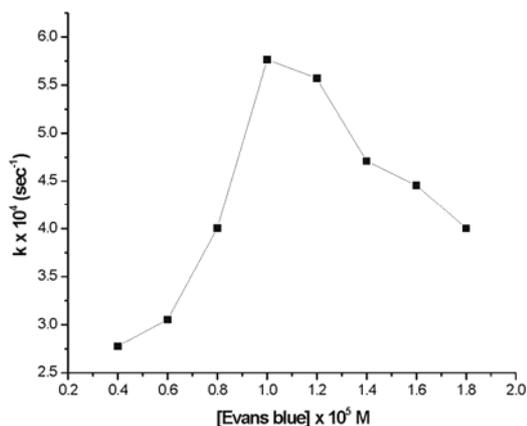

Figure 7. Effect of dye concentration

This may be explained on the basis that initially, on increasing the concentration of dye, the reaction rate increases as more molecules are available for degradation. But further increase in concentration beyond 1.0×10^{-5} M causes retardation of reaction due to increasing number of collision among dye molecules resulting in decrease in number of collision among dye molecule and $^\bullet OH$ radicals. As consequence, the rate of reaction is retarded.

It was observed that rate of degradation increases up to 0.06 g of catalyst, but decreases on increasing the amount further above 0.06 g (Figure 8). On increasing the amount of catalyst, the rate of reaction increases to a certain amount of catalyst (0.06 g). Beyond this point, the rate of reaction decreases with increase in amount of catalyst. This may be explained by the fact that with increase in the amount of catalyst, the surface area of catalyst will increase. Hence, the rise in the rate of reaction has been observed. But after a certain limiting amount of catalyst (0.06 g), any increase in the amount of catalyst would also increase the number of vanadium and copper ions and then there is a possibility of short circuiting between Cu^+ and Cu^{2+} & V^{4+} and V^{5+} ions.[30] As a result, less number of hydroxyl radical are formed and rate of reaction is retarded.
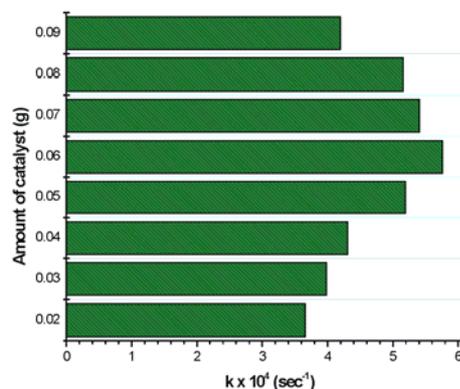

Figure 8. Effect of amount of catalyst

The effect of variation of amount of H_2O_2 on the photo-Fenton degradation of Evans blue has also been investigated in the range from 0.15 to 0.50 mL (Figure 9). It has been observed that initially upon increasing H_2O_2 from 0.15 mL to 0.35 mL, the rate of degradation increases due to availability of more hydroxyl radicals by decomposition of more hydrogen peroxide molecules.
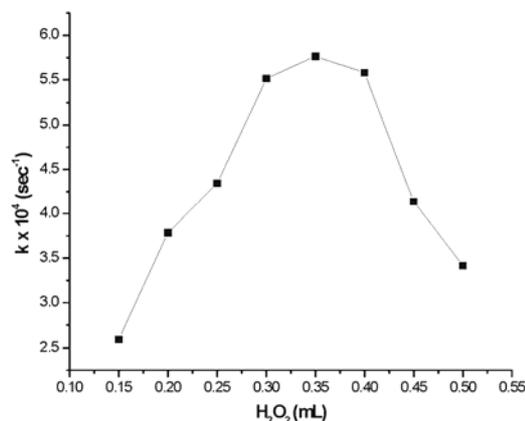

Figure 9. Effect of amount of H_2O_2

However, beyond 0.35 mL, the rate of photo-Fenton degradation decreases. Since propagation step in the oxidative cycle will be hindered by excess of H_2O_2, which

scavenges the $^•OH$ radicals in solution. As a result, less hydroxyl radicals are available resulting into a decrease in the rate of degradation of Evans blue.

It was observed that on increasing light intensity, the rate of reaction also increases and maximum rate has been found at 70.0 mWcm^{-2} (Figure 10). It may be explained on the basis that as light intensity was increased, the number of photons striking per unit area also increases, resulting into higher rate of degradation.
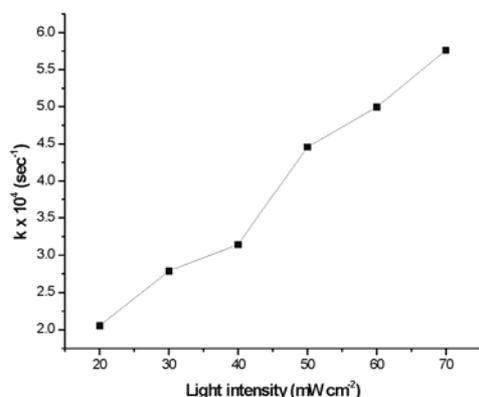

Figure 10. Effect of light intensity

Determination of water quality parameters

Quality of water before and after photo-Fenton degradation has been tested by measuring some parameters. The results are summarized in Table 1.

Table 1. Water quality parameters

Various parameters studied	Before photo-Fenton degradation	After photo-Fenton degradation
COD (mg/L)	27.0	6.0
DO (ppm)	8.1	14.3
Conductivity (μS)	132.0	189.0
Salinity (ppt)	0.10	0.18
TDS (ppm)	63.1	85.5
pH	6.0	6.52

Chemical oxygen demand of dye solution before and after illumination has been determined by redox method. The photodegradation efficiency after 2 hours of illumination has been found to be 77.78 %.

Dissolved oxygen analysis measures the amount of gaseous oxygen dissolved in an aqueous solution. Increase in dissolved oxygen after photo-Fenton degradation indicates mineralization of dye to a significant extent.

Conductivity (as a summation parameter) is a measure of the level of concentration of ions in solution. Conductivity parameter has been increased after the treatment because dye has been mineralized into ions like CO_3^{2-}, NO_3^{-}, SO_4^{2-} etc. Because of this reason, total dissolved solids (TDS) and salinity of the dye solution was also found greater after photo-Fenton degradation of dye.

Before the treatment, pH of reaction mixture was in basic range, but after this degradation, pH becomes neutral because dye particles are mineralized to a significant extent.

Mechanism

On the basis of the experimental observations and corroborating the existing literature, a tentative mechanism has been proposed for the degradation of Evans blue dye in presence of copper pyrovanadate, H_2O_2 and light. V and Cu may simultaneously activate H_2O_2 to give $^•OH$ radicals.

The participation of $^•OH$ radical as an active oxidizing species was confirmed by using hydroxyl radical scavengers, e.g. 2-propanol and butylated hydroxy toluene (BHT), where the rate of photodegradation was found to be drastically reduced.

$$[EB] \xrightarrow{h\nu} {}^1[EB]^* \qquad (3)$$

$$ {}^1[\dot{E}B]^* \xrightarrow{ISC} {}^3[EB]^* \qquad (4)$$

$$ {}^1[EB]^* + {}^•OH \longrightarrow \text{Smaller products} \qquad (5)$$

The involvement of singlet state of dye has been confirmed by conducting the reaction in the presence of a small amount of potassium ferrocyanide as triplet state quencher.[31] The rate of reaction was found to be reduced.

Conclusion

Researches on the heterogeneous photo-Fenton process are expected to grow more rapidly in the near future prompted by the increasing amount of released recalcitrant pollutants. Subsequently, the stability of the produced catalyst needs to be examined under various experimental conditions to prevent the adverse effects of transition metals on the receiving environment. An efficient heterogeneous photo-Fenton catalysts copper pyrovanadate ($Cu_3V_2(OH)_2O_7.2H_2O$) was successfully prepared by using wet chemical method.

The degradation could occur efficiently over a wide pH range of 5.0−8.5. Good degradation effeciency of Evans blue in aqueous solution (77.78 %) was achieved with in 2 h reaction time. This catalyst has good stability for the degradation of Evans blue even after 5 cycles, and therefore, has a great potential. At optimal conditions, (pH = 6.0; [Evans blue] = 1.0 x 10^{-5} M; Amount of catalyst = 0.06 g; H_2O_2 = 0.35 mL; Light intensity = 70 mW cm^{-2}), rate of degradation for Evans blue dye was found to be $k = 5.76 \times 10^{-4}$ sec^{-1}.

During heterogeneous photo-Fenton process, $^•OH$ radicals react with dye and degrade it into smaller products like H_2O, CO_2, NO_3^{-} ions etc.

Acknowledgements

References

[1]Neamtu, M., Siminiceanu, I., Yediler, A. and Kettrup, A., *Dyes and Pigments,* **2002**, *53*, 93.

[2]Gomathi Devi, L., Girish Kumar, S., Mohan, K., Reddy, and Munikrishnappa, C., *J. Hazard. Mater.,* **2009**, *164,* 459.

[3]Pagga, U. and Drown, D., *Chemosphere,* **1986**, *15*, 479.

[4]Brown, D. and Hamberger, B., *Chemosphere,* **1987**, *16*, 1539.

[5]Farias, J., Rossetti, G. H., Albizzati, E. D. and Alfano, O. M., *Ind. Eng. Chem. Res.,* **2007**, *46*, 7586.

[6]Pignatello, J. J., Oliveros, E. and MacKay, A., *Environ. Sci. Technol.,* **2006,** *37*, 273.

[7]Shin, S., Yoon, H. and Jang, J., *Catal. Commun.,* **2008**, *10*, 178.

[8]Heckert, E. G., Seal, S. and Self, W. T., *Environ. Sci. Technol.,* **2008**, *42*, 5014.

[9]Giordano, G., Perathoner, S., Centi, G., De Rosa, S., Granato, T., Katovic, A., Siciliano, A., Tagarelli, A. and Tripicchio, F., *Catal. Today,* **2007**, *124*, 240.

[10]Ghauch, A., Abou Assi, H. and Tuqan, A., *J. Hazard. Mater.,* **2010**, *176*, 48.

[11]Costa, R. C. C., Oliveira, L. C. A., Lelis, M. F. F., Fabris, J. D. and Ardisson, J. D., *Catal. Commun.,* **2003**, *4*, 525.

[12]Thomas, C. L., *Catalytic Processes and Proven Catalysts,* Academic Press, New York, **1970.**

[13]Pradier, C., Rodrigues, F., Marcus, P., Landau, M., Kaliya, M., Gutman, A. and Herskowitz, M., *Appl. Catal. B: Environ.,* **2000**, *27*, 73.

[14]Bosch, H. and Janssen, F., *Catal. Today,* **1988**, *2*, 369.

[15]Mariscal, R., Galan-Fereres, M., Anderson, J., Alemany, L., Palacios J. and Fierro, J., *Environ. Catal.,* **1995**, 223.

[16]De Rossi, S., Ferraris, G., Fermiotti, S., Cimini, A. and Indovina, V., *J. Appl. Catal. A: Gen.,* **1992**, *81*, 113.

[17]Wittgen, P., Groeneveld, C., Zwaans, P., Morgenstern, H., Van Heughten, A., Van Heumen, C. and Schuit, G., *J. Catal.,* **1982**, *77*, 360.

[18]Iwasawa, Y. and Ogasawa, S., *Chem. Lett.,* **1980**, *8*, 127.

[19]Iwasawa, Y., *J. Mol. Catal.,* **1982**, *17*, 93.

[20]De Rossi, S., Ferraris, G., Fremiotti, S., Cimino, A. and Indovina, V., *Appl. Catal.,* **1992,** *81* 113.

[21]Soudan, P., Pereira-Ramos, J. P., Farcy, J., Gregoire, G. and Baffier, N., *Solid State Ionics,* **2000**, *135*, 291.

[22]Melghit, K., Belloui, B. and Yahya, A. H., J. *Mater. Chem.,* **1999**, *9*, 1543.

[23]Melghit, K., Yahaya, A. H. and Yaacob, I. I., *Mater. Lett.,* **2003**, *57*, 1423.

[24]Chirayil, T., Zavalij, P. Y. and Whittingham, M. S., *Chem. Mater.,* **1998**, *10*, 2629.

[25]Baudrin, E., Denis, S., Orsini, F., Seguin, L., Touboul, M. and Tarascon, J.-M., *J. Mater. Chem.,* **1999**, *9*, 101.

[26]Kalal, S., Chauhan, N. P. S., Ameta, N., Ameta, R., Kumar, S. and Punjabi. P. B., *Korean J. Chem. Eng.,* **2014**, *31*, 2183.

[27]Surca, A. and Orel, B., *Electrochim. Acta,* **1999**, *44,* 3051.

[28]Filipek, E., Walczak, J. and Tabero, P. *J., Alloys Comp.,* **1998**, *265*, 121.

[29]Lafontaine, M. A., Le- Bail, A. and Ferey, G., *J. Solid State Chem.,* **1990**, *85*, 220.

[30]Litter, M. I., *Appl. Catal. B: Environ.,* **1999**, *23*, 89.

[31]Zakharova, G. V., Korobov, V. E., Shabalov, V. V. and Chibisov, A. K., *J. Appl. Spectro.* **1983**, *39*, 765.

CHARACTERIZATION OF AIRBORNE PARTICLES AND SOURCE IDENTIFICATION USING SEM/EDS

Silvana Mico[a]*, Eleni Tsaousi[b], Antoneta Deda[c] and Philippos Pomonis[b]

Samples of particulate matter were collected during the winter season from the urban area of Tirana, Albania. Qualitative analyses of particulate matter were performed using Scanning Electron Microscope (SEM) coupled with high Energy Dispersive X-Ray Spectrometer (EDS). Based on chemical analysis and the morphology (the size and shape of particles), the most abundant groups in all sampling days were aluminosilicates (fly ash and soil particles), calcium rich and carbonaceous particles. Air mass trajectories show the presence of Saharan dust during 80 % of sampling days.

*Corresponding author
    E-Mail: silvana.mico@yahoo.com
[a]   Department of Physics, University of Vlora, L.Pavaresia, Skele, Vlora, Albania
[b]   Department of Chemistry, University of Ioannina Ioannina 45110, Greece
[c]   Department of Physics, Faculty of Natural Sciences, Blv. "Zog I", Tirana, Albania

Introduction

Suspended particulate matter is one of the major air pollutants affecting human health.[1,2] Sources of particulate matter are both natural and anthropogenic. Aerosol particles are complex and heterogenic from their physical characteristics, chemical composition, and origin, and have toxic effects on human health. Depending on particle dimensions they remain suspended for long time enough to penetrate into the respiratory tract.[3-6] The physical and chemical characteristics of particles are different, due to large variability of emission sources, and formation and post formation processes. Information about particle size, shape and elemental composition are essential to understand the contribution of emission sources. These data cannot be taken from chemical analysis only. Scanning Electron Microscopy (SEM) coupled with energy dispersed X-ray spectroscopy (EDS) provides a powerful tool for the physico-chemical characterization of particulate matter. Several environmental studies have been carried out for the characterization of airborne particulates and their source apportionment using SEM/EDS techniques.[7-14]

This study aims the characterization of particulate matter in Tirana. Due to rapid urbanization and demographic movement toward Tirana city, about 27 % of the population in Albania lives in Tirana. With a population density of 454 inhabitant/km^2 and about 88.6 % urban population,[15] the pressure on the environment is very high and the city of Tirana is facing serious problems of air pollution. Vehicles fleet in Tirana is mostly private cars using diesel fuel. Tirana has Mediterranean climate with annual average temperature of 16 $^\circ$C. It is located in Central Albania and is mostly covered by hills. Geological formations in Tirana area include coal, quaternary sediments, clays, limestone, quartz sand, schist, conglomerates, volcano sedimentary formations and bauxites.

Materials and methods

Sampling

Samples of suspended particulate matter were collected at the second floor of four storey building of the Faculty of Natural Sciences (Figure 1). This building is located alongside with Zogu I Boulevard, a busy traffic street, and near a busy intersection with heavy traffic. A low volume sampler (Escort ELF air pump) was set to operate at 3 L min^{-1} for air sampling. Suspended particles were collected on Sartorius nuclepore polycarbonate filters having a diameter of 37 mm and 0.45 μm pore size. Each sample was collected continuously for twenty four hours to prevent overloading and formation of secondary aerosol particles due to the recrystallization process. Particulate matter sampling was carried out from 16 January to 25 January 2014 and a total of 7 samples were collected for analysis. Filter samples were weighed before and after sampling time using a microbalance. TSP mass concentrations were measured gravimetrically. Collected samples were put in plastic cassettes and stored until analysis time in the laboratory at 25-30 ºC and relative humidity under 50 %.

Figure 1. Location of sampling site.

SEM-EDS analysis

Individual characterization of aerosol particles was performed using scanning electron microscope JEOL JSM-5600 equipped with an Oxford Link ISIS L300 for EDX analysis, at the Department of Chemistry, University of Ioannina, Greece. SEM/EDS analyses were performed according to EPA Guidelines[16]. Sections 5 mm by 5 mm of filters were cut from each sample and mounted with a carbon film on aluminium SEM stubs for analysis. The working conditions of accelerating voltage of 20 kV, probe current under 100 μA and 21 mm working distance were set. To provide representative results and minimize subjectivity, the results were taken from three randomly selected fields for each filter examined. Each of the particles within a field was analyzed. Manual SEM particle examinations were carried out at magnifications up to 8000 and secondary electron images were acquired. EDX spectra for the centre of particles on SE images with energy range of 0-20 keV and count rate 5-89 cps with approximately measuring time of 100 s were accumulated. Agglomerates with variable chemical composition present in PM samples were examined in different parts. All photomicrographs of individual particles and EDX data were collected for particle classification. Chemical elemental analyses were performed for C, Ca, Al, Si, Cl, Na, K, P, S, Mg, Fe, Cr, Cd, Mn, Pb, Cu, Ti, Zn, Ni, Cs and Co.

Backward trajectories

In order to analyze the sources and transport of aerosol particles at the sampling site, the air mass backward trajectories were calculated for the sampling period. Isobaric backward trajectories were calculated using Hybrid Single-Particle Lagrangian Integrated Trajectory (HYSPLIT) model and the meteorological data of NOAA Air Resources Lab. website (http://www.arl.noaa.gov/ready/hysplit4.html). The calculation method of NOAA HYSPLIT model is hybridization between Lagrangian and Eulerian methods.[17]

Five-day backward trajectories, during sampling period, were calculated for 500 m, 1000 m and 1500 m above the ground level ending at 06:00 UTC, corresponding to the changing time of the filters, and are presented in the Figure 2. The results show the dominance of long trajectories (80 % of the sampling days) that start from the Sahara desert and Mediterranean Sea and arriving in Tirana at low latitudes, smaller than 1000m, where aerosol concentrations are commonly high. Many studies have shown that air masses from Mediterranean Sea transport aerosols from different continental sources and are rich with Sahara dust.[18,19]

Analysis of backward trajectories of air masses for specific days show the presence of air masses from Sahara (Sample S3) and Central Mediterranean region (Sample S2 and S6) and reflect the transport of aerosol particles with natural origin. The samples S4 and S5 are influenced by air masses from Western Mediterranean air masses passing over the South of Italy which can transport both aerosols with anthropogenic and natural origin. The sample Si is influenced by air masses from North Adriatic and S7 is influenced from air masses from Peloponnese area of Greece, suggesting the transport of continental aerosol particles with anthropogenic origin.
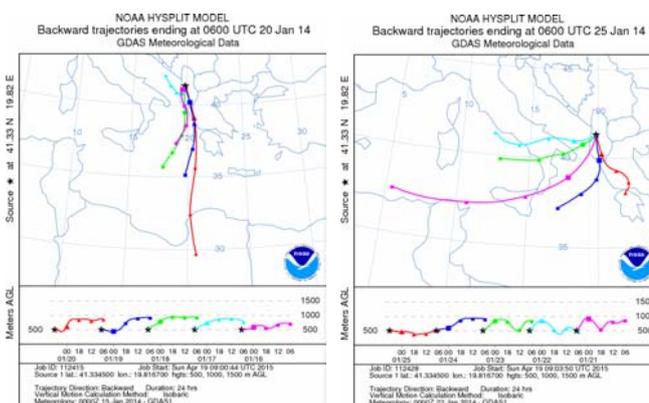

Figure 2. Five-day air-mass backward trajectories at 500, 1000 and 1500 m AGL latitudes, ending at 06:00 (UTC), for the sampling days: a) 16-20 January 2014, b) 21-25 January 2014.

Results and Discussions

Table 1 gives sampling dates and TSP mass concentrations. The mean TSP mass concentration ranged from 56.42 μg m^{-3} to 98.46 μg m^{-3}. Meteorological data during the study period were provided by Meteo Tirana station located in Tirana (N 41° 18' 55"; E 19° 48' 55" and elevation 404 m). During the study period calm conditions and wind directions blowing out from the south to east were dominant.

SEM images of particles showed a wide range of particle sizes and shapes. According to their size, shape and elemental composition 650 particles having a physical diameter greater than 0.5 μm were analyzed. According to the diameter size, the dominant particles corresponded to the fine fraction (smaller than 2 μm). A very small number of particles having a diameter between 10-20 μm were detected. Based on individual particle X-ray spectra performed by EDS the most abundant elements detected were Ca, C, O, Si, Al, Mg, Mn, Pb, Fe and Cd, present in both coarse and fine fractions. Other elements such as Na, K, P, S, Ti, Cs, Ni and Cr were present in minor amounts in the most of the particles.

Based on their morphology and chemical analysis two main particle classes were detected, natural and anthropogenic. Natural particles consist mostly soil dust (minerals) and biogenic (biological fragments, spores, pollen, fungi, etc) particles. Soil particles have irregular shapes and rough surfaces and sometimes form aggregates with irregular shapes and sizes, while biogenic particles were highly structured, with rounded shapes and smooth surface. Anthropogenic particles emitted from combustion processes were predominantly spherical and rounded with smooth surface. The most abundant particles were classified into 7 groups in the decreasing order, aluminosilicates (fly ash and soil particles), Ca-rich particles, carbonaceous particles (soot aggregates and biological particles), mixed particles, Si-rich, Fe-rich and aged sea salt particles.

Table 2 gives a summary of particle groups, corresponding relative abundances, elemental composition and their morphology characteristics for total examined samples.

Table 1. A summary of sampling data

Samples	Sampling date	TSP, µg m⁻³	Weather conditions			
			Wind speed (m s⁻¹)	Wind direction	Temperature, ºC	Relative humidity, %
S1	16-17/01/201	64.17	0.41	SSE	11.4	85
S2	17-18/01/201	75.35	0.5	SE	11.6	75
S3	19-20/01/201	81.68	1.2	SE	9.1	66
S4	20-21/01/201	98.46	1.36	ESE	6.3	83
S5	22-23/01/201	72.63	0.83	SE	6	89
S6	23-24/01/201	56.42	0.72	SE	10.3	84
S7	24-25/01/201	61.39	0.61	SE	10.6	84

Table 2. Particle groups of particulate matter from 16 January to 25 January in Tirana

Particle groups	Abundance, %	Subgroups	Elemental composition	Morphology
Aluminosilicates	13	Si- Al- / Fly ash	Si and Al dominant, moderate amounts of Fe, with Na, Mg, Ca, P and S content	Spherical
	30.2	Si- Al- Ca/ Soil	Dominant Si, Al and Ca with moderate amounts of Fe, Mg and Cr; minor amounts S, Co, Ni, Cu and Pb	Irregular
Ca-rich compds.	19.6	Calcite (CaCO3)	Ca dominant with minor amounts Al, Si, Mg, S and K	Irregular
		Ca-Mn-Pb	Ca, Mn and Pb dominant; variable amounts of Al Mg, Na, Mg, Si, S and Cd, trace of Cs, Cr, Fe, Co Ni and Cu	Irregular
		Ca-Mn-Mg-Al	Ca, Mn, Mg and Al dominant; variable amounts of Na, Si, S and Cd, trace of Cs, Cr, Fe, Co Ni and Cu	Irregular
		Ca-Cd	Ca and Cd dominant; minor amounts of K, Si, Al, Mg, P, and S; trace metals Cr, Fe, Co Ni and Cu	Irregular
Soot	11.5	C-O	C content higher than O	Aggregates
Biogenic	8.7	C-O	C and O in the same amounts and N, P, Cl and S contents	Well-defined
Si-rich	4.1	Si-O	Si dominant variable amounts of Al, Na, Mg and trace of S, K and Ca	Irregular and rounded
Fe-rich particles	1.6	Fe-0	Fe dominant with traces of Na, Mg, Al, Si, K Ca, Cr, Mn, Co and Zn	Irregular and rounded
Aged sea salt	1.1	Na	Na and S with contents of Mg, K, Cl, Si and Cu	Irregular
Mixed particles	10.2	Variable components	Variable combination of Ca, Si, Al, Mn, Cd, Pb, Mg and Fe with trace of P, S, Na, Cu, Co and Ni	Irregular

SEM photomicrographs and respective EDX spectra of the typical particles, which are described in detail with regard to their characteristics, are shown in Figure 3.

Relative number abundances (%) of the particle groups on different sampling days are shown in Figure 4. Both Figure 2 and Figure 4 clearly demonstrate the dependence of the chemical composition of particulate matter on the trajectory of air masses.

Aluminosilicates (43.2 % relative abundance), divided in two subgroups, fly ash and soil particles, were the most abundant particles. They are characterized by high amounts of both Si and Al, moderate amounts of Fe, variable combinations of Ca, Mg, Na, P, S, Ti, and other metals in trace amounts. Aluminosilicates with spherical shapes (Figure 3a) were characterized as fly ash particles and were present in all examined samples. Fly ash particles were distributed mainly in the size range of 1-5 μm. They come from anthropogenic source and can be produced by different combustion processes. These particles consist 30.4 % of aluminosilicates group. Sample S3 (weekend day) is less abundant with fly ash, 9.6 % of aluminosilicates and 4 % of all particles analyzed in this sample. All the other samples taken during weekdays have closely relative amounts of fly ash particles. These results reflect the influence of traffic emissions as major source of fly ash particles. Soil particles with irregular shapes (Figure 3b) were dominant ones within the aluminosilicates group (56.1 %). A part of these particles are seen as aggregations of smaller particles rich in Si, Al

and Fe. They come from soil, and in urban atmosphere may be derived mostly from resuspension of road dust caused by vehicles or carried by air masses.[20]
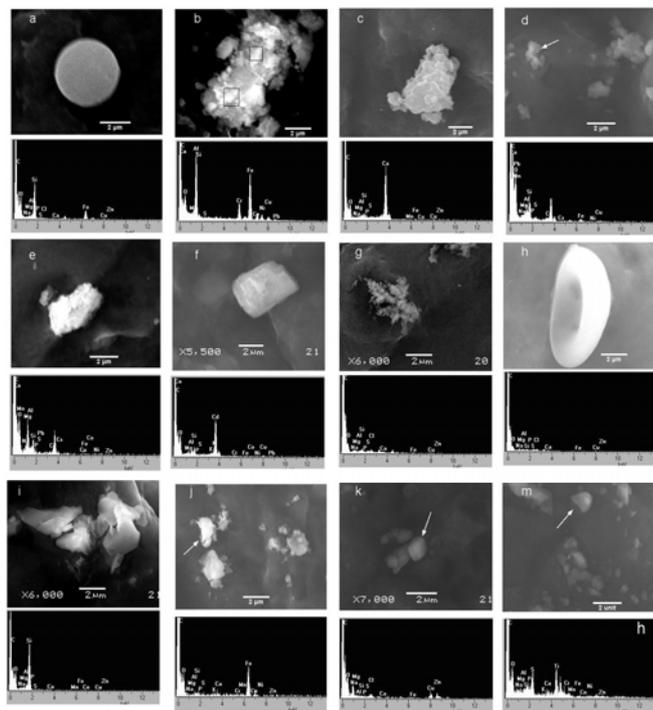

Figure 3. SEM photomicrographs and respective EDX spectra for: aluminosilicates- a) fly ash particles, b) soil particles; Ca-rich particles- c) calcite (CaCO₃), d) Ca- Mn- Pb particles, e) Ca-Mn-Al particles, f) Ca-Cd particles; Carbonaceous particles- g) soot aggregates, h) biogenic particles (pollen or spore); i) Si-rich(natural quartz particles); j) Fe-rich mineral particles; k) aged sea salt particles; m) mixed particles.
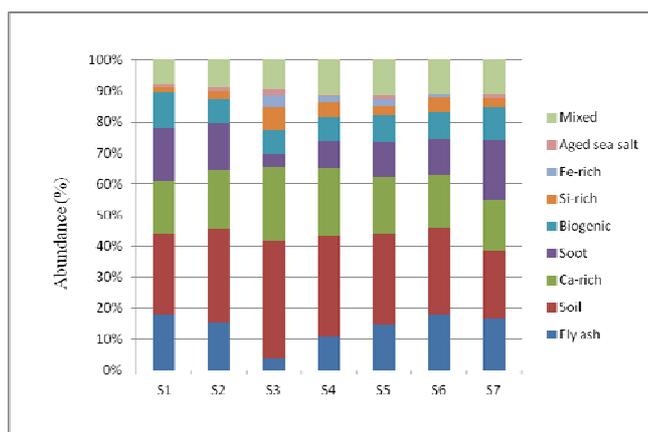

Figure 4. The relative number abundance (%) of the particle groups on different sampling days.

These particles can also contain much higher ratio of potentially anthropogenic phases (amorphous phases, salts, magnetite), while they can be hidden by the large amount of coarse particles of soil origin.[21] The Figure 4 shows that all samples are dominated by soil particles but, the samples S3

and S4 are largely dominated. Soil particles consist 37.6 % and 32.2 % of all analysed particles and 91.4 % and 74.5 % of aluminosilicate group particles in the samples S3 and S4 respectively, reflecting the influence of Saharan dust in particulate matter in Tirana.

Ca-rich particles (19.6 % abundance) group was the second most abundant, in the range from 16.4 % (S7) to 24 % (S3). The major part of this group is made up by calcite particles, which are dominated by Ca (> 60 %) with minor amounts of Al, Si, Mg, S and K (Figure 3c). These particles were present in all aerosol samples. They result mainly from geogenic origin and are composed of carbonate minerals including calcite and dolomite[7,13]. Calcite particles (CaCO₃) can be generating from lime production, cement manufacturing and building construction. These particles can also come from the rocky hills which form the background of Tirana. Particles such as Ca-Mn-Pb (Figure 3d), Ca-Mn-Mg-Al (Figure 3e) and Ca-Cd (Figure 3f) are included in the group of calcite particles. Particles rich in Ca, Mn and Pb were found in fine fraction and contained minor amounts of Al, Na, Mg, Si, S, Cd and trace of Cs, Cr, Fe, Co, Ni and Cu. The analysis of shape cannot yield any information about the possible source. The airborne Ca particles are mainly derived from earth crust. Pb is typically derived from anthropogenic combustion processes such as the use of leaded gasoline, coal combustion or may be the use of paints and plasters during construction activities. Mn is a metal of both natural and anthropogenic origin. Mn may be derived as one of additive elements in gasoline or is naturally occurring in many types of rocks. The presence of Ca, Pb and Mn in moderate amounts indicated that these Ca-rich particles cannot come from traffic emission. These particles were present only in the samples S3, S4 and S6, suggesting that may be from Saharan dust. Some authors have suggested that lead concentration in soils can be seen as tracer of the potential anthropogenic contamination occurring during Saharan aerosol transport and fallout.[22]

Soot aggregates (11.5 % abundance) are composed by spheres with diameter smaller than 0.1 μm, and the C content is higher than O and are thus easily distinguished from other particles. These particles are of much interest because these are considered as second largest contributor to global warming. They may originate in different ways from incomplete combustion of gasoline, oil, diesel and other fuels, being so these are good tracer of vehicle emissions.[23] SEM photomicrographs and respective EDX spectra for soot aggregates are presented in the Figure 3g. The variation on different days of soot particles like fly ash particles suggests that its major source is traffic related. Few particles can be attributed to the combustion of fossil fuels for domestic heating.

Biogenic particles (8.7 % abundance) are the most easily identified among other particles and include a wide range of spores, pollens, bacteria, fungi and fragments of plants and insects. Biogenic particles contain C and O in the same amount and minor amounts of P, Cl and S. They were present in all samples and were indifferently distributed on sampling days. These particles of natural origin are seasonal dependent. They have highly structured and symmetrical shape and different sizes mainly in coarse fraction. SEM photomicrographs and respective EDX of typical biogenic particle are shown in Figure 3h.

Si-rich (4.1 % abundance) particles, classified as quartz (Figure 3i), contain predominately silicon (SiO_2). They also contain variable amounts of Al, Na, Mg, P and traces of S, K and Ca. More than 60 % of these particles were found in coarse fraction. The major part (55.5 %) of all Si-rich particles was observed in two samples, S3 and S4. They can be derived from soil and carried by wind or from construction activities and transported materials.

Fe-rich particles (1.6 % abundance) may be of both anthropogenic and natural origin. They contain mainly Fe with traces of Na, Mg, Al, Si, K Ca, Cr, Mn, Co and Zn. Fe-rich particles were absent in the samples S1, S2 and S7. Very few irregular Fe-rich particles from soil origin were detected, their diameter is mostly smaller than 5 μm (Figure 3j).

Aged sea salt (1.1 % abundance) particles differ from fresh sea salt of marine aerosol. These particles contain mainly Na with some amount of Mg, S and K and traces of Cl, Si, Cu and Zn. The crystals of fresh sea salt undergo chemical and morphological changes during the long transport, especially depleting Cl content of particles and driving it into the atmosphere.[24,25] Detected aged sea salt particles were found to be rounded or well-shaped (Figure 3k). They come from Mediterranean air masses.

Mixed particles (10.2 % abundance) contain variable combination of Ca, Si, Al, S, Ti, Mn, Cd, Pb, Mg and Fe. These particles, which could not be classified as one of described groups, were mostly in the fine fraction and with rounded shape. They may be either from mineral origin transported by winds or anthropogenic origin such as construction activities, tire wear debris and abrasion of different materials. Another source can be direct traffic emissions mixed with road dust resuspended several times. An example of mixed particles is presented in Figure 3m.

Conclusions

Gravimetric measurements show that the mean TSP mass concentrations range from 56.42 μg m^{-3} to 98.46 μg m^{-3}. The air mass backward trajectories indicate that urban atmosphere of Tirana during the sampling period was affected by Saharan dust event and air masses from Mediterranean Sea. The conduction of SEM/EDX analysis provided information on individual particle morphology and chemical composition, important characteristics to assess the contribution of major sources to the particulate matter. Morphology analyses of individual particles show that nonspherical particles of crystal origin were dominant in all dust samples. For all samples, both in the fine and coarse fractions, predominant elements were Si, Al, Ca, and variable amounts of Fe, Mn, Pb, Cd and Cr. These results confirm the influence of Saharan dust of particulate matter composition in urban atmosphere of Tirana. For the sampling period, two major sources of particulate matter affect urban atmosphere in Tirana, anthropogenic and natural sources. Anthropogenic emission sources include traffic emissions, resuspended road dust induced by traffic and construction activities. Natural sources include mineral particles of local origin and carried by air masses over Mediterranean region mainly from Saharan dust origin.

With extended data and further statistical analysis the source apportionment can be clarified.

References

[1]Dockery, D. W., Pope, C. A., Xu, X., Spengler, J. D., Ware, J. H., Fay, M. E., Ferris, B. G. and Speizer, F. E., *New Engl. J. Med.*, **1993**, *329*, 1753–1759.

[2]Pope, C. A., Dockery, D. W., and Schwartz, J., *Inhalation Toxicol.*, **1995**, *7*, 1–18.

[3]Heyder, J., Gebhart, J., Rudolf, G., Schiller, C. F., Stahlhofen, W., *J. Aerosol Sci.*, **1986**, *17*, 811-825.

[4]Peters, A., Wichmann, H. E., Tuch, T., Heinrich, J. and Heyder, J. *Am. J. Respir. Crit. Care Med.*, **1997**, *155*, 1376–1383.

[5]Hinds, W. C., *Aerosols technology: properties, behavior, and measurements of airborne particles*, 2nd Ed., J. Wiley and Sons, N.Y., **1999**,

[6]Taunton, E. A, Gunter, E. M, Nolan, P. R, Phillips, I. J., *Period. Mineral.,* **2011**, *80(1)*, 167-179.

[7]Xie, R. K., Seipa, H M., Leinumb, J. R., Winjec, T., Xiao, J. S. *Sci. Total Env.,* **2005**, *343*, 261– 272.

[8]Iordanidis, A., Buckman, J., Triantafyllou, A. G., and Asvesta, A.I., *Bull. Geol. Soc. Gr.,* **2007**, *40*, 1421-1432,*Proc. 11th Int. Congr*. Athen, May, **2007**

[9]Post, J. E. and Buseck, P. R. *Environ. Sci. Technol.*, **1984**, *18*, 35–42.

[10]Sielicki, P., Janik, H., Guzman A., and Namiesnik, J., *Crit, Rev, Anal, Chem,* **2011**, *41(4)*, 314-334.

[11]Perez, N., Pey, J., Querol, X., Alastuey, A., Lopez, J. M., Viana, M., *Atm. Environ.,* **2008**, *42*, 1677–1691.

[12]Sinha, B. W., Hoppe, P., Huth, J., Foley, S., and Andreae, M. O., *Atm. Chem. Phys.*, **2008**, *8*, 7217–7238.

[13]Pachauri, T., Singla, V., Satsangi, A., Lakhani, A., Kumari, K., *Aerosol Air Qual. Res.,* **2013**, *13*, 523–536.

[14]Armiento, G., Inglesis, M., Taglioni, M. S., Montreali, R. M., Nardi, E., Palleschi, S., Piga, L., Sacco, F., Leopoldo, S., Gianfagna, A., *Period. Mineral.,* **2013**, *82(1)*, 199-216.

[15]INSTAT, *Censusi i popullsisë dhe banesave 2011*, (Population and housing census 2011), *Adel Print*, **2012**, 11-12.

[16]EPA, *Guidelines for the application of SEM/EDX analytical techniques to particulate matter samples,* **2002**, *EPA* 600/R-02/070.

[17]Draxler, R. R. and Rolph, G. D., **2003**, *Model Access via the NOAA ARL READY Website:(http://www.arl.noaa.gov/ ready/hysplit4.html).*

[18]Papayannis, A., Balis, D., Amiridis, V., Chourdakis, G., Tsaknakis, G., Zerefos, C., Castanho, ADA., Nickovic, S., Kazadzis, S., Grabowski, J., *Atm. Chem. Phys.* **2005**, *5,* 2065–2079.

[19]Querol, X. Pey J., Pandolfi, M., Alastuey, A., Cusack, M., Pérez, N., Moreno, K. G., Kleanthous, S., *Atm. Env.* **2009**, *43(28),* 4266-4277.

[20]Thibodeaux, L. J. and Mackay, D., *Handbook of Chemical Mass Transport in the Environment*, CRC Press, **2010**, 1st ed., 453-477.

[21]Sipos, P., Kis, K. V., Márton., E., Németh, T., May, Z. and Szalai, Z., *Eur. Chem. Bull.,* **2012**, *1(11),* 449-454.

[22]Guieu, C., Loÿe-Pilot, M.-D., Ridame, C., and Thomas C., J. *Geophys. Res.*, **2002**, *107(D15)*, 4258.

[23]Fruhstorfer, P. and Niessner, R., *Microchim. Acta*, **1994**, *113(3)*, 239-250.

[24]Hoffman, R. C., Laskin, A., and Finlayson-Pitts, B. J., *J. Aerosol Sci.*, **2004**, *35*, 869–887

[25]Targino, A. C., Krejci, R., Noone, K. J., and Glantz, P., *Atm.. Chem. Phys.*, **2006**, **6**, 1977–1990.